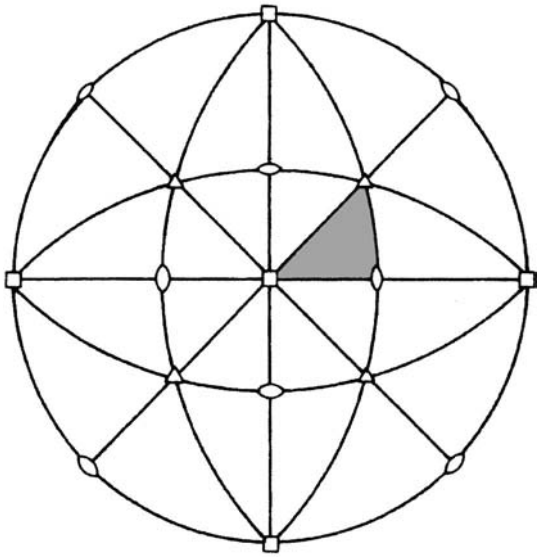

Fig. 6.7 Standard [001] stereographic projection divided into 24 triangles.

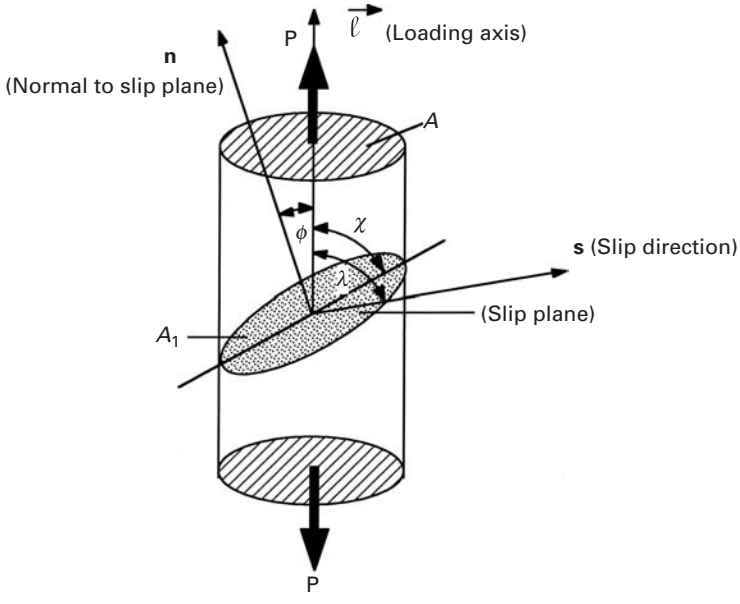

Fig. 6.8 Relationship between loading axis and slip plane and direction.

Figure 6.8 shows a crystal with a normal cross-sectional area A upon which a tensile load P acts, generating a uniaxial stress P/A. The slip plane and direction are indicated, respectively, by the angles ϕ and λ that they make with the tensile axis. The normal **n** of the slip plane, cross-sectional area A_1, that makes an angle ϕ with the loading direction ℓ.

The areas A_1 and A are related by the angle ϕ. Area A is the projection of A_1 onto the horizontal plane; thus, we can write

$$A = A_1 \cos\phi.$$

The shear stress τ acting on the slip plane and along the slip direction **s** is obtained by dividing the resolved load along the slip direction ($P \cos \lambda$) by A_1:

$$\tau = \frac{P \cos \lambda}{A_1} = \frac{P}{A} \cos\phi \cos \lambda.$$

But $P/A = \sigma$ is the normal stress applied to the specimen. Hence,

$$\tau = \sigma \cos\phi \cos\lambda.$$

Note that $\cos \phi = \sin \chi$.

This equation shows that τ will be zero when either λ or ϕ is equal to 90°. On the other hand, the shear component is maximum when both ϕ and λ are equal to 45°. We have, in this case,

$$\tau_{\max} = \sigma \cos 45^\circ \cos 45^\circ = \frac{\sigma}{2}.$$

The angle between any two directions **a** and **b** can be obtained from the scalar product of these vectors:

$$\mathbf{a} \cdot \mathbf{b} = |\mathbf{a}||\mathbf{b}| \cos\theta$$

or

$$\cos \theta = \frac{\mathbf{a} \cdot \mathbf{b}}{|\mathbf{a}||\mathbf{b}|}.$$

For cubic crystals, planes and directions with the same indices are perpendicular, and the angle is determined from the coefficients, h, k, and l. For two vectors

$$\mathbf{a} = h_1\mathbf{i} + k_1\mathbf{j} + l_1\mathbf{k}$$

and

$$\mathbf{b} = h_2\mathbf{i} + k_2\mathbf{j} + l_2\mathbf{k},$$

the angle θ is given by

$$\boxed{\cos\theta = \frac{h_1h_2 + k_1k_2 + l_1l_2}{(h_1^2 + k_1^2 + l_2^2)^{1/2}(h_2^2 + k_2^2 + l_2^2)^{1/2}}.} \tag{6.1}$$

If two directions are perpendicular, their dot product is zero; and the same is true for a direction that is contained in a plane. From Equation 6.1, it is possible to obtain the $\cos \phi$ and $\cos \lambda$ terms for all desired crystallographic directions of a crystal. For instance, if the loading direction is [123] for an FCC crystal, then the Schmid factors (see below) of the various slip systems are found by obtaining the angles of [123] with <111> (perpendicular to slip planes) and <110> (slip directions). Note that each slip plane contains three slip directions and that 12 values (4×3) have to be obtained.

Schmid and coworkers[1] used the variation in the resolved shear stress to explain the great differences in the yield stresses of monocrystals of certain metals. They proposed the following rationalization, known as the *Schmid law*: *Metal flows plastically when the resolved shear stress acting in the plane and along the direction of slip reaches the critical value*

$$\boxed{\tau_c = \sigma_0 \sin\chi \cos\lambda = M\sigma_0,} \tag{6.2}$$

$$M = \sin\chi \cos\lambda = \cos\phi \cos\lambda, \tag{6.3}$$

where the factor M is usually known as the *Schmid factor*.

Schmid's law has found experimental confirmation principally in hexagonal crystals. Figure 6.9 shows the experimental results, compared with Schmid's prediction for high-purity zinc. The full line shows the hyperbola obtained by the use of Equation 6.3, assuming a critical resolved shear stress of 184 kPa. It is worth noting that the yield stress is minimum for $M = 0.5$.

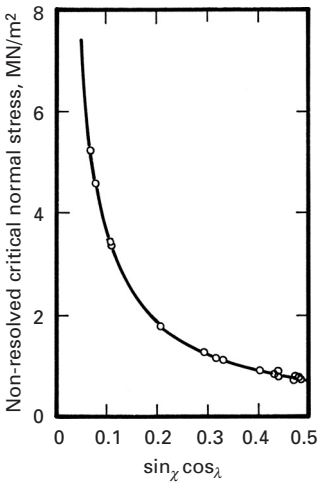

Fig. 6.9 Comparison of Schmid law prediction with experimental results for zinc. (Adapted with permission from D. C. Jillson, *Trans. AIME*, 188 (1950) 1120.)

For cubic crystals, the correspondence between Schmid's law and experiments is not as good. This is mainly due to the great number of slip systems in these structures. For nickel, the critical resolved shear stress is practically orientation independent. On the other hand, for copper, the critical resolved shear stress is dependent on orientation, being constant in the center of the stereographic triangle and assuming higher values close to the sides. Figure 6.10 shows the inverse of Schmid's factor in the stereographic triangle based on a $\{111\}$ <110> slip: This is the situation for FCC crystals. The orientation for which FCC crystals are softest is $M = 0.5$, or $M^{-1} = 2$, which occurs approximately at the center of the triangle. The dependence of τ_c on the orientation for cubic systems is thought to be because the components of compressive stresses acting normal to the slip planes are different for different orientations at the same applied stress level. These compressive stresses should have an effect on τ_c. Easy glide in FCC crystals is greatest in the center of the stereographic projection, in the region closer to (but not coinciding with) the <110> corner. It is affected by a number of parameters, the most notable being the following.

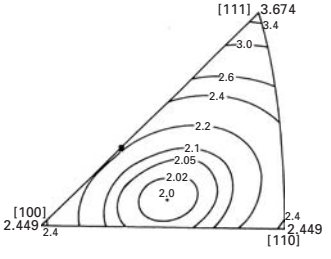

Fig. 6.10 Effect of orientation on the inverse of Schmid's factor ($1/M$) for FCC metals. (Adapted with permission from G. Y. Chin, "Inhomogeneities of Plastic Deformation," in *The Role of Preferred Orientation in Plastic Deformation* (Metals Park, OH: ASM, 1973), pp. 83, 85.)

1. *Specimen size*. Specimens with a smaller cross-sectional area tend to have a more extended easy-glide region.
2. *Temperature*. Easy glide is more pronounced at lower temperatures and may vanish completely at high temperatures.
3. *Stacking-fault energy*. FCC metals with low stacking-fault energy tend to have a more pronounced easy-glide region. Why?
4. *Solute atoms*. If solute atoms pin the dislocations, they will shorten their mean free path and the extent of easy glide. If solute atoms contribute primarily to the lowering of the stacking-fault energy or to ordering, they will increase the easy glide range.

[1] E. Schmid and W. Boas, *Kristalplastizitat* (*Plasticity of Crystals*) (Berlin and London: Springer and Hughes, 1950).

Example 6.1

A single crystal of copper is deformed in tension. The loading axis is [112].

(a) Calculate the Schmid factors for the different slip systems.
(b) If the critical resolved shear stress is 50 MPa, what is the tensile stress at which the material will start to deform plastically?

Solution:

(a) Copper is FCC, which has 12 slip systems of the type $\{111\}\langle 110\rangle$; thus, we have

$$\cos\phi = \frac{\mathbf{n}\cdot\ell}{|\mathbf{n}|\cdot|\ell|},$$
$$\cos\lambda = \frac{\mathbf{s}\cdot\ell}{|\mathbf{s}|\cdot|\ell|},$$

and the following table:

Slip plane ($\boldsymbol{n}$)	Slip direction ($\boldsymbol{s}$)	Cos ϕ	Cos λ	Schmid factor (cos ϕ cos λ)	σ (*MPa*)
(111)	$[\bar{1}10]$	$2\sqrt{2}/3$	0	0	Not deformed
	$[\bar{1}01]$	$2\sqrt{2}/3$	$\sqrt{3}/6$	$\sqrt{6}/9$	184
	$[0\bar{1}1]$	$2\sqrt{2}/3$	$\sqrt{3}/6$	$\sqrt{6}/9$	184
$(\bar{1}11)$	$[110]$	$\sqrt{2}/3$	$\sqrt{3}/3$	$\sqrt{6}/9$	184
	$[101]$	$\sqrt{2}/3$	$\sqrt{3}/2$	$\sqrt{6}/6$	122
	$[0\bar{1}1]$	$\sqrt{2}/3$	$\sqrt{3}/6$	$\sqrt{6}/18$	367
$(1\bar{1}1)$	$[110]$	$\sqrt{2}/3$	$\sqrt{3}/3$	$\sqrt{6}/9$	184
	$[\bar{1}01]$	$\sqrt{2}/3$	$\sqrt{3}/6$	$\sqrt{6}/18$	367
	$[011]$	$\sqrt{2}/3$	$\sqrt{3}/2$	$\sqrt{6}/6$	122
$(11\bar{1})$	$[\bar{1}10]$	0	0	0	Not deformed
	$[101]$	0	$\sqrt{3}/2$	0	Not deformed
	$[011]$	0	$\sqrt{3}/2$	0	Not deformed

A diagram showing the loading axis [112] is given in Figure E6.1.

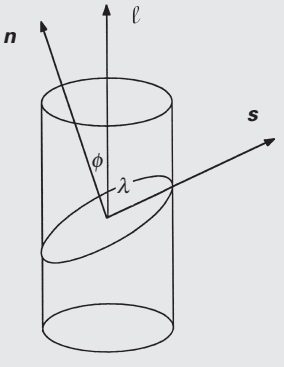

Fig. E6.1

(b) $\tau_{\text{crss}} = \sigma \cos\phi \cos\lambda,$

$$\sigma = \frac{\tau_{\text{crss}}}{\cos\phi \cos\lambda} = \frac{50}{\cos\phi \cos\lambda}.$$

Results are shown in the foregoing table.

Example 6.2

Calculate the total energy due to dislocations in iron in the annealed condition, after 20% plastic deformation and 100% plastic deformation. Use both the exact (Equation 4.20) and the approximate equation (Equation 4.21) ($U = Gb^2/2$). Assume that the core has a radius equal to $5b$ and that dislocations are evenly distributed between edge and screw types. Given the following information:

$G = 81.6$ GPa,

$\nu = 0.293$,

$r = 0.124$ nm.

The relationship between the stress and dislocation density is (see Section 6.3):

$$\tau = 40 \times 10^6 + 16.67\sqrt{\rho} \quad (\text{in Pa}).$$

The stress–strain relationship is:

$$\tau = \tau_0 + k\gamma^n,$$

where $\tau_0 = 50 \times 10^6$, $k = 100 \times 10^6$, and $n = {}^1/_2$.

Solution: The stress levels for $\gamma = 0$, 0.4, and 2 ($\gamma = 2\varepsilon$) are

$$\tau = 50{,}113, \text{ and } 191.4 \times 10^6 \text{ Pa}.$$

The dislocation density is:

$$\rho = (\tau - 40 \times 10^6)^2 \times \frac{1}{16.67^2} = 3.5 \times 10^{-3}(\tau - 40 \times 10^6)^2.$$

Hence, for

$\varepsilon = 0, \quad \rho = 3.5 \times 10^9 \text{ m}^{-2},$

$\varepsilon = 0.2, \quad \rho = 3.71 \times 10^{13} \text{ m}^{-2},$

$\varepsilon = 1, \quad \rho = 1.15 \times 10^{14} \text{ m}^{-2}.$

We now obtain the dislocation spacing. It is known that

$$\ell = \frac{1}{\rho^{1/2}}.$$

So, for

$\varepsilon = 0, \quad l \approx 1.69 \times 10^{-5} \text{ m},$

$\varepsilon = 0.2, \quad l \approx 1.64 \times 10^{-7} \text{ m},$

$\varepsilon = 1, \quad l \approx 0.93 \times 10^{-7} \text{ m},$

and we have

$$U_T = \frac{Gb^2}{10} + \frac{Gb^2}{4\pi(1-\nu)}(1-\nu\cos^2\alpha)\frac{\rho^{-1/2}}{5b}.$$

For 50% edge and 50% screw dislocations, we make $\alpha = 45^\circ$. The Burgers vector can then be calculated from the radius of the atoms. If the lattice parameter is a, the Burgers vector is, along [111]

$$|\mathbf{b}| = a\sqrt{1^2+1^2+1^2} = 4r$$
$$= 0.496\,\text{nm}.$$

Thus, for

$$\varepsilon = 0, \quad U_T = (0.1 + 0.847)G\,b^2 = 0.947\,Gb^2,$$
$$\varepsilon = 0.2, \quad U_T = (0.1 + 0.402)G\,b^2 = 0.502\,Gb^2,$$
$$\varepsilon = 1, \quad U_T = (0.1 + 0.34)G\,b^2 = 0.44\,Gb^2.$$

The approximate expression for the dislocation self-energy ($U_T = Gb^2/2$) becomes gradually better as the density is increased. The total energy of dislocations per unit volume is

$$U = U_T\rho,$$

and for

$$\varepsilon = 0, \quad U = 696.3\ \text{J/m}^3,$$
$$\varepsilon = 0.2, \quad U = 74.2 \times 10^4\ \text{J/m}^3,$$
$$\varepsilon = 1, \quad U = 2.3 \times 10^5\ \text{J/m}^3.$$

6.2.3 Shear Deformation

Just as a tensile test does not directly provide the shear stress in the slip plane and along the slip direction, it does not directly provide the corresponding deformation. Accordingly, one must determine shear by taking into account the relative orientations of the tensile axis and the slip system. If a tensile specimen is attached to the grips of a tensile-testing machine by means of universal joints, it can be seen that the slip plane will rotate with respect to the tensile axis as deformation proceeds. Therefore, it is important to know the deformation and, consequently, the change in orientation, along with the attendant alteration in Schmid's factor. In a similar way, it can be shown that the shear strain $d\gamma$ in the slip system is related to the longitudinal strain $d\varepsilon$ by

$$d\lambda = \frac{d\varepsilon}{\sin\chi\cos\lambda} = \frac{d\varepsilon}{M}. \tag{6.4}$$

Therefore, when $M = 0.5$, we have $\tau = 0.5\sigma$ and $\gamma = 2\varepsilon$. (Notice that $\tau = \sigma/2$!).

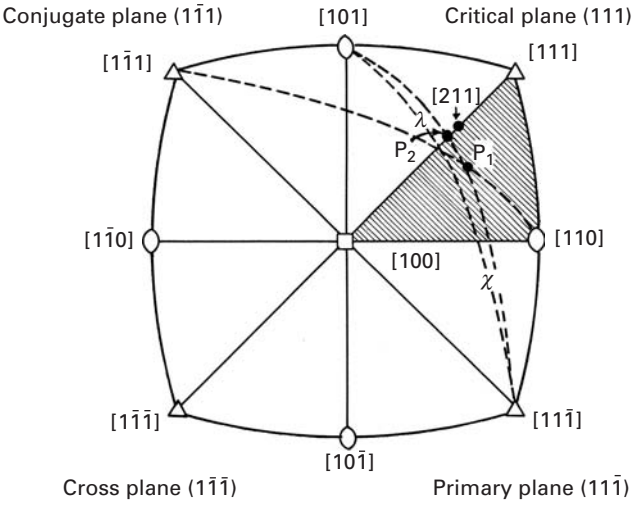

Fig. 6.11 Stereographic projection showing the rotation of slip plane during deformation. Direction P_1, inside stereographic triangle moves toward P_2 on boundary [100]–[111]. Then, P_2 moves toward [211].

6.2.4 Slip in Systems and Work-Hardening

Equations 6.3 and 6.4 establish the stress and strain in the plane and in the direction of shear and are therefore important from the point of view of dislocation motion. In HCP structures, the slip is more easily maintained in one plane. However, in BCC and FCC structures, other slip systems are easily activated. The rotation and direction of the slip plane will easily put other systems in a favorable position. This situation is shown in the stereographic projection of Figure 6.11. A certain crystal has its tensile axis within the crosshatched stereographic triangle. The first slip system to be activated will be the one with the highest Schmid factor. (See Equations 6.2 and 6.3). There are eight slip systems around axis P_1 in the figure. There are other ones in the total stereographic projection. By using great circles, the reader can check whether the following systems of directions really belong to the planes:

$(11\bar{1})[101]$, $(11\bar{1})[1\bar{1}0]$,
$(111)[1\bar{1}0]$, $(111)[10\bar{1}]$,
$(1\bar{1}1)[10\bar{1}]$, $(1\bar{1}1)[110]$,
$(1\bar{1}\bar{1})[110]$, $(1\bar{1}\bar{1})[101]$.

The maximum value of Schmid's factor, $M = 0.5$, is obtained for $\chi = \lambda = 45^\circ$. The angles between P_1 and the <100> directions are determined by means of a Wulff net, passing a great circle through the two poles. Among the preceding eight systems, the slip system having the highest Schmid factor is $(11\bar{1})$ [101]; slip will initially take place in this system. Plane $(11\bar{1})$ is therefore called the *primary slip plane*. As deformation proceeds, χ and λ will rotate. In the stereographic projection, this is indicated by rotation of the axis P_1. Actually, the specimen rotates with respect to the axis. P_1 will tend to align itself with direction [101], decreasing λ in the process; this is shown in

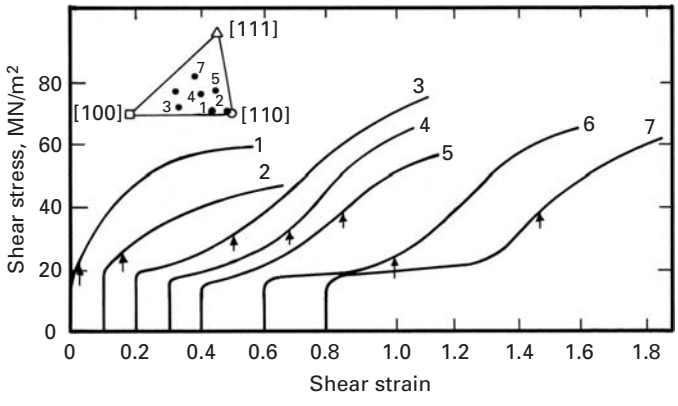

Fig. 6.12 Shear-stress vs. shear-strain curves for Nb(BCC) monocrystals at different crystallographic orientations; arrows indicate calculated strain at which conjugate slip is initiated. (From T. E. Mitchell, *Prog. App. Matls. Res.* 6 (1964) 117.)

Figure 6.11. However, when the great circle passing through [100] and [111] is reached, the primary system and the *conjugate slip system* $(1\bar{1}1)$ [110] will have the same Schmid factor. The typical behavior in this case is double slip in both systems: The axis P_1 will tend toward the direction [211], as shown in the figure. In reality, there are deviations from this behavior, and there is a tendency to "overshoot" and subsequent correction. The two other slip systems are called the *cross* system and the *critical* system. This nomenclature, however, is not universal: Often, the term "cross-slip" is used to describe a different situation – small slip segments in a secondary slip system joining slip lines in a primary slip system.

As a conclusion to the foregoing discussion, it can be said that a cubic crystal will initially undergo slip in one system if P_1 is within the stereographic triangle. If P_1 is on the sides of the triangle, two systems have the same Schmid factor. On the other hand, if P_1 coincides with one of the edges, the situation is more complicated: Eight systems will have the same Schmid factor if P_1 coincides with [100], four if it coincides with [110], and six if it coincides with [111]. The term "polyslip" refers to a crystal oriented in such a way that more than one system is activated.

When a cubic monocrystal with an orientation inside the stereographic triangle is deformed, one single slip system is often activated. Such orientations in the center of the stereographic triangle are considered "soft" orientations, and Figure 6.12 illustrates the different stress–strain curves obtained for niobium. Orientations 1 and 2 are close to polyslip, and the stress–strain curves have the characteristic parabolic hardening shape. Several slip systems are activated at the onset of yielding. For orientations 3 through 7, inside the sterographic triangle, one single slip system is activated first. The onset of conjugate slip requires rotation of the crystal toward an orientation along the sides of the triangle; this occurs only at a certain amount of strain, which depends on the orientation. Single slip is characterized by a very low work-hardening rate; once the conjugate slip becomes operative, the work-hardening rate increases significantly.

Figure 6.13 shows generic shear-stress–shear-strain curves for FCC single crystals. Any such curve can be divided, conveniently, into three regions: I, II, and III; θ_I, θ_{II}, and θ_{III} are the respective work-hardening slopes ($d\tau/d\gamma$) of the regions. In what follows, we describe the salient points of the various stages.

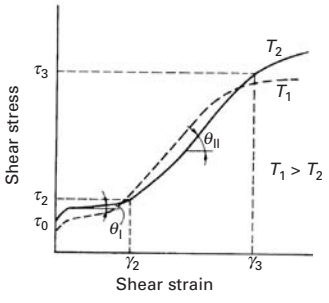

Fig. 6.13 Generic shear-stress–shear-strain curves for FCC single crystals for two different temperatures.

Stage I starts after elastic deformation at the critical stress τ_0. This stage, called "easy glide," is a linear region of low strain-hardening rate. θ_I is approximately $G/3000$. Stage I is characterized by long slip lines (100 to 1,000 μm), straight and uniformly spaced (10 to 100 nm apart). We adopt the nomenclature used by A. Seeger.[2] *Slip lines* are the "elementary structure" of slip and can be observed only via the electron microscope. With the optical microscope, one observes *slip bands*; they occur at the higher strains and are made up of clusters of slip lines. On the other hand, *slip markings* are observed as steps at the surface of the specimen. Stage I does not exist in polycrystals or in monocrystals oriented for polyslip. The extent of this stage depends strongly on the crystal orientation. The strain at the end of stage I (γ_2) has a maximum value when the crystal orientation is located in the center of the standard stereographic triangle. The end of stage I is considered to be the start of secondary slip (when, in Figure 6.11, point P_1 has moved to P_2).

Stage II, or the linear hardening stage, has the following important characteristics.

1. A linear hardening regimen with a high θ_{II}.
2. $\theta_{II}/G \approx 1/300$. This parameter is relatively constant for a great majority of metals. (The maximum variation is a factor of about 2).

θ_{II} is approximately equal to $10\theta_I$ and is relatively independent of temperature, although temperature has a significant effect on the extent of stage II.

Stage III is characterized by cross-slip. Stage III is difficult to occur at a low level of stresses, and its operation is aided by high temperatures. Thus, one expects that the stress necessary at the start of stage III, τ_3, would depend on temperature, and such, indeed, is the case in practice: τ_3 increases with a decrease in temperature.

The start of Stage III is also markedly dependent on the stacking-fault energy of the metal. Metals with relatively low stacking-fault energies – for example, brasses, bronzes, and austenitic steels – have a rather wide stacking-fault ribbon and, consequently, need a higher activation energy for cross-slip to occur. (See Figure 6.14.) This is so because, for cross-slip to occur in these metals, it is necessary to form a constriction over a wide ribbon of the stacking fault, in order to have a certain length of perfect dislocation. Thus, in metals and alloys with low stacking-fault energies, cross-slip will be difficult to bring about at normal stress levels. This, in turn, makes it difficult for the screw dislocations to change their slip plane. The dislocation density is high,

[2] A. Seeger, in J. C. Fischer, W. G. Johnston, and T. Vreeland (eds.), *Dislocations and Mechanical Properties of Crystals* (New York: John Wiley, 1957), p. 243.

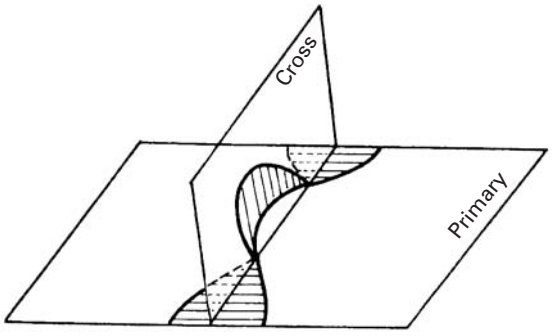

Fig. 6.14 Model of cross-slip.

and the transition from stage II to stage III is retarded. Aluminum, on the other hand, has a higher stacking-fault energy. Thus, the stress necessary for cross-slip to occur in aluminum, at a given temperature, is much lower than in, say, copper or brass.

6.2.5 Independent Slip Systems in Polycrystals

For any FCC crystal whose tensile axis is near the center of the stereographic triangle, deformation should start on the primary system. However, if the crystal is surrounded by other crystals with different crystallographic orientations – as is likely in a polycrystalline aggregate – all the crystals (grains) are not likely to start deforming in the same manner. The strain taking place in the first grain must be compatible with the neighboring grains. In other words, it is not possible to form discontinuities along the grain boundaries; deformation has to propagate from one grain to another if continuity at the boundary is to be maintained. Five independent slip systems are required to produce a general homogeneous strain in a crystal by slip.

The slip along several parallel systems produces, macroscopically, a translation of one part of the crystal with respect to the other and, consequently, a certain shear. Since the plastic flow generally occurs without any appreciable change in volume, we have $\varepsilon_{11} + \varepsilon_{22} + \varepsilon_{33} = 0$. This relationship reduces the components of strain from six (ε_{11}, ε_{22}, ε_{33}, ε_{12}, ε_{13}, ε_{23}) to five; the operation of one slip system produces only one independent component of the strain tensor. Therefore, one may conclude that five independent slip systems are required for the deformation of one grain in a polycrystalline aggregate. Consequently, polycrystals do not exhibit stage I (easy glide) of work-hardening.

6.3 Work-Hardening in Polycrystals

In the preceding sections, work-hardening in single crystals was attributed to the interaction of dislocations with other dislocations and barriers that impede the motion of dislocations through the crystal lattice. In polycrystals, too, this basic idea remains valid.

However, due to the mutual interference of neighboring grains and the problem of compatible deformations among adjacent grains, multiple slip occurs rather easily, and, consequently, there is an appreciable work-hardening right at the beginning of straining.

In a manner similar to that in single crystals, primary dislocations interact with secondary dislocations, giving rise to dislocation dipoles and loops which result in local dislocation tangles and, eventually, a three-dimensional network of subboundaries. Generally, the size of these cells decreases with increasing strain. The structural differences between one metal and another are mainly in the sharpness of these cell boundaries. In BCC metals and in FCC metals with high stacking-fault energy, such as Al, the dislocation tangles rearrange into a well-defined cell structure, while in metals or alloys with low stacking-fault energy (e.g., brasses, bronzes, austenitic steels, etc.), where the cross-slip is rather difficult and the dislocations are extended, the sharp subboundaries do not form even at very large strains.

The plastic deformation and the consequent work-hardening results in an increase in the dislocation density. An annealed metal, for example, will have about 10^6 to 10^8 dislocations per cm^2, while a plastically cold-worked metal may contain up to 10^{12} dislocations per cm^2. The relationship between the flow stress and the dislocation density is the same as that observed for single crystals – that is,

$$\tau = \tau_0 + \alpha G b \sqrt{\rho}, \tag{6.5}$$

where α is a constant with a value between 0.3 and 0.6. This relationship has been observed to be valid for a majority of the cases. τ_0 is the stress necessary to move a dislocation in the absence of other dislocations. Figure 6.15 shows that Equation 6.5 is obeyed for copper monocrystals (with one, two, and six slip systems operating), as well as polycrystals. The relationship is very important and serves as a basis for work-hardening theories. In ceramics, only limited observations of such kind have been made. Nevertheless, they show the same trend. Measurements of dislocation densities in sapphire (single-crystal α-alumina) subjected to plastic deformation at high temperatures (1,400–1,720 °C), above the ductile-to-brittle transition, are shown in Figure 6.16. These dislocation densities were measured at strains $\gamma < 0.23$, and it was observed that the dislocation density showed a stress dependence analogous to Equation 6.5, with $\tau_0 = 0$. The proportionality coefficient was dependent on temperature and varied in the range 0.2–0.5, which is very similar to the corresponding range for metals.

Many theories have been advanced to explain the phenomenon of work-hardening. The most important and difficult part in the attempt to predict work-hardening behavior is to determine how the density and distribution of dislocations vary with the plastic strain. The problem is that stress is a state function in the thermodynamic sense

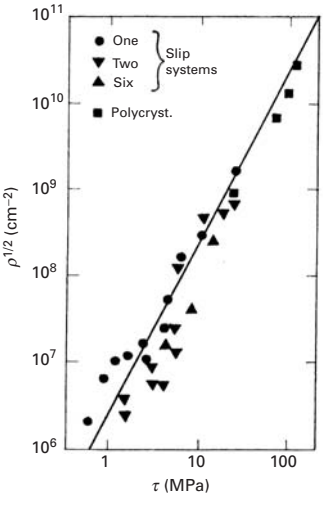

Fig. 6.15 Average dislocation density ρ as a function of the resolved shear stress τ for copper. (Adapted with permission from H. Wiedersich, *J. Metals*, 16 (1964) p. 425, 427.)

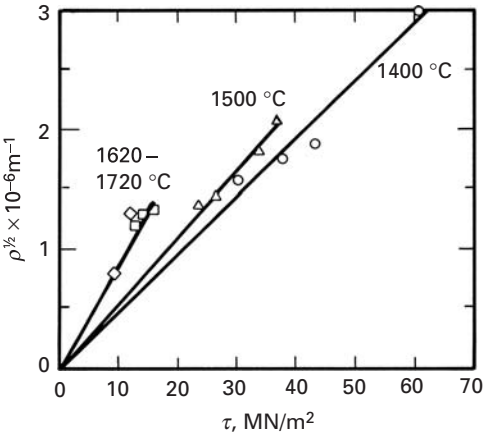

Fig. 6.16 Relationship between flow shear stress and dislocation density for monocrystalline sapphire (Al_2O_3) deformed at different temperatures. (Adapted from B. J. Pletka, A. H. Heuer, and T. E. Mitchell, *Acta Met.*, 25 (1977) 25.)

(i.e., it depends only on its position or value, not on how that particular value of stress was attained.) Plastic strain, on the other hand, is a path function of its position (i.e., it depends on the actual path traversed in reaching a certain strain value.) In other words, plastic strain is dependent on its history. Thus, the presence or absence of dislocations and their distributions can tell us nothing about how a certain amount of strain was accumulated in the crystal, because we do not know the path that dislocations traversed to accumulate that strain. Hence, one constructs models that recreate the processes by means of which the various dislocation configurations emerge; one then tries to correlate the models with the configurations observed experimentally. Both the density and the distribution of dislocations are very sensitive functions of the crystal structure, stacking-fault energy, temperature, and rate of deformation. In view of all this, it is not surprising that a unique theory of work-hardening which would explain all of its aspects does not exist.

In what follows, we briefly review three of the best-known theories of workhardening – those of Taylor, Seeger, and Kuhlmann–Wilsdorf.

6.3.1 Taylor's Theory

Taylor's theory[3] is one of the oldest theories of work-hardening. At the time the theory was postulated (1934), the stress–strain curve for metallic crystals such as aluminum was considered to be parabolic. (The single-crystal stress–strain curve consisting of three stages was unknown; see Figure 6.13.) This being so, Taylor proposed a model that would predict the parabolic curve. The principal idea, which, incidentally, is still used in one form or another by modern theories, was that the dislocations, on moving, elastically interact with other dislocations in the crystal and become trapped. These trapped dislocations give rise to internal stresses that increase the stress necessary for deformation (i.e., the flow stress).

[3] G. I. Taylor, *Proc. Roy. Soc. (London)*, A145 (1934) 362.

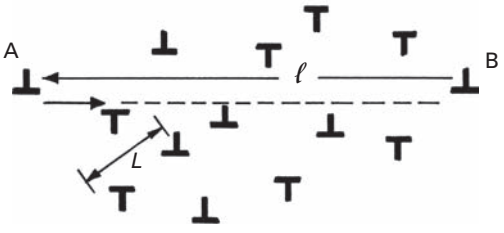

Fig. 6.17 Taylor model of interaction among dislocations in a crystal.

Let ℓ be the average distance that a dislocation moves before it is stopped. The initial and final positions A and B are marked in Figure 6.17. Let ρ be the dislocation density after a certain strain. Then the shear strain is given by (see Equation 4.29)

$$\gamma = k\rho b\ell, \tag{6.6}$$

where k is an orientation-dependent factor and b is the Burgers vector.

Taylor considered only edge dislocations and assumed that the dislocation distribution was uniform; thus, the separation between dislocations, L, will be equal to $\rho^{-1/2}$. (See Figure 6.17.) The effective internal stress τ, caused by these interactions among dislocations, is the stress necessary to force two dislocations past each other. The interactions among dislocations are complex, involving attraction, repulsion, reactions, etc. Taylor considered only a very simple case: As the dislocation moves from A to B, it will approach the other dislocations, with the minimum distance being $L/2$. Taking into account just the repulsion from the dislocations, we can assume that, for an edge dislocation, the shear stress fields given in Chapter 4 are (Equation 4.12)

$$\sigma_{12} = \frac{Gb}{2\pi(1-\nu)} \frac{x_1(x_1^2 - x_2^2)}{(x_1^2 + x_2^2)}.$$

Supposing that $x_2 = L/2$ and $x_1 = 0$, we arrive at

$$\sigma_{12} = \frac{Gb}{\pi(1-\nu)L} = \frac{K\,Gb}{L},$$

where K is a constant. In order for the moving dislocation to overcome this stress field, a shear stress

$$\tau = \frac{K\,Gb}{L}$$

has to be applied. Or, recalling that $L = \rho^{-1/2}$, we obtain

$$\tau = K\,Gb\sqrt{\rho}. \tag{6.7}$$

From Equations 6.6 and 6.7, we get

$$\tau = K\,Gb\sqrt{\frac{\gamma}{kb\ell}} = k'G\sqrt{\frac{\gamma}{\ell}}. \tag{6.8}$$

We could add a frictional term τ_0 that is required to move the dislocation in the absence of other dislocations, and arrive at:

$$\tau = \tau_0 + k''\gamma^{1/2}$$

Equation 6.8 is a parabolic relation between the stress τ and the strain γ. It describes, approximately, the behavior of many materials at large deformations. Among the criticisms of the Taylor theory, one may include the following.

1. Such regular configurations of dislocations are rarely observed in cold-worked crystals.
2. Screw dislocations are not involved, and thus, the cross-slip is excluded; edge dislocations cannot cross-slip.
3. Two dislocations on neighboring planes may be trapped in each other's stress fields and may thus become incapable of moving independently of each other. But the pair of dislocations may be pushed by a third dislocation.
4. We know now that stress–strain curves for hexagonal crystals, as well as those for stage II of cubic crystals, are linear. Taylor's theory does not explain this linear hardening.
5. Taylor's parabolic relation derives from the supposition that there is a uniform distribution of deformed regions inside the crystal. In reality, the distribution is not uniform, and experimentally, we observe slip bands, cells, and other nonuniform arrangements.

6.3.2 Seeger's Theory

Seeger's theory, (see the suggested reading for details) addresses the three stages of work-hardening of a monocrystal (easy glide, linear hardening, and parabolic hardening) and proposes specific mechanisms for each stage. The values of the slopes for the three stages are obtained from dislocation considerations. In stage I, long-range interactions between well-spaced dislocations are considered. The dislocation loops are blocked by unspecified obstacles, all on the primary system. Slip activity on secondary slip systems begins in stage II of hardening. The secondary activity furnishes barriers such as Lomer–Cottrell barriers. The dislocations pile up against such barriers in Stage II and give rise to long-range internal stresses that control the flow stress. Without going into complex details, we can say that the long-range theory of Seeger *et al*. does predict that $\theta_{II}/G \approx 1/300$ for FCC metals.

6.3.3 Kuhlmann–Wilsdorf's Theory

The substructures developed during metal deformation processes resemble the idealized models only in the initial stages. As the imposed deformation increases, dislocation cells start to form in alloys with medium and high stacking-fault energies. With increasing deformation, the cell diameters decrease, and the cells become elongated in the general direction of the deformation. The cell walls

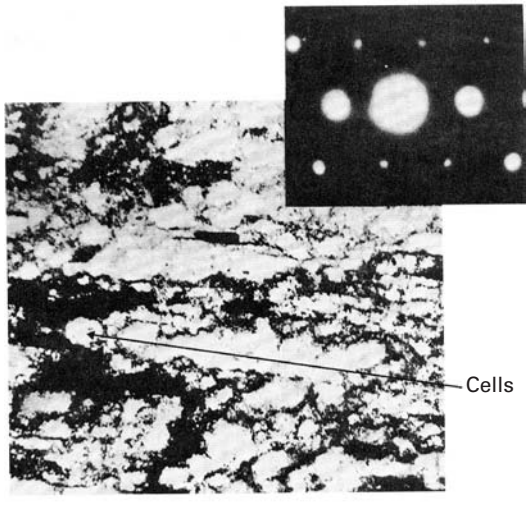

(a)

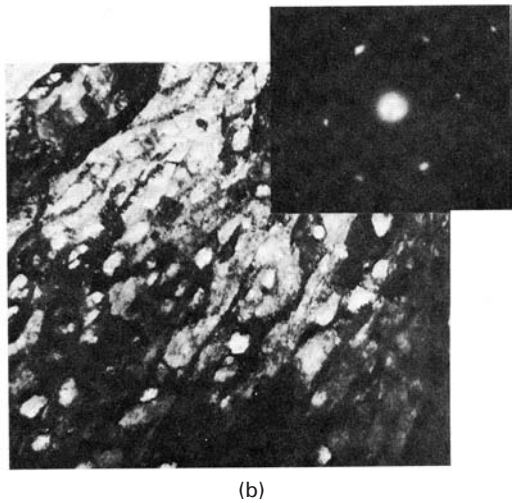

(b)

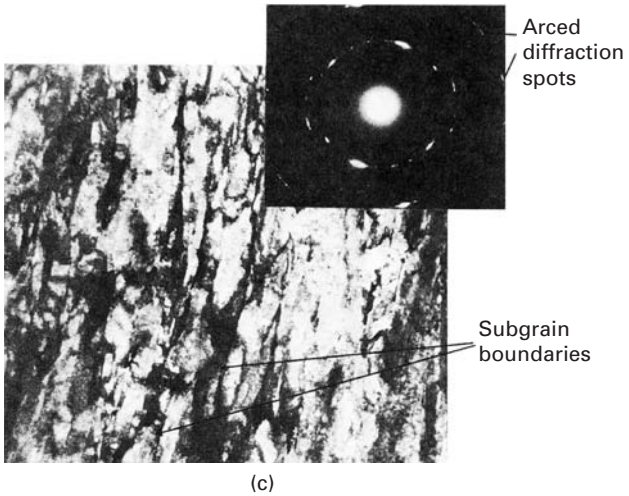

(c)

Fig. 6.18 Development of substructure of Nickel-200 as a function of plastic deformation by cold rolling. (a) 20% reduction. (b) 40% reduction. (c) 80% reduction.

tend to become progressively sharper as the misorientation between two adjacent cells increases. A cell wall is essentially a low-angle grain boundary, but when the misorientation between adjacent cell walls reaches a certain critical value, we can no longer refer to the boundary in these terms. The boundary between two cells becomes freer of dislocations, and subgrains are formed in a process called *polygonization*. This transition from cells to subgrains occurs at different effective strains for different materials: 0.80 for 99.97% pure Al and 1 to 1.20 for copper. A detailed treatment of the work-hardening and formation of texture at large imposed plastic strains is given by Gil Sevillano *et al*.[4] For metals with low stacking-fault energies, the development of a fine lamellar substructure consisting of microtwins, twin bundles, shear bands, and stacking faults is the characteristic feature of high-strain deformation.

Figure 6.18 shows the changes in substructure observed in nickel rolled at room temperature. At reductions up to 40%, we clearly have a cellular structure. We can see that at 40% (Figure 6.18(b)) we already have a large dislocation density. At 80% reduction, we can clearly see that many of the cell walls have disappeared and are replaced by well-defined boundaries. The observation is made more difficult because of the large density of dislocations. The electron diffraction patterns (right-hand corner of photomicrographs) show the effect very well. Up to 40% reductions, the diffraction spots are fairly clear, with little asterism (elliptical distortion). At 80% (Figure 6.18(c)), the asterism is very pronounced, and elongated spots break down into smaller spots, indicating that a distorted grain has broken down into subgrains, which have relatively little distortion. Based on observations of dislocation cells in plastically deformed metals with medium and high stacking-fault energies, Kuhlmann-Wilsdorf[5] proposed the so-called mesh-length theory, which is based on the stress necessary for dislocation bowing. In stage I, the dislocations multiply into certain restricted regions and penetrate into regions as yet substantially free of mobile dislocations, until a quasiuniform distribution of dislocations is obtained. The only resistance to deformation is the dislocation line tension. Thus, hardening occurs because free segments of dislocations become ever smaller. Stage II starts when there are no more "virgin" areas left for penetration by new dislocations. The stress required to bow segments of dislocation is responsible for a great part of stage II hardening: Dislocation segments can bow out inside the cells. Figure 6.19 shows, in a schematic manner, dislocation cells of size L in which the cell walls occupy a fraction f of the total crystal. Dislocation sources with mean width ℓ are activated and form loops, as shown in the figure. As these loops are formed, the dislocation density increases and the cell size decreases. Kuhlmann-Wilsdorf was able to explain, in quantitative manner, the three stages of work-hardening.

[4] J. Gil Sevillano, P. van Houtte, and E. Aernoudt, *Prog. Mater. Sci*., 25 (1981) 69.
[5] D. Kuhlmann–Wilsdorf, *Met. Trans*. 11A (1985) 2091.

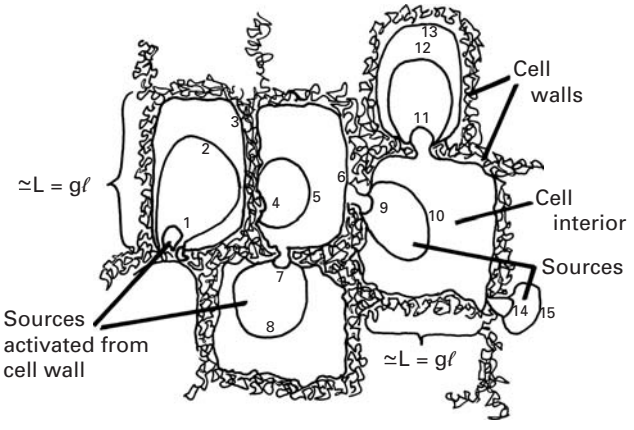

Fig. 6.19 Schematic representation of dislocation cells of size L, with activation of dislocation sources from the cell walls and bowing out of loops into the cell interior. (Courtesy of D. Kuhlmann-Wilsdorf.)

Example 6.3

Consider dislocations blocked in a copper crystal. If the flow stress is controlled by the stress necessary to operate a Frank–Read source, compute the dislocation density ρ in this crystal when it is deformed to a point where the resolved shear stress in the slip plane is 42 MPa. Take $G = 50$ GPa.

Solution: The dislocation line length is related to the dislocation density by

$$\ell = \rho^{-1/2}.$$

The flow stress is the shear stress necessary to operate a Frank–Read source. Hence (from Equation 4.22d),

$$\tau = G\,b/\ell = G\,b\sqrt{\rho}.$$

For copper, $b = 3.6 \times 10^{-10}(\sqrt{2}/2)$ m $= 2.55 \times 10^{-10}$ m, where 3.6×10^{-10} m is the Cu lattice parameter. Rearranging the preceding expression, we obtain the dislocation density

$$\rho = \tau^2/G^2b^2 = (42 \times 10^6)^2/(50 \times 10^9)^2 \times (2.55 \times 10^{-1})^2,$$

or

$$\rho = 1.09 \times 10^{13}\ \text{m}^{-2}.$$

Example 6.4

For the single crystal of an FCC metal, the work-hardening rate in shear is $d\tau/d\gamma = 0.3$ GPa. Compute the work-hardening rate in tension, $d\sigma/d\varepsilon$, for a polycrystal of this metal. Take the Schmid factor M_p to be 1/3.1.

Solution: The tensile stress is related to the shear stress by the Schmid factor

$$\sigma = M_p^{-1}\tau.$$

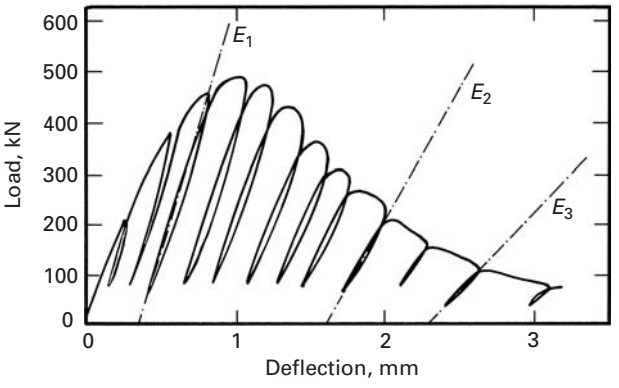

Fig. 6.20 Typical load deformation curve for concrete under uniaxial compression; the specimen was unloaded and reloaded at different stages of deformation. (From G. A. Hegemier and H. E. Reed, *Mech. Mater.*, 4 (1985) 215; data originally from A. Anvar.)

Thus,

$$d\sigma = M_p^{-1} d\tau. \tag{1}$$

Also, the tensile strain ε is related to the shear strain γ by

$$\varepsilon = M_p y.$$

Thus,

$$d\varepsilon = M_p^{-1} d\tau. \tag{2}$$

Dividing Equation 1 by Equation 2, we have

$$d\sigma/d\varepsilon = M_p^{-2}(d\tau/d\gamma) = (d\tau/d\gamma)(3.1)^2,$$

or

$$d\sigma/d\varepsilon = 9.61(d\tau/d\gamma) = 9.61 \times 0.3 = 2.88\,\text{GPa}.$$

6.4 Softening Mechanisms

Under special circumstances, materials can undergo softening during plastic deformation. This degradation of a material's strength can be caused by a number of mechanisms. *Damage accumulation* is the most common mechanism in ceramics and composites. Damage can be of many types: microcracks forming in the material, a breakup of the matrix/reinforcement interface, cracking of second phase, etc. Figure 6.20 shows softening observed in concrete. The compression was halted at several points, and the specimen was unloaded and subsequently reloaded. The damage consists of microcracks, which results in the reduction in the Young's modulus of concrete as the compression evolves ($E_1 > E_2 > E_3$). In Chapter 2, we saw how microcracks affect the Young's modulus of brittle materials. A discussion of damage accumulation in composites is given in Chapter 15.

Softening of radiation-hardened materials occurs when the sweeping of radiation induced defects (point defects) by dislocations leads to the formation of "soft" channels.

In *geometric softening*, during plastic deformation, individual grains rotate toward crystallographic orientations for which the Schmid factor is increased. This rotation can lead to global softening of the material in spite of the hardening along the individual slip systems.

We describe the last of the major softening mechanisms, *thermal softening*, in detail. The plastic deformation of a metal is an irreversible process, and most of the work of deformation is converted into heat. At most, only 10% of plastic deformation is stored as defects (primarily dislocations) as shown in the example below.

Example 6.5

Calculate the stored energy in a copper crystal with a dislocation density of $\sim 10^{11}$ cm^{-2}, typical of a highly deformed metal.

Solution: We first find the total energy in the crystal which is equal to

$$U = \rho \frac{G b^2}{2}.$$

For copper, $G = 48.3$ GPa and $b = 0.25$ nm. Thus, the total deformation energy is ($\rho = 10^{11}$ cm$^{-2} = 10^{15}$ m^{-2}):

$$\begin{aligned} U &= \frac{1}{2} \times 10^{15} \times 48.3 \times 10^{9} \times 0.0625 \times 10^{-18} \\ &= 1.5 \times 10^{6}\ \text{J/m}^3. \end{aligned}$$

Assuming that this sample of copper exhibits work-hardening and that the constitutive equation is (see Equation 3.11)

$$\sigma = \sigma_0 + K \varepsilon^n,$$

where

$$\begin{aligned} \sigma_0 &= 50\ \text{MPa}, \\ n &= 0.5, \\ K &= 500\ \text{MPa}. \end{aligned}$$

We can calculate the total deformation energy per unit volume at a strain of 0.5:

$$\begin{aligned} U &= \int_0^{\varepsilon} \sigma\, d\varepsilon = \int_0^{\varepsilon_1} (\sigma_0 + K \varepsilon^n) d\varepsilon \\ &= \sigma_0 \varepsilon_1 + K \frac{\varepsilon_1^{n+1}}{n+1} = 50 \times 10^6 \times 0.5 + 500 \times 10^6 \times \frac{0.35}{1.5} \\ &= (25 + 116) \times 10^6 \\ &= 1.41 \times 10^8\ \text{J/m}^3. \end{aligned}$$

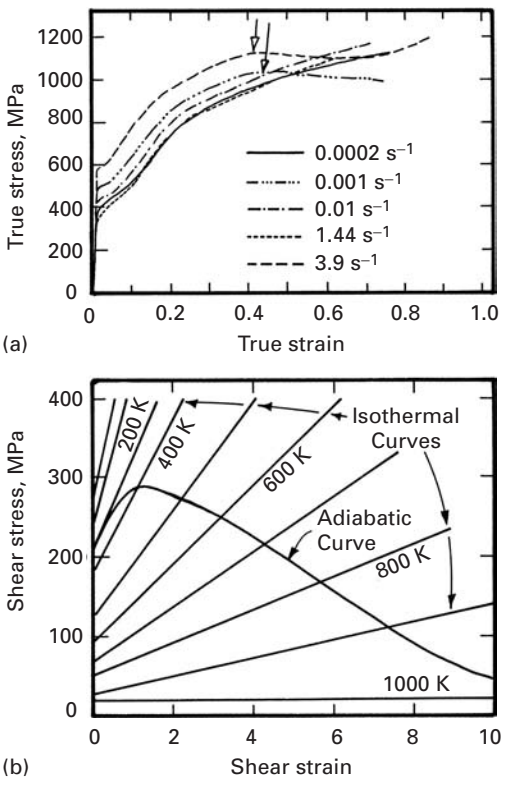

Fig. 6.21 (a) Compressive true-stress–true-strain curves for titanium at different strain rates; notice the onset of softening at the arrows. (Adapted from M. A. Meyers, G. Subhash, B. K. Kad, and L. Prasad, *Mech. Mater.*, 17 (1994) 175.) (b) Schematic linear shear-stress–shear-strain curves for titanium at different temperatures, with superimposed adiabatic curve constructed from isothermal curves by incrementally converting deformation work into heat (and a consequent rise in temperature.) (Adapted from M. A. Meyers and H.-R. Pak, *Acta Met.*, 34 (1986) 2493.)

Thus, the dislocation energy represents 1.4% of the total work of deformation. The work of deformation leads to a rise in the temperature of the specimen.

If there is insufficient time for the heat to escape from the specimen during deformation, the material cannot be considered isothermal any longer, and the loss of strength caused by the increase in temperature will, at a certain point, exceed the increase in strength due to work-hardening. At this point, the stress–strain curve starts to go down, and thermal softening sets in. This is shown in Figure 6.21(a). At lower strain rates (2×10^{-4} s^{-1}, 10^{-3} s^{-1}, and 10^{-2} s^{-1}), the curves show the normal work-hardening behavior up to high strains. However, for the strain rates of 1.44 s^{-1} and 3.9 s^{-1}, the stress–strain curves show maxima beyond which softening sets in. It is easy to understand and to predict this softening. Figure 6.21(b) shows shear-stress–shear-strain curves for titanium at different temperatures. For simplicity, linear work-hardening was assumed. These curves are all isothermal. We now compute the temperature elevation produced by plastic deformation, by applying the following equation:

$$dT = \frac{\beta}{\sigma C_p} \sigma d\varepsilon,$$

where β is the conversion factor for mechanical energy into heat, C_p is the heat capacity and ρ the density of the material. By taking small increments of strain, we obtain

$$\Delta T = \frac{\beta}{\rho C_p}\sigma \Delta\varepsilon.$$

In Figure 6.21(b), an adiabatic curve was built in such a fashion. The work-to-heat conversion factor β is usually taken to be in the range 0.9–1.0. (Most of the work is converted to heat.) The adiabatic curve shows a maximum at γ approximately equal to 1; this marks the shear strain at which softening starts.

The softening of the material will lead to the phenomenon of adiabatic shear localization. Adiabatic shear bands are narrow regions where softening occurs and where concentrated plastic deformation takes place. Steels, titanium alloys, and aluminum alloys are quite prone to shear-band formation, which occurs in machining and which is responsible for the breakup of the machining chips. Shear-band formation also occurs in high-strain-rate operations, such as forging and shearing, as well as in ballistic impact.

Shear bands formed during forging operations are highly undesirable, because they can lead to subsequent fracture of the specimen. The microstructure within shear bands is quite different from that of the surrounding material. The shear bands often undergo dynamic recrystallization, due to the high local temperature.

In the ballistic impact of projectiles against armor, shear bands play a major role both in the defeat of the armor and in the breakup of the projectiles. Since recrystallization occurs very rapidly, the resultant grain size is very small, typically 0.1 μm. Figure 6.22(a) shows a shear band in titanium with a width of approximately 10 μm. The fine microcrystalline structure inside of the shear band is seen in the photomicrograph of Figure 6.22(b); the initial grain size of the material was 50 μm.

6.5 Texture Strengthening

A single crystal rotates when it deforms plastically in a particular slip system. (See Section 6.2.4.) When a polycrystal is deformed in rolling, forging, drawing, and so on, the randomly oriented grains will slip on their appropriate glide systems and rotate from their initial conditions, but this time under a constraint from the neighboring grains. Consequently, a strong preferred orientation or texture develops after large strains; that is, certain slip planes tend to align parallel to the rolling plane, while certain slip directions tend to align in the direction of rolling or wire drawing. In metals, annealing can also result in a texture generally different from that obtained by mechanical working, but still dependent on the history of the mechanical working. As an illustration, Figure 6.23 shows the microstructures along three perpendicular planes for nickel cold-rolled to a reduction in

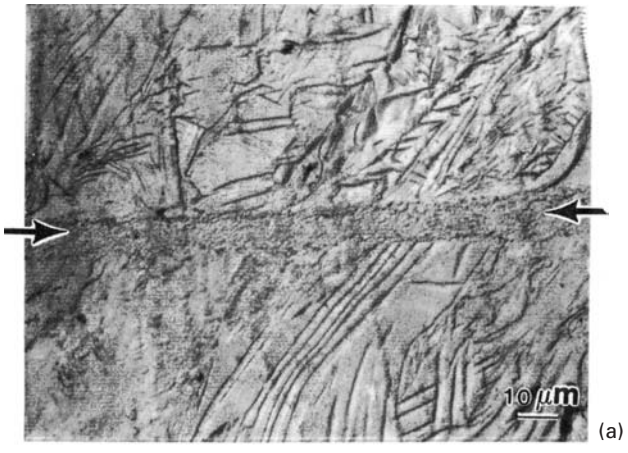

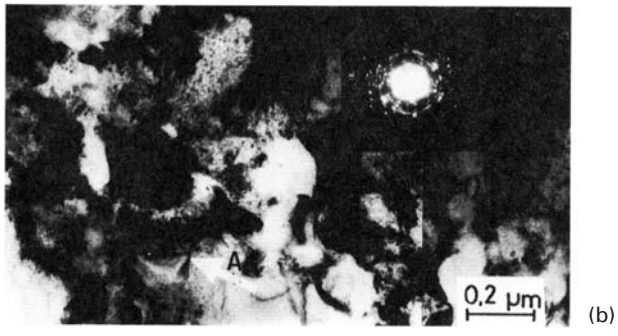

Fig. 6.22 Shear bands in titanium. (a) Optical micrograph, showing band. (b) Transmission electron micrograph, showing microcrystalline structure, with grain size approximately equal to 0.2 μm. The original grain size of the specimen was 50 μm.

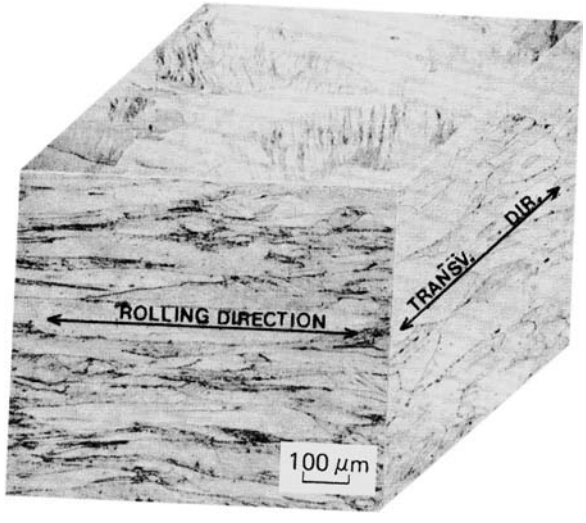

Fig. 6.23 Perspective view of microstructure of Nickel-200 cold-rolled to a reduction in thickness of 60%.

thickness of 60%. The highly elongated grains along the rolling direction are readily seen.

A strongly textured material can exhibit highly anisotropic properties. This is not intrinsically bad; in fact, controlled anisotropy in sheet metals can be exploited to obtain an improved final product. The

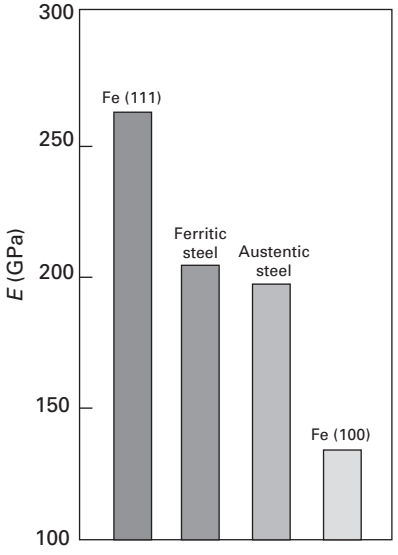

Fig. 6.24 Theoretical bounds on the Young's modulus E of steel.

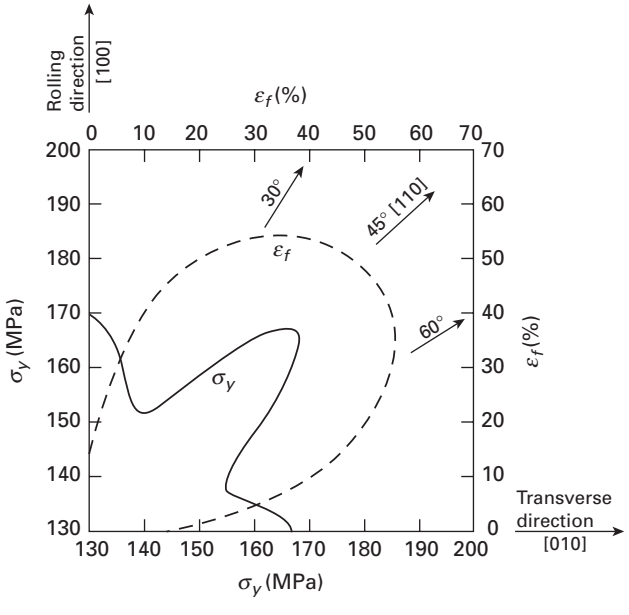

Fig. 6.25 Orientation dependence of yield strength σ_y and strain to fracture, ε_f, of a rolled copper sheet.

Young's modulus E of steel can, theoretically, have a value between the extreme values of the iron monocrystal (i.e., between Fe[111] and Fe[100]), as shown in Figure 6.24. The Young's modulus cannot be changed much by alloying, but texture can – again, theoretically – have some influence. We caution the reader that the effect on E, for all practical purposes, is rather small. This is not the case, however, for many other properties. For example, Figure 6.25 shows the rather marked orientation dependence of the yield strength σ_y and the strain to fracture, ε_f, of a rolled copper sheet. Clearly, cups made out of this material by deep drawing would show "earing" at 90° intervals due to this texture (see Figure 3.45 for illustration of

Table 6.1 Some Common Wire and Sheet Textures

	Wire (Fiber Texture)	Sheet (Rolling Texture)
FCC	[111] + [100]	(110) [1$\bar{1}$2] + (112) [11$\bar{1}$]
BCC	110	(100) [011]
HCP	[10$\bar{1}$0]	(0001) [11$\bar{2}$0]

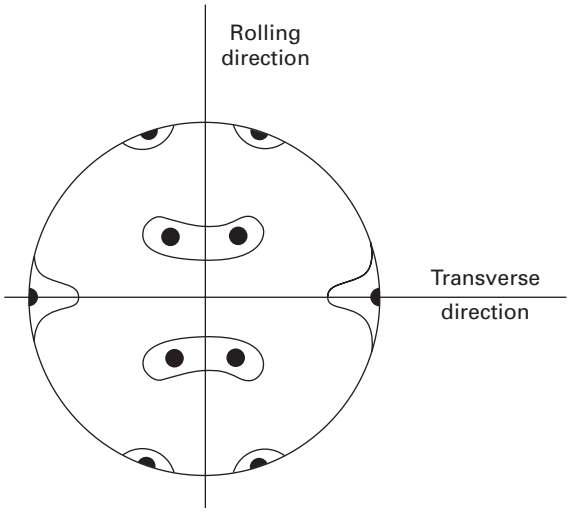

Fig. 6.26 [111] pole figure of a rolled-brass sheet.

"earing"). Use is made of such texture development in Fe–3% Si. Sheets of this material are used to make transformer cores, wherein thermomechanical treatments are given to develop a desirable magnetic anisotropy that improves electrical performance.

Crystallographic texture is commonly represented in the form of normal-pole or inverse-pole figures. A normal-pole figure is a stereographic projection showing the intensity of normals to a specific plane in all directions, while an inverse-pole figure is a sterographic projection showing the intensities of all planes in a specific direction. The experimental procedure involves measuring relative intensities of X-ray reflections from the polycrystalline material at different angular settings. Details of the experimental determination of pole figures can be found in standard texts on the subject.

Figure 6.26 shows the [111] pole figure of a heavily deformed α-brass (70% Cu−30% Zn) sheet. This texture, called brass-type texture, is a (110) [1$\bar{1}$2] texture, i.e., with (110) planes parallel to the rolling plane and [1$\bar{1}$2] directions parallel to the rolling direction. The double texture indicated for FCC structures in Table 6.1 is not obtained in α-brass, but single (110) [1$\bar{1}$2] texture develops, owing to the material's low stacking-fault energy or (probably) to mechanical twinning.

Suggested Reading

Geometry of Deformation

J. GilSevillano, P. van Houtte, and E. Aernoudt, "Large Strain Work Hardening and Textures", in *Progress in Materials Science*, vol. 25, J. W. Christian, P. Haasen, and T. B. Massalski, eds., Elmsford, NY: Pergamon Press, 1981, p. 69.

R. W. K. Honeycombe and H. K. D. H. Bhadeshia. *The Plastic Deformation of Metals*. New York, NY: St. Martin's Press, 1995.

W. F. Hosford, *The Mechanics of Crystals and Textured Polycrystals*. New York, NY: Oxford University Press, 1993.

Work-Hardening

L. M. Clarebrough and M. E. Hargreaves. "Work Hardening of Metals," in *Progress in Metal Physics*, Vol. 8, B. Chalmers and W. Hume-Rothery, eds. New York, NY: Pergamon Press, 1959, p. 1.

A. H. Cottrell. *Dislocations and Plastic Flow in Crystals*. Oxford: Clarendon Press, 1953.

P. B. Hirsch, ed. *The Physics of Metals, Vol. 2: Defects*. Cambridge, U.K.: Cambridge University Press, 1975.

J. P. Hirth and J. Lothe. *Theory of Dislocations*, 2nd. ed. New York, NY: J. Wiley, 1982.

D. Kuhlmann–Wilsdorf, *Met. Trans.* 11A (1985) 2091.

A. Seeger, in *Work Hardening*, TMS-AIME Conf., Vol. 46, 1966, p. 27.

A. W. Thompson, ed. *Work Hardening in Tension and Fatigue*. New York, NY: TMS-AIME, 1977.

Exercises

6.1 Discuss the merits and demerits of the use of transmission electron microscopy techniques to study the dislocation behavior in crystalline materials.

6.2 Explain why a metal like lead does not work-harden when deformed at room temperature, whereas a metal such as iron does.

6.3 What is the effect of cold work and annealing on the Young's modulus of a metal?

6.4 If we strain an FCC and an HCP single crystal, which of the two will have a larger amount of easy glide, and why?

6.5 In a cold-worked metal, a dislocation density of 1×10^{16} m^{-2} was measured after a shear strain of 10%. Assuming that the dislocations are uniformly distributed, estimate the flow stress of this metal. Take $G = 25$ GPa.

6.6 Consider dislocations blocked with an average spacing of ℓ in a copper crystal. If the flow stress is controlled by the stress necessary to operate a Frank–Read source, compute the dislocation density ρ in this crystal when it is deformed to a point where the resolved shear stress in the slip plane is 42 MPa. Take $G = 50$ GPa.

6.7 Make a schematic plot showing the variation in the following parameters with percent cold work:

(**a**) ultimate tensile strength,
(**b**) yield strength in tension,
(**c**) strain to failure,
(**d**) reduction in area.

6.8 The stress axis in an FCC crystal makes angles of 31° and 62° with the normal to the slip plane and with the slip direction, respectively. The applied stress is 10 MN/m^2.

(**a**) Determine the resolved stress in the shear plane.
(**b**) Is the resolved stress larger when the angles are 45° and 32°, respectively?
(**c**) Using a stereographic projection, determine the resolved stresses on the other slip systems.

6.9 Magnesium oxide is cubic (having the same structure as NaCl). The slip planes and directions are [110] and <110>, respectively. Along which directions, if any, can a tensile (or compressive) stress be applied without producing slip?

6.10 A Cu monocrystal (FCC) of 10 cm length is pulled in tension. The stress axis is [$\bar{1}$23].

(**a**) Which is the stress system with the highest resolved shear stress?
(**b**) If the extension of the crystal continues until a second slip system becomes operational, what will this system be?
(**c**) What rotation will be required to activate the second system?
(**d**) How much longitudinal strain is required to activate the second system?

6.11 Flow stress varies with strain rate; one equation that has been used to express this dependence is

$$\sigma = c\dot{\varepsilon}^{m'} f(\varepsilon, T),$$

where m' is the strain-rate sensitivity, which is generally less than 0.1. Some metals, called superplastic, can undergo elongations of up to 1,000% in uniaxial tension. Assuming that these tests are performed at a uniform velocity of the crosshead, will the metals have a very high or a very low value of m'? Explain, in terms of the formation and inhibition of the neck.

6.12 Johnston and Gilman[6] experimentally determined the relationship between dislocation velocity and applied stress

$$v = A\sigma^m,$$

where A is the constant of proportionality. Assuming that the mobile dislocation density does not depend on the velocity of the dislocations, obtain a relationship between m and m' (from Exercise 6.11).

6.13 The following results were obtained in an ambient-temperature tensile test, for an aluminum monocrystal having a cross-sectional area of 9 mm^2 and a stress axis making angles of 27° with [100], 24.5° with [110], and 29.5° with [111]:

[6] W. G. Johnston and J. J. Gilman, *J. Appl. Phys.*, 30 (1959) 129.

Load (N)	Length (cm)
0	10.000
12.40	10.005
14.30	10.040
16.34	10.100
18.15	10.150
21.10	10.180
23.60	10.200
26.65	10.220

(a) Plot the results in terms of true stress versus true strain.
(b) Determine the resolved shear stress on the system that will slip first.
(c) Determine the longitudinal strain at the end of the easy-glide stage (when a second slip system becomes operative).

6.14 Take a stereographic triangle for a cubic metal. If the FCC slip systems are operative, indicate the number of slip systems having the same Schmid factor if the stress axis is:

(a) [111],
(b) [110],
(c) [100],
(d) [123].

Use the stereographic projections to show your results.

6.15 A copper bicrystal is composed of two monocrystals separated by a coherent twin boundary (111). The bicrystal is being compressed in a homogeneous upset test in such a way that the twin boundary is perpendicular to machine plates. The compression direction is the same for both crystals, namely, [134].

(a) Is this crystal isoaxial?
(b) Is deformation in the two crystals compatible or incompatible?

6.16 The flow stress σ is related to the dislocation density ρ by the relationship

$$\sigma_1 = \sigma_i + \alpha G b \sqrt{\rho},$$

where the symbols have their usual significance. If the dislocation density is inversely related to the grain size d, show that a Hall–Petch type of dependence of flow stress on grain size is obtained.

6.17 For an FCC polycrystalline metal, TEM analysis showed that the dislocation density after cold working was 5×10^{10} m^{-2}. If the friction stress is 100 MPa, $G = 40$ GPa, and $b = 0.3$ nm, compute the flow stress of this metal.

6.18 The stress–strain curve of a polycrystalline aluminum sample can be represented by

$$\sigma = 25 + 200\varepsilon^{0.5}.$$

Calculate the energy of deformation per unit volume corresponding to uniform strain (i.e., just prior to the onset of necking) in this material.

6.19 An FCC crystal is pulled in tension along the [100] direction.

(**a**) Determine the Schmid factor for all slip systems.
(**b**) Identify the slip system(s) that will be activated first.
(**c**) What is the tensile stress at which this crystal will flow plastically? (τ = 50 MPa.)

6.20 Calculate the total energy due to dislocations for copper that underwent 20% plastic deformation, resulting in a dislocation density of 10^{14} m^{-2}. Assume that $b = 0.3$ nm.

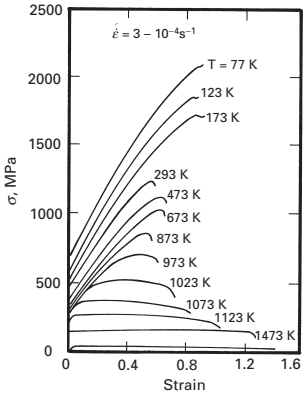

Fig. Ex6.21 (After D Viereck, G. Merckling, K. H. Lang, D. Eifler, and D. Löhe, in *Festigkeit und Verformung bei Höher Temperatur*, K. Schneider, ed. (Oberursel: Informationsgesellshaft, pp. 102–208.)

6.21 Using data from Figure Ex6.21 for (Ni–22%Cr–12%Co–9%Mo), obtain appropriate parameters for the Johnson–Cook equation (see Chapter 3). Assume $\dot{\varepsilon}_0 = 3 \times 10^{-4}$ s^{-1} and T_m = 1,600 K.

(**a**) Using the Johnson–Cook equation, plot stress–strain curves for temperatures of 77, 173, 473, and 1,473 K.
(**b**) If $C = 0.02$, plot the stress strain curves for a strain rate of 3×10^4 s^{-1}.

6.22 A monocrystal (diameter 4 mm, length 100 mm) is being pulled in tension.

(**a**) What is the elongation undergone by the specimen if 1,000 dislocations on slip planes making 45° with the tension axis cross the specimen completely? Take $b = 0.25$ nm.
(**b**) What would the elongation be if all dislocations existing in the crystal (10^6 cm^{-2}) were ejected by the applied stress? Assume a homogeneous distribution of dislocations. Assume that the crystal is FCC and all the dislocations are in the same slip system.

6.23 A long crystal with a square cross section (1 × 1 cm) is bent to form a semicircle with radius $R = 25$ cm.

(**a**) Determine the total number of dislocations generated if all bending is accommodated by edge dislocations.
(**b**) Determine the dislocation density ($b = 0.3$ nm).

6.24 The response of copper to plastic deformation can be described by Hollomon's equation $\sigma = K\varepsilon^{0.7}$.

It is known that for $\varepsilon = 0.25$, $\sigma = 120$ MPa. The dislocation density varies with flow stress according to the well-known relationship

$$\sigma = K'\rho^{1/2}.$$

(**a**) If the dislocation density at a plastic strain of 0.4 is equal to 10^{11} cm^{-2}, plot the dislocation density versus strain.
(**b**) Calculate the work performed to deform the specimen.
(**c**) Calculate the total energy stored in the metal as dislocations after a plastic deformation of 0.4, and compare this value with the one obtained in part
(**d**) Explain the difference.

6.25 A single crystal of silver is pulled in tension along the [100] direction. Determine the Schmid factor for all slip systems. What is the tensile stress at which this crystal will flow plastically? (τ = 100 MPa.)

6.26 Determine the area of the slip plane in Ni deformed parallel to [100] and under a load $P = 150 \times 10^3$ N. The shear stress is 600 MPa.

6.27 Compute the dislocation density in tungsten if the flow stress is controlled by the stress necessary to operate a Frank–Read source. The shear stress in the slip plane is 50 MPa. Take $G = 166$ GPa.

6.28 List all the slip systems in single crystal copper. Calculate the Schmid factors for them with loading axis as [221]. Which system will be activated first when we apply the load?

6.29 Obtain the parameters for the relationship between the flow stress and the dislocation density for copper with one, two, and six slip systems from the data in Figure 6.15. Use the equation:

$$\tau = \tau_0 + \alpha G b \sqrt{\rho}.$$

6.30 What is the dislocation density in iron with a shear strain of 0.4?

Given:

(a) $\tau = \tau_0 + K\gamma^n$, $\tau_0 = 50 \times 10^6$ MPa, $K = 10^8$ MPa, $n = 0.5$,
(b) $\tau = \tau_0 + \alpha G b\sqrt{\rho}$, $G = 81.6$ GPa, $b = 0.25$ nm, $\alpha = 0.5$.

6.31 The flow stress for an alloy is 100 MPa when its dislocation density is 10^6 cm^{-2}, and 150 MPa when its dislocation density is 10^8 cm^{-2}. When the flow stress is 190 MPa, what is the dislocation density?

6.32 A copper sample exhibits work-hardening described by:

$$\sigma = \sigma_0 + K\varepsilon^n,$$

where $\sigma_0 = 50$ MPa, $n = 0.5$, $K = 500$ MPa.

Calculate the temperature rise when the sample is deformed up to a strain of 0.2. Assume that the conversion factor is 1.0, and given: density = 8.9 g/cm^3; heat capacity = 360 J/kg K.

Chapter 7

Fracture: Macroscopic Aspects

7.1 Introduction

The separation or fragmentation of a solid body into two or more parts, under the action of stresses, is called *fracture*. The subject of fracture is vast and involves disciplines as diverse as solid-state physics, materials science, and continuum mechanics. Fracture of a material by cracking can occur in many ways, principally the following:

1. Slow application of external loads.
2. Rapid application of external loads (impact).
3. Cyclic or repeated loading (fatigue).
4. Time-dependent deformation (creep).
5. Internal stresses, such as thermal stresses caused by anistropy of the thermal expansion coefficient or temperature differences in a body.
6. Environmental effects (stress corrosion cracking, hydrogen embrittlement, liquid metal embrittlement, etc.)

The process of fracture can, in most cases, be subdivided into the following categories:

1. Damage accumulation.
2. Nucleation of one or more cracks or voids.
3. Growth of cracks or voids. (This may involve a coalescence of the cracks or voids.)

Damage accumulation is associated with the properties of a material, such as its atomic structure, crystal lattice, grain boundaries, and prior loading history. When the local strength or ductility is exceeded, a crack (two free surfaces) is formed. On continued loading, the crack propagates through the section until complete rupture occurs. Linear elastic fracture mechanics (LEFM) applies the theory of linear elasticity to the phenomenon of fracture – mainly, the propagation of cracks. If we define the fracture toughness of a material as its resistance to crack propagation, then we can use LEFM to

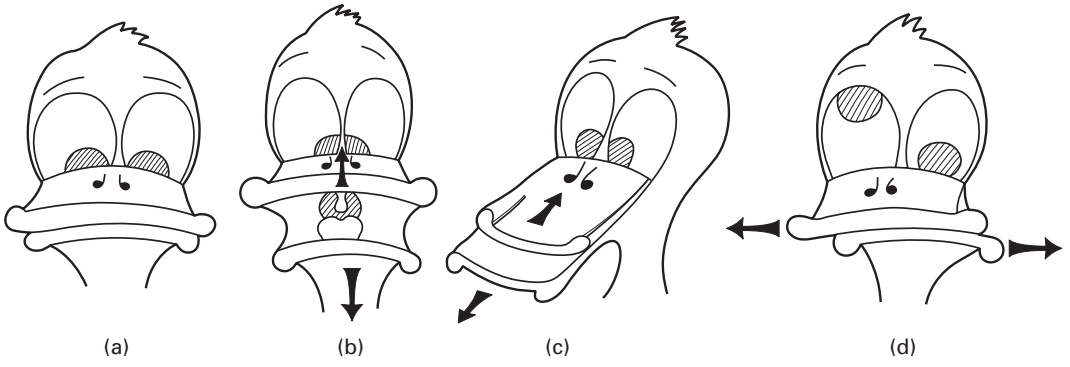

Fig. 7.1 "Goofy duck" analog for three modes of crack loading. (a) Crack/beak closed. (b) Opening mode. (c) Sliding mode. (d) Tearing mode. (Courtesy of M. H. Meyers.)

provide us with a quantitative measure of fracture toughness. Various standardization bodies, such as the American Society for Testing and Materials (ASTM), British Standards Institution (BSI), and Japan Institute of Standards (JIS), have standards for fracture toughness tests.

In this chapter, we will develop a quantitative understanding of cracks. It is very important to calculate the stresses at the tip (or in the vicinity of the tip) of a crack, because these calculations help us answer a very important practical question: At what value of the external load will a crack start to grow?

Figure 7.1 shows a simple analog that will assist the student in the visualization of different types of crack. In Figure 7.1(a), "goofy duck" has its beak initially closed. Let us consider the spacing between the upper and lower beaks as a crack. Depending on how the goofy duck moves its beak, different modes of crack loading are generated:

- The opening mode, shown in Figure 7.1(b) is caused by loading that is perpendicular to the crack plane.
- The sliding mode, shown in Figure 7.1(c) is produced by forces parallel to the crack plane and perpendicular to the crack "line" (crack extremity).
- The tearing mode (Figure 7.1d) is produced by forces parallel to the crack surface and to the crack "line."

Among the parameters and tests that have been developed, mostly during the last quarter of the twentieth century, to describe the resistance to fracture of a material in a quantitative and reproducible manner, is the *plane strain fracture toughness*, defined as the critical stress intensity factor under plane strain conditions and mode I loading. This is the stress intensity factor at which a crack of a given size starts to grow in an unstable manner. The fracture toughness is related to the applied stress by an equation of the following form:

$$\boxed{K_{Ic} = Y\sigma\sqrt{\pi a},}$$

where K_{Ic} is the fracture toughness in mode I loading, a is the characteristic dimension (semilength) of the crack and Y is a

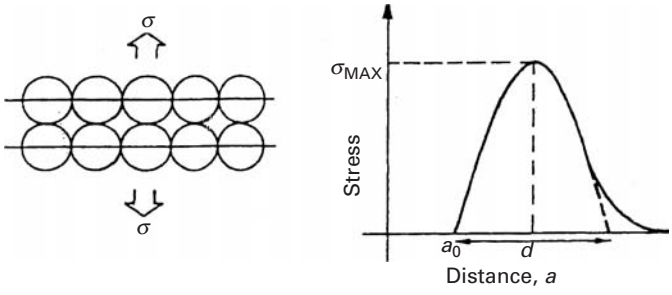

Fig. 7.2 Stress required to separate two atomic layers.

factor that depends on the geometry of the specimen, the location of the crack, and the loading configuration. One can see that the stress which can be safely applied decreases with the square root of the size of the crack. Also, note that K_{Ic} is a parameter of the material in the same manner as are hardness and yield strength. We will explain this in detail in Section 7.5. First we derive an expression for the theoretical tensile strength of a crystal.

7.2 Theorectical Tensile Strength

A material is said to *cleave* when it breaks under normal stress and the fracture path is perpendicular to the applied stress. The process involves the separation of the atoms along the direction of the applied stress. Orowan developed a simple method for obtaining the theoretical tensile strength of a crystal.[1] With his method, no stress concentrations at the tip of the crack are assumed; instead, it is assumed that all atoms separate simultaneously once their separation reaches a critical value. Figure 7.2 shows how the stress required to separate two planes will vary as a function of the distance between planes. The distance is initially equal to a_0. Naturally, σ for $a = a_0$; σ will also be zero when the separation is infinite. The exact form of the curve of σ versus a depends on the nature of the interatomic forces. In Orowan's model, the curve is simply assumed to be a sine function – hence the generality of the model. The area under the curve is the work required to cleave the crystal. This work of deformation – and here there is a certain similarity with Griffith's crack propagation theory to be presented in Section 7.4 – cannot be lower than the energy of the two new surfaces created by the cleavage. If the surface energy per unit area is γ and the cross-sectional area of the specimen is A, the total energy is $2\gamma A$ (two surfaces formed). The stress dependence on plane separation is then given by the following equations, admitting a sine function and assuming a periodicity of $2d$:

$$\sigma = K \sin \frac{2\pi}{2d}(a - a_0). \tag{7.1}$$

[1] E. Orowan, "Fracture and Strength of Solids," *Rep. Prog. Phys.*, 12 (1949) 185.

K is a constant that can be determined by the following artifice: When a is close to a_0, the material responds linearly to the applied loads (Hookean behavior). Assuming that the elastic defomation is restricted to the two planes shown in Figure 7.2 and that the material is isotropic, the fractional change in the distance between the planes, da/a_0, is defined as the incremental strain $d\varepsilon$.

$$\frac{da}{a_0} = d\varepsilon$$
$$\frac{d\sigma}{d\varepsilon} = \frac{d\sigma}{da/a_0} = E\,, \tag{7.2}$$

where E is Young's modulus, which is defined as $d\sigma/d\varepsilon$ in the elastic region. Thus,

$$a_0 \frac{d\sigma}{da} = E\,.$$

Taking the derivative of Equation 7.1 and substituting into Equation 7.2 for $a = a_0$,

$$a_0 \frac{d\sigma}{da} = K \frac{\pi}{d} a_0 \cos\frac{\pi}{d}(a - a_0) = E\,,$$
$$K = \frac{E}{\pi}\frac{d}{a_0}. \tag{7.3}$$

However, d is not known; to determine d, the area under the curve has to be equated to the energy of the two surfaces created:

$$\int_{a_0}^{a_0+d} \sigma\, da = 2\gamma. \tag{7.4}$$

Substituting Equation 7.1 into 7.4, we get

$$\int_{a_0}^{a_0+d} K \sin\frac{2\pi}{2d}(a - a_0)\, da = 2\gamma. \tag{7.5}$$

From a standard mathematics text, the preceding integral can be evaluated:

$$\int \sin ax dx = \frac{1}{a}\cos ax. \tag{7.6}$$

A substitution of variables is required to solve Equation 7.5; applying the standard Equation 7.6, we have $a - a_0 = y$; therefore, $da = dy$, and

$$K\int_0^d \sin\frac{\pi}{d} y dy = 2\gamma,$$
$$K\frac{d}{\pi} = \gamma,$$

and

$$d = \frac{\pi\gamma}{K}. \tag{7.7}$$

The maximum value of σ is equal to the theoretical cleavage stress. From Equation 7.1, and making the sine equal to 1, we have,

Table 7.1 | Theorectical Cleavage Stresses According to Orowan's Theory*

Element	Direction	Young's Modulus (GPa)	Surface Energy (mJ/m^2)	σ_{max} (GPa)	σ_{max}/E
α-Iron	<100>	132	2	30	0.23
	<111>	260	2	46	0.18
Silver	<111>	121	1.13	24	0.20
Gold	<111>	110	1.35	27	0.25
Copper	<111>	192	1.65	39	0.20
	<100>	67	1.65	25	0.38
Tungsten	<100>	390	3.00	86	0.22
Diamond	<111>	1,210	5.4	205	0.17

* Adapted with permission from A. Kelly, *Strong Solids*, 2nd ed. (Oxford, U.K.: Clarendon Press, 1973), p. 73.

from Equation 7.3,

$$\sigma_{max} = K = \frac{E}{\pi}\frac{d}{a_0}. \tag{7.8}$$

Substituting Equation 7.7 into Equation 7.8 yields

$$K = \sigma_{max} = \frac{E\gamma}{a_0 K},$$

and

$$K^2 = (\sigma_{max})^2 = \frac{E\gamma}{a_0},$$

or

$$\sigma_{max} = \sqrt{\frac{E\gamma}{a_0}}. \tag{7.9}$$

According to Orowan's model, the surface energy is given by

$$\gamma = \frac{Kd}{\pi} = \frac{E}{a_0}\left(\frac{d}{\pi}\right)^2 \tag{7.10}$$

$$\gamma = \frac{Ea_0}{10} \quad \text{and} \quad \boxed{\sigma_{max} \cong \frac{E}{\pi}} \tag{7.11}$$

We can conclude from Equation 7.9 that, in order to have a high theoretical cleavage strength, a material must have a high Young's modulus and surface energy and a small distance a_0 between atomic planes. Table 7.1 presents the theoretical cleavage strengths for a number of metals. The greatest source of error is γ: it is not easy to determine γ with great precision in solids, and the values used in the table come from different sources and were not necessarily determined at the same temperature.

7.3 Stress Concentration and Griffith Criterion of Fracture

The most fundamental requisite for the propagation of a crack is that the stress at the tip of the crack must exceed the theoretical cohesive strength of the material. This is indeed the fundamental criterion, but it is not very useful, because it is almost impossible to measure the stress at the tip of the crack. An equivalent criterion, called the Griffith criterion, is more useful and predicts the force that must be applied to a body containing a crack for the propagation of the crack. The Griffith criterion is based on an energy balance and is described in Section 7.4. Let us first grasp the basic idea of stress concentration in a solid.

7.3.1 Stress Concentrations

The failure of a material is associated with the presence of high local stresses and strains in the vicinity of defects. Thus, it is important to know the magnitude and distribution of these stresses and strains around cracklike defects.

Consider a plate having a through-the-thickness notch and subjected to a uniform tensile stress away from the notch (Figure 7.3). We can imagine the applied external force being transmitted from one end of the plate to the other by means of lines of force (similar to the well-known magnetic lines of force). At the ends of the plate, which is being uniformly stretched, the spacing between the lines is uniform. The lines of force in the central region of the plate are severely distorted by the presence of the notch (i.e., the stress field is perturbed). The lines of force, acting as elastic strings, tend to minimize their lengths and thus group together near the ends of the elliptic hole. This grouping together of lines causes a decrease in the line spacing locally and, consequently, an increase in the local stress (a stress concentration), there being more lines of force in the same area.

7.3.2 Stress Concentration Factor

The theoretical fracture stress of a solid is on the order $E/10$ (see Section 7.2), but the strength of solids (crystalline or otherwise) in practice is orders of magnitude less than this value. The first attempt

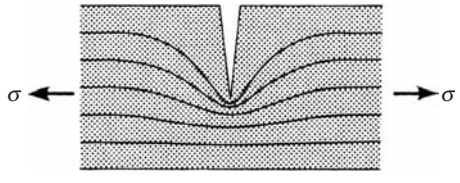

Fig. 7.3 "Lines of force" in a bar with a side notch. The direction and density of the lines indicate the direction and magnitude of stress in the bar under a uniform stress σ away from the notch. There is a concentration of the lines of force at the tip of the notch.

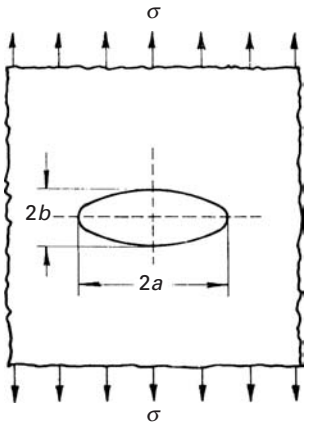

Fig. 7.4 Griffith model of a crack.

at giving a rational explanation of this discrepancy was attributed to Griffith. His analytical model was based on the elastic solution of a cavity elongated in the form of an ellipse.

Figure 7.4 shows an elliptical cavity in a plate under a uniform stress σ away from the cavity. The maximum stress occurs at the ends of the major axis of the cavity and is given by Inglis's formula,[2]

$$\boxed{\sigma_{\max} = \sigma\left(1 + 2\frac{a}{b}\right).} \tag{7.12}$$

where $2a$ and $2b$ are the major and minor axes of the ellipse, respectively.[3] The value of the stress at the leading edge of the cavity becomes extremely large as the ellipse is flattened. In the case of an extremely flat ellipse or a very narrow crack of length $2a$ and having a radius of curvature $\rho = b^2/a$, Equation 7.12 can be written as

$$\boxed{\sigma_{\max} = \sigma\left(1 + 2\sqrt{\frac{a}{\rho}}\right) \cong 2\sigma\sqrt{\frac{a}{\rho}} \qquad \text{for } \rho \ll a.} \tag{7.13}$$

We note that as ρ becomes very small, $\sigma_{\max}$ becomes very large, and in the limit, as $\rho \to 0$, $\sigma_{\max} \to \infty$. We define the term $2\sqrt{a/\rho}$ as the stress concentration factor K_t (i.e., $K_t = \sigma_{\max}/\sigma$). K_t simply describes the geometric effect of the crack on the local stress (i.e., at the tip of the crack). Note that K_t depends more on the *form* of the cavity than on its size. A number of texts and handbooks give a compilation of stress concentration factors K_t for components containing cracks or notches of various configurations.

As an example of the importance of stress concentration, we point out the use of square windows in the COMET commercial jet aircraft. Fatigue cracks, initiated at the corners of the windows, caused catastrophic failures of several of these aircraft.

In addition to producing a stress concentration, a notch produces a local situation of biaxial or triaxial stress. For example, in the case of a plate containing a circular hole and subject to an axial force, there exist radial as well as tangential stresses. The stresses in a large plate containing a circular hole (with diameter $2a$) and axially loaded (Figure 7.5(a)) can be expressed as[4]

$$\begin{aligned}
\sigma_{rr} &= \frac{\sigma}{2}\left(1 - \frac{a^2}{r^2}\right) + \frac{\sigma}{2}\left(1 + 3\frac{a^4}{r^4} - 4\frac{a^2}{r^2}\right)\cos 2\theta, \\
\sigma_{\theta\theta} &= \frac{\sigma}{2}\left(1 + \frac{a^2}{r^2}\right) - \frac{\sigma}{2}\left(1 + 3\frac{a^4}{r^4}\right)\cos 2\theta, \\
\sigma_{r\theta} &= -\frac{\sigma}{2}\left(1 - \frac{3a^4}{r^4} + \frac{2a^2}{r^2}\right)\sin 2\theta.
\end{aligned} \tag{7.14}$$

[2] C. E. Inglis, *Proc. Inst. Naval Arch.*, 55 (1913) 163, 219.

[3] The derivation of this equation, which can be found in more advanced tests [e.g., J. F. Knott, *Fundamentals of Fracture Mechanics*, (London: Butterworths, 1973), p. 51], involves the solution of the biharmonic equation, the choice of an appropriate Airy stress function, and complex variables.

[4] See, for example, S. Timoshenko and J. N. Goodier, *Theory of Elasticity*, 2nd ed. (New York: McGraw-Hill, 1951), p. 78.

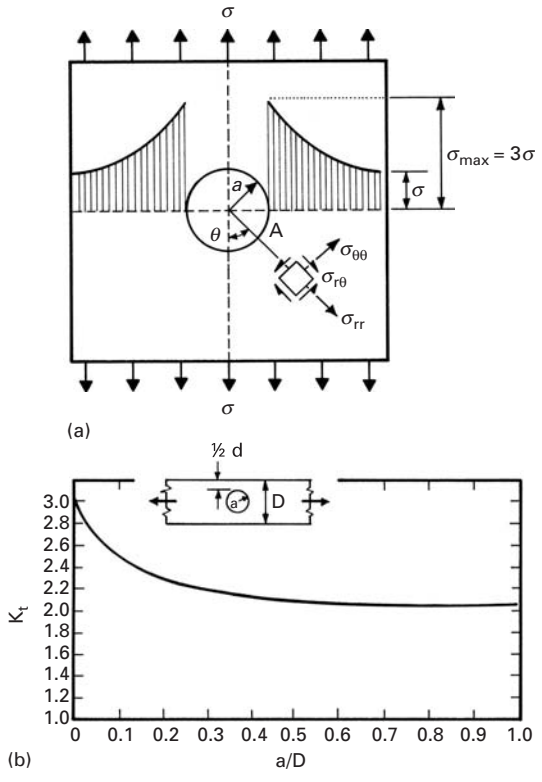

Fig. 7.5 (a) Stress distribution in a large plate containing a circular hole. (b) Stress concentration factor K_t as a function of the radius of a circular hole in a large plate in tension.

The maximum stress occurs at point A in Figure 7.5(a), where $\theta = \pi/2$ and $r = a$. In this case,

$$\sigma_{\theta\theta} = 3\sigma = \sigma_{\max},$$

where σ is the uniform stress applied at the ends of the plate. The stress concentration $K_t = \sigma_{\max}/\sigma = 3$. Figure 7.5(b) shows the stress concentration for a circular hole in a plate of finite lateral dimensions. When D, the lateral dimension, decreases, or the radius of the hole increases, the stress concentration K_t drops from 3 to 2.2.

Goodier[5] calculated the stresses around spherical voids in perfectly elastic materials. Although his solution was obtained when the applied stress was tensile, it can be extended to compressive stress by changing the signs. The stresses given by Timoshenko and Goodier can be determined from the methods of elasticity theory. At the equatorial plane ($\theta = \pi/2$), the tangential stress $\sigma_{\theta\theta}$ is equal to

$$\sigma_{\theta\theta} = \left[1 + \frac{4 - 5\nu}{2(7 - 5\nu)}\frac{a^3}{r^3} + \frac{9}{2(7 - 5\nu)}\frac{a^5}{r^5}\right]\sigma, \tag{7.15}$$

where a is the radius of the hole, r is the radial coordinate, and ν is the Poisson's ratio. For $r = a$, $\nu = 0.3$, and we have

$$(\sigma_{\theta\theta})_{\max} = \frac{45}{22}\,\sigma \approx 2\sigma.$$

[5] J. N. Goodier, *App. Mech.* 1 (1933) 39; see also Timoshenko and Goodier, *op. cit.*

Thus, as expected, the stress concentration for a spherical void is approximately 2. The stress $\sigma_{\theta\theta}$ decays quite rapidly with r, as can be seen from Equation 7.15; the decay is given by r^{-3}. For $r = 2a$, we have $\sigma_{\theta\theta} = 1.054$. This decay is faster than for the circular hole, where it goes with r^{-2} (Equation 7.14). For $\theta = 0$ (north and south poles), Timoshenko and Goodier have the equation

$$(\sigma_{rr})_\theta = (\sigma_{\theta\theta})_{\theta=0} = -\frac{3 + 15\nu}{2(7 - 5\nu)}\sigma.$$

Hence, a compressive stress generates a tensile stress at $\theta = 0$. This result is very important and shows that compressive stress can generate cracks at spherical flaws such as voids. Taking $\nu = 0.2$–0.3 (typical of ceramics), one arrives at the following values:

$$\frac{1}{2} \leq (\sigma_{\theta\theta})_{\theta=0} \leq \frac{7.5}{11}.$$

Thus, the tensile stress is 50–80% of the applied compressive stress. If failure is determined by cracking at spherical voids, cracking should start at a compressive stress level equal to $-4\sigma_t$ (depending on ν; in this case, for $\nu = 0.2$), where σ_t is the tensile strength of the material. This value represents, to a first approximation, the marked differences between the tensile and compressive strengths of cast irons, intermetallic compounds, and ceramics. The result is fairly close to the stress generated around a circular hole, given in Equation 7.14. In that case, for $r = a$, we find that

$$\sigma_{\theta\theta} = -\sigma.$$

In tensile loading, the stress $\sigma_{\theta\theta} = 3\sigma$, which would predict a threefold difference in tensile and compressive strengths. More general (elliptical) flaws can be assumed, and their response under compressive loading provides a better understanding of the compressive strength of brittle materials. The generation and growth of cracks from these flaws also needs to be analyzed, for more realistic predictions. This will be carried out in Section 8.3.4.

Stress concentration caused by an elliptical hole is shown in Figure 7.6. In this figure, σ_L is the longitudinal stress applied along x_2. It is also referred to as the far-field stress. Locally at the crack tip we have a biaxial or triaxial stress situation. In particular, for an elliptical hole, with $a = 3b$, Figure 7.6 shows that σ_{22} falls from its maximum value at the crack tip and attains σ_L asymptotically. The stress component, σ_{11}, however is zero at the crack tip, increases to a peak value and then falls to zero with the same tendency as σ_{22}. The general result is that a major perturbation in the applied stress state occurs over a distance approximately equal to a from the boundaries of the cavity, with the major stress gradients being confined to a region of dimensions roughly equal to ρ surrounding the maximum concentration position.

Although the exact formulas vary according to the form of the crack, in all cases K_t increases with an increase in the crack length a and a decrease in the root radius at the crack tip, ρ.

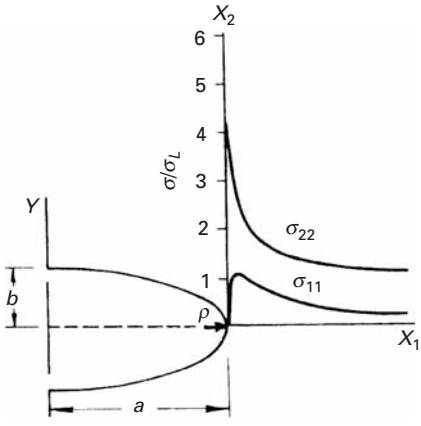

Fig. 7.6 Stress concentration at an elliptical hole for $a = 3b$.

Despite the fact that the analysis of Inglis represented a great advance, the fundamental nature of the fracture mechanism remained obscure. If the Inglis analysis was applicable to a body containing a crack, how does one explain that, in practice, larger cracks propagate more easily than smaller cracks? What is the physical significance of the root radius at the tip of the crack?

Example 7.1

Although the elastic modulus of silica-based glass is rather low ($E =$ 70 GPa), the theoretical strength of a defect-free glass can be as high as 3 GPa. Generally, such high strength values are not measured in practice. Why?

Solution: Extremely minute crack-like defects form rather easily on the glass surface. Such imperfections can lead to a drastic reduction in the strength of glass. This is the reason that, in the making of a glass fiber, a protective coating called a *size* is applied to the fiber immediately as it comes out of the spinneret. Just to get an estimate of the reduction in strength caused by a tiny imperfection – say, a 1-μm-long, atomically sharp scratch – we can use the Inglis expression (Equation 7.13),

$$\sigma_{\text{th}} = 2\sigma(a/\rho)^{0.5}, \quad \text{or} \quad \sigma = 0.5\ \sigma_{\text{th}}(\rho/a)^{0.5},$$

where σ_{th} is the theoretical strength (3 GPa), a is the crack length (1 μm), and ρ is the root radius at the crack tip, which, since the tip is atomically sharp, can be taken to be 0.25 nm. Plugging these values into the preceding expression, we find that the real strength of such a glass is only 24 MPa! Note that in this problem we made an estimate of the notch root radius. In practice, this is very difficult to measure. That is why the concept of stress intensity factor, involving the far-field stress and the square root of the crack length, is much more convenient to deal with in fracture toughness problems, as we shall see later in this chapter (Section 7.6).

Example 7.2

Determine the stresses at distances equal to 0, $a/2$, a, $3a/2$, and $2a$ from the surface of a spherical hole and for $\theta = 0$ and $\pi/2$.

Solution: We use Equation 7.14. By setting $\theta = 0$, we have

$$\sigma_{rr} = \frac{\sigma}{2}\left(2 - \frac{5a^2}{r^2} + \frac{3a^4}{r^4}\right),$$
$$\sigma_{\theta\theta} = \frac{\sigma}{2}\left(\frac{a^2}{r^2} - \frac{3a^2}{r^4}\right),$$
$$\tau_{r\theta} = 0.$$

For $\theta = \pi/2$,

$$\sigma_{rr} = \frac{\sigma}{2}\left(\frac{3a^2}{r^2} - \frac{3a^4}{r^4}\right),$$
$$\sigma_{\theta\theta} = \frac{\sigma}{2}\left(2 + \frac{a^2}{r^2} + \frac{3a^4}{r^4}\right),$$
$$\tau_{r\theta} = 0.$$

We calculate the stresses for $r = 0$, a, $3a/2$, and $2a$ and plot them as shown in Figure E7.2 in terms of a dimensionless parameter r/a.

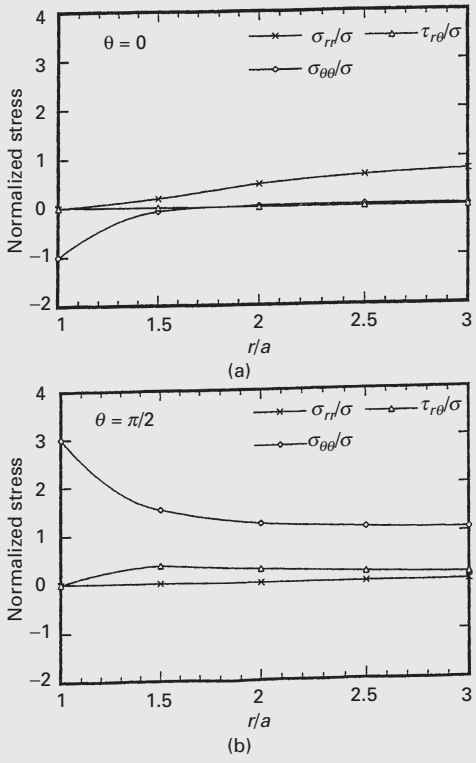

Fig. E7.2

Example 7.3

Two flat plates are being pulled in tension. (See Figure E7.3.) The flow stress of the materials is 150 MPa.

(a) Calculate the maximum stresses in the plate.
(b) Will the material flow plastically?
(c) For which configuration is the stress higher?

Solution:

(a) Normal stress:

$$\sigma = \frac{P}{A} = \frac{100\,\text{kN}}{10\,\text{cm} \times 1\,\text{cm}}$$

$$= 100\ \text{MPa},$$

$$\sigma_{\max} = \sigma\left(1 + 2\frac{a}{b}\right).$$

Circular hole:

$$a = b = 3/2\ \text{cm} = 1.5\ \text{cm},$$

$$\sigma_{\max} = 100 \times \left(1 + 2 \times \frac{1.5}{1.5}\right) = 300\ \text{MPa}.$$

Elliptical hole:

$$a = 3/2\ \text{cm} = 1.5\ \text{cm}, b = 1/2\ \text{cm} = 0.5\ \text{cm},$$

$$\sigma_{\max} = 100 \times \left(1 + 2 \times \frac{1.5}{0.5}\right) = 700\ \text{MPa}.$$

(b) Yes, because in both cases, the stress is greater than the flow stress (150 MPa).
(c) The elliptical hole has higher stress than the circular one.

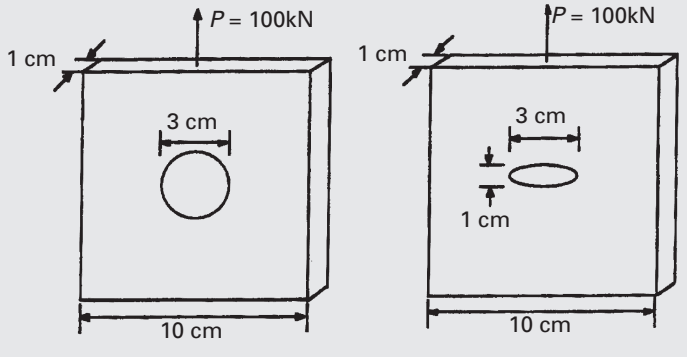

Fig. E7.3

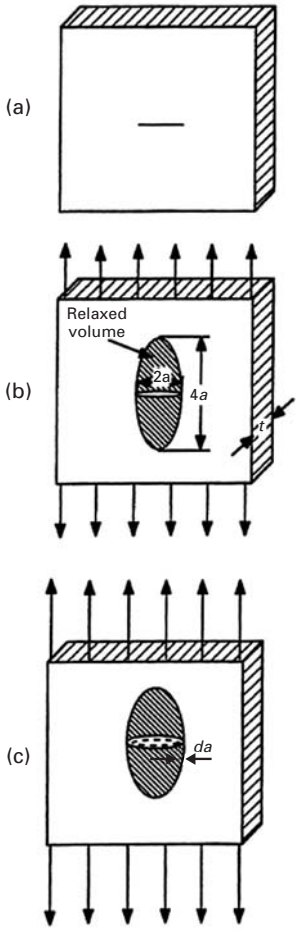

Fig. 7.7 A plate of thickness t containing a crack of length $2a$. (a) Unloaded condition. (b) and (c) Loaded condition.

7.4 Griffith Criterion

Griffith proposed a criterion based on a thermodynamic energy balance. He pointed out that two things happen when a crack propagates: Elastic strain energy is released in a volume of material, and two new crack surfaces are created, which represent a surface-energy term. Thus, according to Griffith, an existing crack will propagate if the elastic strain energy released by doing so is greater than the surface energy created by the two new crack surfaces. Figure 7.7(a) shows an infinite plate of thickness t that contains a crack of length $2a$ under plane stress. As the stress is applied, the crack opens up. The shaded region denotes the approximate volume of material in which the stored elastic strain energy is released (Figure 7.7(b)). When the crack extends a distance da on the extremities, the volume over which elastic energy is released increases, as shown in Figure 7.7(c). The elastic energy per unit volume in a solid under stress is given by $\sigma^2/2E$. (See Chapter 2.) To get the total strain energy released, we need to multiply this quantity by the volume of the material in which this energy is released. In the present case, this volume is the area of the ellipse times the plate thickness. The area of the shaded ellipse is $\pi\ (2a)a = 2\ \pi a^2$; therefore, the volume in which the strain energy is relaxed is $2\ \pi a^2 t$. The total strain energy released is thus

$$\left(\frac{\sigma^2}{2E}\right)(2\pi a^2 t) = \frac{\pi\sigma^2 a^2 t}{E},$$

or, in terms of the per-unit thickness of the plate under plane stress, the energy released is

$$U_e = \pi\sigma^2 a^2/E\,.$$

The decrease in strain energy, U_e, when a crack propagates is balanced by an increase in the surface energy, U_s, produced by the creation of the two new crack surfaces. The increase in surface energy equals:

$$U_s = (2at)(2y_s),$$

here γ_s is the specific surface energy, i.e., the energy per unit area. In terms of the per-unit thickness of the plate, the increase in surface energy is $4a\gamma_s$. Now, when an elliptical crack is introduced into the plate, we can write, for the change in potential energy of the plate,

$$\Delta U = U_s - U_e,$$
$$\Delta U = 4a\gamma_s - \frac{\pi\sigma^2 a^2}{E},$$

where ΔU is the change in the potential energy per unit thickness of the plate in the presence of the crack, σ is the applied stress, a is half the crack length, E is the modulus of elasticity of the plate, and γ_s is the specific surface energy (i.e., the surface energy per unit area) of the plate.

As the crack grows, strain energy is released, but additional surfaces are created. The crack becomes stable when these energy components balance each other. If they are not in balance, we have an unstable crack (i.e., the crack will grow). We can obtain the equilibrium condition by equating to zero the first derivative of the potential energy ΔU with respect to the crack length. Thus,

$$\frac{\Delta U}{\partial a} = 4\gamma_s - \frac{2\pi\sigma^2 a}{E} = 0, \tag{7.16a}$$

or

$$\boxed{2\gamma_s = \frac{\pi\sigma^2 a}{E}.} \tag{7.16b}$$

The reader can check the nature of this equilibrium further by taking the second derivative of U with respect to a. A negative second derivative would imply that Equation 7.16a represents an unstable equilibrium condition and that the crack will advance.

Rearranging Equation 7.16b, we may write, for the critical stress required for the crack to propagate in the plane-stress situation,

$$\boxed{\sigma_c = \sqrt{\frac{2E\gamma_s}{\pi a}} \quad \text{(plane stress).}} \tag{7.17a}$$

We can rearrange Equation 7.17a to get the following expression:

$$\sigma\sqrt{\pi a} = \sqrt{2E\gamma_s}.$$

The reader should note that the left-hand side of this expression involves critical stress for crack propagation and square root of crack length. This product is called fracture toughness. Note that the right-hand side of the expression consists only of material parameters: E and γ_s, i.e., the above expression represents a material property, viz., fracture toughness.

For the plane-strain situation, we will have the factor $(1 - \nu^2)$ in the denominator because of the confinement in the direction of thickness. The expression for the critical stress for crack propagation then becomes

$$\boxed{\sigma_c = \sqrt{\frac{2E\gamma_s}{\pi a(1-\nu^2)}} \quad \text{(plane strain).}} \tag{7.17b}$$

The distinction between plane stress and plane strain is shown in Figure 7.8. Normal and shear stresses at free surfaces are zero; hence, for a thin plate, $\sigma_{33} = \sigma_{23} = \sigma_{13} = 0$. This is the plane-stress state (Figure 7.8(a)). In very thick plates ($t_2 > t_1$), the flow of material in the x_3 direction is restricted. Therefore, $\varepsilon_{33} = 0$, and so are, $\varepsilon_{23} = \varepsilon_{13} = 0$. This is the plane-strain condition (Figure 7.8(b)). Note that the factor $(1 - \nu^2)$ is less than unity and is in the denominator. Therefore, the critical stress corresponding to fracture in the plane-strain situation will be higher than that in the plane-stress state. This is as expected,

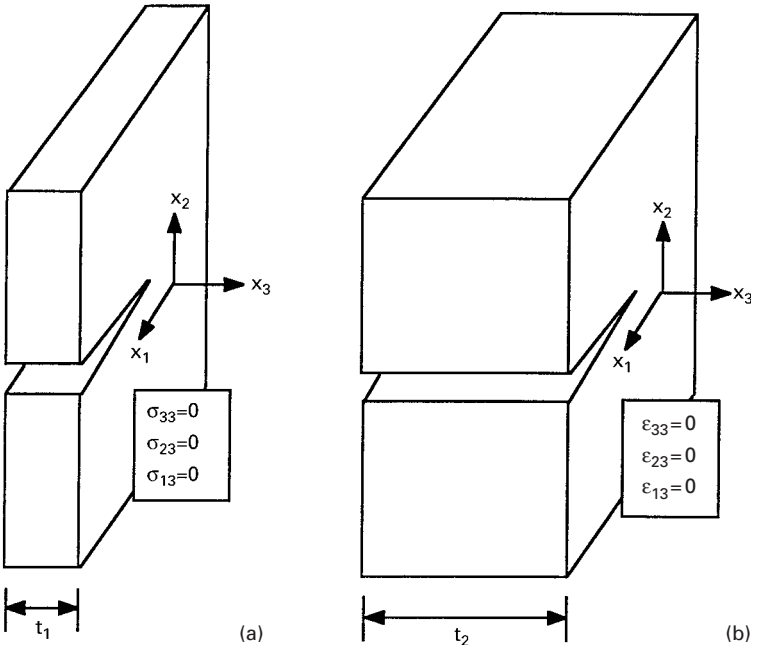

Fig. 7.8 Crack in (a) thin (t_1) and (b) thick (t_2) plates. Note the plane-stress state in (a) and the plane-strain state in (b).

because of the confinement in the direction of thickness in the case of plane strain. For many metals, $\nu \approx 0.3$, and $(1 - \nu^2) \approx 0.91$. Thus, the difference is not very large for most metals.

The importance of the length of the crack is implicit in Griffith's analysis. In modern fracture mechanics, as we shall see later, the crack length enters as a square-root term in the product $\sigma\sqrt{a}$. According to Griffith's thermodynamic analysis, a necessary condition for crack propagation is

$$-\frac{\partial U_e}{\partial a} \geq \frac{\partial U_s}{\partial a},$$

where U_e is the elastic energy of the system (i.e., the machine plus the test piece) and U_s is the surface energy of the two crack faces. This is a necessary condition for fracture by rapid crack propagation. But it may not always be sufficient: if the local stress at the crack tip is not sufficiently large to break the atomic bonds, the energy criterion of Griffith will be inadequate.

Let us consider Equation 7.17a or 7.17b again. Note that the fracture stress, or critical stress required for crack propagation, σ_c, is inversely proportional to $\sqrt{a}$. More importantly, the quantity $\sigma_c\sqrt{a}$ depends only on material constants. It is instructive, then, to examine the Inglis result, Equation 7.13, and the Griffith result, Equation 7.17a or 7.17b in the form

$$\sigma_c\sqrt{a} = \frac{1}{2}(\sigma_{\max})_c\ \sqrt{\rho} = \text{constant}.$$

Here, σ_c is the critical far-field or uniform stress (i.e., the stress at fracture), a is the crack length corresponding to σ_c, $(\sigma_{\max})_c$ is the

stress at the crack tip at fracture, and ρ is the root radius at the tip of the crack.

Both analyses, Inglis's and Griffith's lead to the same result, viz., that a crack will propagate when an appropriate quantity with dimensions of stress times the square root of length reaches a critical value, a material constant. It is easy to see that the parameters in the Inglis analysis, $(\sigma_{\max})_c$ and ρ, are local parameters and very difficult to measure, while the Griffith analysis allows us to use the far-field applied stress and crack length, which are easy to measure. It is this quantity, $\sigma_c\sqrt{a}$, that is called the fracture toughness and is denoted by K_{Ic}. We treat fracture toughness in detail in Section 7.6.

Example 7.4

Consider a brittle material with $\gamma_s = 1$ J/m^2 and $E = 100$ GPa. (a) What is the breaking strength of this material if it contains crack-like defects as long as 1 mm? (b) Should it be possible to increase γ_s to 3,000 J/m^2, what would be the breaking strength for a 1-mm-long crack?

Solution

(a) We have

$$\gamma_s = 1 \text{ J/m}^2 \quad \text{and} \quad E = 100 \text{ GPa},$$

and

$$2a = 1 \text{ mm} \quad \text{and} \quad a = 0.5 \text{ mm}.$$

Thus,

$$\sigma_c = \sqrt{\frac{2E\gamma_s}{\pi a}} = \sqrt{\frac{2 \times 100 \times 10^9 \times 1}{\pi \times (0.5 \times 10^{-3})}}$$
$$= 11.3 \text{ MPa}.$$

(b) If γ_s increases to 3,000 J/m^2,

$$2a = 1 \text{ mm} \quad \text{and} \quad a = 0.5 \text{ mm},$$

so that

$$\sigma_c = \sqrt{\frac{2E\gamma_s}{\pi a}} = \sqrt{\frac{2 \times 100 \times 10^9 \times 3{,}000}{\pi \times (0.5 \times 10^{-3})}}$$
$$= 618 \text{ MPa}.$$

7.5 Crack Propagation with Plasticity

If the material in which a crack is propagating can deform plastically, the form of the crack tip changes because of plastic strain. A sharp crack tip will be blunted. Another important factor is time: because

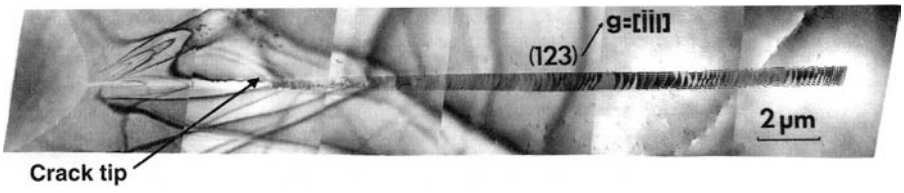

Fig. 7.9 Dislocations emitted from a crack tip in copper. (Courtesy of S. M. Ohr.)

plastic deformation requires time, the amount of plastic deformation that can occur at the crack tip will depend on how fast the crack is moving. Figure 7.9, a TEM micrograph, shows dislocations that were generated at a crack tip and that propagated along crystallographic planes. The crack is at the left-hand side, and the plane of the copper foil is (123). In a great majority of materials, localized plastic deformation at and around the crack tip is produced because of the stress concentrations there. In such a case, a certain amount of plastic work is done during crack propagation, in addition to the elastic work done in the creation of two fracture surfaces. The mechanics of fracture will, then, depend on the magnitude of γ_p, the plastic work done, which in its turn depends on the crack speed, temperature, and the nature of the material. For an inherently brittle material, at low temperatures and at high crack velocities γ_p is relatively small ($\gamma_p < 0.1\gamma_s$). In such a case, the crack propagation would be continuous and elastic. These cases are usefully treated by means of linear elastic fracture mechanics, which is dealt with in Section 7.6. In any event, in the case of plastic deformation, the work done in the propagation of a crack per unit area of the fracture surface is increased from γ_s to $(\gamma_s + \gamma_p)$. Consequently, the Griffith criterion (Equation 7.17a or 7.17b) is modified to

$$\sigma_c = \sqrt{\frac{2E}{\pi a}(\gamma_s + \gamma_p)} \quad \text{(plane stress)} \tag{7.18a}$$

and

$$\sigma_c = \sqrt{\frac{2E}{\pi a(1-\nu^2)}(\gamma_s + \gamma_p)} \quad \text{(plane strain).} \tag{7.18b}$$

Rearranging Equation 7.18a, we get

$$\sigma_c = \sqrt{\frac{2E\,\gamma_s}{\pi a}\left(1 + \frac{\gamma_p}{\gamma_s}\right)}.$$

For $\gamma_p/\gamma_s \gg 1$,

$$\sigma_c \cong \sqrt{\frac{2E\,\gamma_p}{\pi a}}.$$

Thus, the plastic deformation around the crack tip makes it blunt and serves to relax the stress concentration by increasing the radius of curvature of the crack at its tip. Localized plastic deformation at the crack tip therefore improves the fracture toughness of the material.

This is the conventional treatment of the plastic work contribution to the fracture process, wherein γ_p is considered to be a constant. However, the reader should be warned that this is not strictly true. As a matter of fact, the value of γ_p increases with the stress intensity factor K ($=Y\sigma\sqrt{a}$). Consider Equation 7.18a. As was pointed out, in the conventional approach γ_p will be very much larger than γ_s for a ductile material such as polycrystalline copper. Thus, according to this conventional treatment, the fracture stress σ_c should be relatively insensitive to changes in γ_s. However, in the embrittlement of copper with beryllium, all we change is the γ_s part of Equation 7.18a (along the grain boundaries where the fracture proceeds). The γ_p part in that equation (i.e., the plastic behavior of copper) does not change appreciably by the addition of beryllium to copper.

As pointed out earlier, equations of the type 7.17a or 7.18 are difficult to use in practice. It is not a trivial matter to measure quantities such as surface energy and the energy of plastic deformation. In a manner similar to that of Griffith, Irwin made a fundamental contribution to the mechanics of fracture when he proposed that fracture occurs at a stress that corresponds to a critical value of the crack extension force

$$G = \frac{1}{2}\frac{\partial U_e}{\partial a} = \text{rate of change of energy with crack length.}$$

G is sometimes called the *strain energy release rate*.

Now, $U_e = \pi a^2\sigma^2/E$, the energy released by the advancing crack per unit of plate thickness. This is for plane stress. For plane strain, a factor of $(1 - \nu^2)$ is introduced in the denominator. Thus,

$$G = \frac{\pi a\sigma^2}{E}.$$

At fracture, $G = G_c$, and

$$\sigma_c = \sqrt{\frac{EG_c}{\pi a}} \quad \text{(plane stress)} \tag{7.19a}$$

or

$$\sigma_c = \sqrt{\frac{EG_c}{\pi a(1-\nu^2)}} \quad \text{(plane strain).} \tag{7.19b}$$

From Equations 7.18 and 7.19, we see that

$$G_c = 2(\gamma_s + \gamma_p).$$

We shall come back to this idea of crack extension force later in the chapter.

7.6 Linear Elastic Fracture Mechanics

A nonductile material has a very low capacity to deform plastically; that is, it is not capable of relaxing peak stresses at crack-like defects.

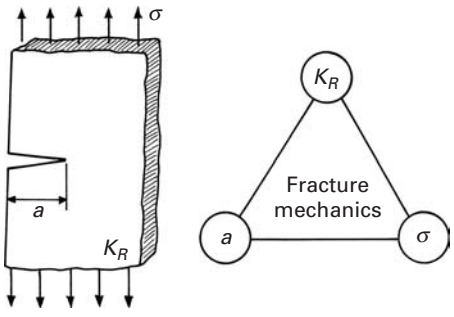

Fig. 7.10 Inherent material resistance to crack growth and its relationship to the applied stress σ and crack size a.

In such a material, a crack will propagate very rapidly with little plastic deformation around the crack tip, resulting in what is called a brittle fracture. Typically, such a fracture is also characterized by a crack propagation that is sudden, rapid, and unstable. In practical terms, this definition of brittleness, which refers to the onset of instability under an applied stress smaller than the stress corresponding to plastic yielding of the material, is very useful. Numerous brittle fractures have occurred in service, and there are abundant examples of them in a great variety of structural and mechanical engineering fields involving ships, bridges, pressure vessels, oil ducts, turbines, and so on. In view of the great importance of brittle fracture in real life, a discipline called linear elastic fracture mechanics (LEFM) has emerged, enabling us to obtain a quantitative measure of the resistance of a brittle material to unstable or catastrophic crack propagation. Extension of these efforts into nonlinear elastic and plastic regimens has led to the development of elasto-plastic fracture mechanics (EPFM), also called post-yield fracture mechanics (see Section 7.9).

7.6.1 Fracture Toughness

Fracture mechanics gives us a quantitative handle on the process of fracture in materials. Its approach is based on the concept that the relevant material property, fracture toughness, is the force necessary to extend a crack through a structural member. Under certain circumstances, this crack extension force (or an equivalent parameter) becomes independent of the dimensions of the specimen. The parameter can then be used as a quantitative measure of the fracture toughness of the material.

Fracture mechanics adopts an entirely new approach to designing against fracture. Admittedly defects will always be present in a structural component. But consider a structure or a component with a crack-like defect. We can simulate this with single edge notch of length a in a plate. (See Figure 7.10.) Alternatively, we can say that we are increasing the applied stress intensity factor K at the crack tip. The material at the tip, however, presents resistance to crack growth. We denote this inherent material resistance by K_R (sometimes the symbol R alone is used in place of K_R.) The discipline of fracture mechanics

can then be represented by a triangle as shown in Figure 7.10; that is, we have an interplay among the following three quantities:

1. The far-field stress, σ.
2. The characteristic crack length, a.
3. The inherent material resistance to cracking, K_R.

Various parameters are used to represent K_R. We discuss their equivalence in Section 7.7.5. Here we wish to clarify one common point of confusion. The symbol K is used to designate the stress intensity factor at the crack tip corresponding to a given applied stress and crack length. The symbol K_R (or one of its equivalents) represents fracture toughness. In this regard, the following analogy is helpful. The stress intensity factor, K, is to stress as fracture toughness, K_R, is to strength. Stress and stress intensity factor vary with the external loading conditions; strength and toughness are material parameters, independent of loading and specimen size considerations.

We now seek an answer to the question: Given a certain applied stress, what is the largest size defect (crack) that can be tolerated without the failure of the member? Once we know the answer to this question, it remains only to use appropriate inspection techniques to select/repair/replace a material so that defects larger than the critical size for the given design stress are not present.

7.6.2 Hypotheses of LEFM

The basic hypotheses of LEFM are as follows:

1. Cracks are inherently present in a material, because there is a limit to the sensibility or resolution of any crack-detecting equipment.
2. A crack is a free, internal, plane surface in a linear elastic stress field. With this hypothesis, linear elasticity furnishes us stresses near the crack tip as

$$\sigma_{r\theta} = \frac{K}{\sqrt{2\pi r}} f(\theta), \tag{7.20}$$

   where r and θ are polar coordinates and K is a constant called the *stress intensity factor* (SIF).
3. The growth of the crack leading to the failure of the structural member is then predicted in terms of the tensile stress acting at the crack tip. In other words, the stress situation at the crack tip is characterized by the value of K. It can be shown by elasticity theory that $K = Y\sigma\sqrt{\pi a}$, where σ is the applied stress, a is half the crack length, and Y is a constant that depends on the crack opening mode and the geometry of the specimen.

7.6.3 Crack-Tip Separation Modes

The three modes of fracture are shown in Figure 7.11. Mode I (Figure 7.11(a)), called the opening mode, has tensile stress normal to the crack faces. Mode II (Figure 7.10(b)) is called the sliding mode or the forward shear mode. In this mode, the shear stress is normal

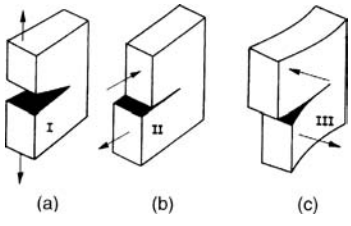

Fig. 7.11 The three modes of fracture. (a) Mode I: opening mode. (b) Mode II: sliding mode. (c) Mode III: tearing mode (see also Figure 7.1).

to the advancing crack front. Mode III (Figure 7.11(c)) is called the tearing mode or transverse shear mode, with the shear stress parallel to the advancing crack front. The "goofy duck" analog of Figure 7.1 shows this in a more illustrative fashion.

7.6.4 Stress Field in an Isotropic Material in the Vicinity of a Crack Tip

The stress components for the three fracture modes in an isotropic material are given next. In the case of anisotropic materials, these relations must be modified to permit the asymmetry of stress at the crack tip. K_{I}, K_{II}, and K_{III} represent stress intensity factors in modes I, II, and III, respectively. We have (the derivation of these expressions is attributed to Westergaard[6]):

Mode I:

$$\begin{bmatrix}\sigma_{11}\\ \sigma_{22}\\ \sigma_{12}\end{bmatrix} = \frac{K_{\mathrm{I}}}{\sqrt{2\pi r}}\cos\frac{\theta}{2}\begin{bmatrix}1-\sin\frac{\theta}{2} & \sin\frac{3\theta}{2}\\ 1+\sin\frac{\theta}{2} & \sin\frac{3\theta}{2}\\ \sin\frac{\theta}{2} & \cos\frac{3\theta}{2}\end{bmatrix},$$

$$\sigma_{13} = \sigma_{23} = 0,$$

$$\sigma_{33} = 0, \quad \text{(plane stress)},$$

$$\sigma_{33} = \nu(\sigma_{11}+\sigma_{22}), \quad \text{(plane strain)}. \tag{7.21}$$

Mode II:

$$\begin{bmatrix}\sigma_{11}\\ \sigma_{22}\\ \sigma_{12}\end{bmatrix} = \frac{K_{\mathrm{II}}}{\sqrt{2\pi r}}\begin{bmatrix}-\sin\frac{\theta}{2} & \left(2\cos\frac{\theta}{2}\cos\frac{3\theta}{2}\right)\\ \sin\frac{\theta}{2} & \cos\frac{\theta}{2}\ \cos\frac{3\theta}{2}\\ \cos\frac{\theta}{2} & \left(1-\sin\frac{\theta}{2}\sin\frac{3\theta}{2}\right)\end{bmatrix},$$

$$\sigma_{13} = \sigma_{23} = 0,$$

$$\sigma_{33} = 0, \quad \text{(plane stress)},$$

$$\sigma_{33} = \nu(\sigma_{11}+\sigma_{22}) \quad \text{(plane strain)}. \tag{7.22}$$

Mode III:

$$\begin{bmatrix}\sigma_{13}\\ \sigma_{23}\end{bmatrix} = \frac{K_{\mathrm{III}}}{2\pi r}\begin{bmatrix}-\sin\frac{\theta}{2}\\ \cos\frac{\theta}{2}\end{bmatrix}$$

$$\sigma_{11} = \sigma_{22} = \sigma_{33} = \sigma_{12} = 0. \tag{7.23}$$

The derivation of this expression for Mode III is given in the Appendix at the end of this chapter

[6] H. M. Westergaard, *J. Appl. Mechan., 5A* (1939) 49.

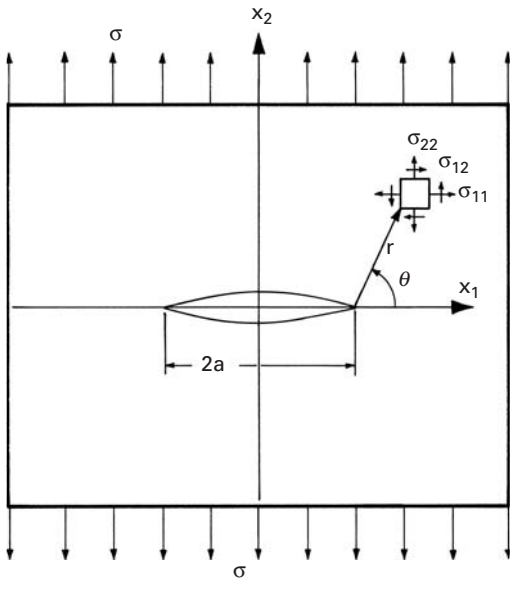

Fig. 7.12 Infinite, homogeneous, elastic plate containing a through-the-thickness central crack of length $2a$, subjected to a tensile stress σ.

7.6.5 Details of the Crack-Tip Stress Field in Mode I

Consider an infinite, homogeneous, elastic plate containing a crack of length $2a$ (Figure 7.12). The plate is subjected to a tensile stress σ far away from and normal to the crack. The stresses at a point (r, θ) near the tip of the crack are given by Equation 7.21. Ignoring the subscript of K, we may write the stress components in expanded form as:

$$\begin{aligned}
\sigma_{11} &= \frac{K}{\sqrt{2\pi r}} \cos\frac{\theta}{2}\left(1 - \sin\frac{\theta}{2}\sin\frac{3\theta}{2}\right),\\
\sigma_{22} &= \frac{K}{\sqrt{2\pi r}} \cos\frac{\theta}{2}\left(1 + \sin\frac{\theta}{2}\sin\frac{3\theta}{2}\right),\\
\sigma_{12} &= \frac{K}{\sqrt{2\pi r}} \cos\frac{\theta}{2}\sin\frac{\theta}{2}\cos\frac{3\theta}{2},\\
\sigma_{13} &= \sigma_{13} = 0,\\
\sigma_{33} &= 0 \quad \text{(plane stress)},\\
\sigma_{33} &= \nu(\sigma_{11} + \sigma_{22}) \quad \text{(plane strain)},
\end{aligned} \tag{7.24}$$

where

$$\boxed{K = \sigma\sqrt{\pi a}} \tag{7.25}$$

is the stress intensity factor for the plate and has the units $(\text{N/m}^2)\sqrt{\text{m}}$, or $\text{Pa}\sqrt{\text{m}}$, or $\text{Nm}^{-3/2}$. Note that Equation 7.25 is applicable in the region $r \ll a$ (i.e., in the vicinity of the crack tip). For larger r, higher order terms must be included.

For a thin plate, one has plane-stress conditions, and $\sigma_{33} = \sigma_{13} = \sigma_{23} = 0$. For a thick plate (infinite in the direction of thickness), there exist plane-strain conditions (i.e., $\sigma_{33}=\nu(\sigma_{11} + \sigma_{22})$ and $\sigma_{13} = \sigma_{23} = 0$).

Consider again Equation 7.24. The right-hand side has three quantities: K, r, and $f(\theta)$, $f(\theta)$ here designating the group of terms containing the angle θ in Equation 7.24. The terms r and $f(\theta)$ describe

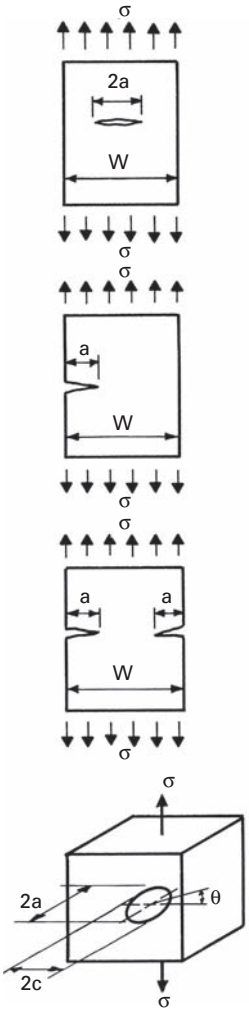

Center crack: $K_1 = Y\sigma\sqrt{\pi a}$

$$Y = 1 + 0.256\left(\frac{a}{W}\right) - 1.152\left(\frac{a}{W}\right)^2 + 12.200\left(\frac{a}{W}\right)^3$$

$$\text{or } Y = \sqrt{\sec\left(\frac{\pi a}{W}\right)}$$

$$\text{or } Y = \frac{1}{\sqrt{1-\left(\frac{2a}{W}\right)^2}}$$

Single edge notch: $K_1 = Y\sigma\sqrt{\pi a}$

$$Y = 1.12 \quad \text{for small cracks}$$

$$\text{or } Y = 1.12 - 0.231\left(\frac{a}{W}\right) + 10.55\left(\frac{a}{W}\right)^2 - 21.72\left(\frac{a}{W}\right)^3 + 30.39\left(\frac{a}{W}\right)^4$$

up to a/W = 0.6

Double edge notch: $K_1 = Y\sigma\sqrt{\pi a}$

$$Y = 1.12 \quad \text{for small cracks}$$

$$\text{or } Y = \frac{1.222 - 0.561\left(\frac{a}{W}\right) - 0.205\left(\frac{a}{W}\right)^2 + 0.471\left(\frac{a}{W}\right)^3 - 0.190\left(\frac{a}{W}\right)^4}{\sqrt{1-\frac{a}{W}}}$$

Embedded Cracks

Elliptical crack: $K_1 = Y\sigma\sqrt{\pi a}$

$$Y = \left(\sin^2\theta + \frac{a^2}{c^2}\cos^2\theta\right)^{1/4} \Big/ \left(\frac{3\pi}{8} + \frac{\pi}{8}\frac{a^2}{c^2}\right)$$

Circular crack: $K_1 = Y\sigma\sqrt{\pi a}$

$$Y = \frac{2}{\pi}$$

Fig. 7.13 Some common load and crack configurations and the corresponding expressions for the stress intensity factor, *K*.

the stress distribution around the crack tip. These two characteristics (i.e., dependence on $\sqrt{r}$ and $f(\theta)$) are identical for all cracks in two- or three-dimensional elastic solids. The stress intensity factor K includes the influence of the applied stress σ and the appropriate crack dimensions, in this case half the crack length a. Thus, K will characterize the external conditions (i.e., the nominal applied stress σ and half the crack length a) that correspond to fracture when stresses and strains at the crack tip reach a critical value. This critical value of K is designated as K_c. It turns out, as we shall see later, that K_c depends on the dimensions of the specimen. In the case of a thin sample (plane-stress conditions), K_c depends on the thickness of the sample, whereas in the case of a sufficiently thick sample (plane-strain conditions), K is independent of the thickness of the specimen and is designated as K_{Ic}.

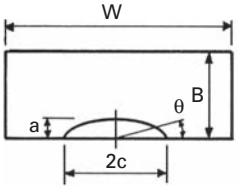

Semi-elliptical surface flaw in tension:

$$K_1 = Y\frac{\sigma\sqrt{\pi a}}{\frac{3\pi}{8} + \frac{\pi}{8}\frac{a^2}{c^2}}\left(\sin^2\theta + \frac{a^2}{c^2}\cos^2\theta\right)^{1/4}$$

$Y = 1.12$ (for W, B Large)

$$Y = \left(\frac{a}{B}, \frac{a}{c}, \frac{c}{W}, \theta\right)$$

$$Y = \left[Y_1 + Y_2\left(\frac{a}{B}\right)^2 + Y_3\left(\frac{a}{B}\right)^4\right]Y_4 g(\theta)g(W)$$

$$Y_1 = 1.13 - 0.09\left(\frac{a}{c}\right)$$

$$Y_2 = -0.54 + \frac{0.89}{0.2 + \left(\frac{a}{c}\right)}$$

$$Y_3 = 0.5 - \frac{1.0}{0.65 + \left(\frac{a}{c}\right)} + 14\left(1.0 - \frac{a}{c}\right)^{24}$$

$$Y_4 = 1 + \left[0.1 + 0.35\left(\frac{a}{B}\right)^2\right](1 - \sin\theta)^2$$

$$g(\theta) = \left[\sin^2\theta + \left(\frac{a}{c}\right)^2\cos^2\theta\right]^{1/8}$$

$$g(W) = \left[\sec\frac{\pi c}{W}\sqrt{\frac{a}{B}}\right]^{1/2}$$

for: $0 < \frac{a}{c} < 1$ $\quad 0 < \frac{a}{B} < 1$

$0 < \frac{c}{B} < 0.5$ $\quad 0 < \theta < \pi$

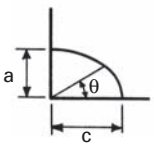

Quarter elliptical corner crack in tension:

$$K_1 = Y\frac{\sigma\sqrt{\pi a}}{\frac{3\pi}{8} + \frac{\pi}{8}\frac{a^2}{c^2}}\left(\sin^2\theta + \frac{a^2}{c^2}\cos^2\theta\right)^{1/4}$$

$Y = 1.2$

Fig. 7.13 (*cont.*)

The stress intensity factor K measures the amplitude of the stress field around the crack tip and should not be confused with the stress concentration factor K_t discussed in Section 7.3.2. It is also important to distinguish between K and K_c or K_{Ic}. The stress intensity factor K is a quantity, determined analytically or not, that varies as a function of configuration (i.e., the geometry of the crack and the manner of application of the external load). Thus, the analytical expression for K varies from one system to another. However, once K attains its critical value, K_{Ic}, in plane strain for a given system and material, it is essentially a constant for all the systems made of this material. The difference between K_c and K_{Ic} is that K_c depends on the thickness of the specimen, whereas K_{Ic} is independent of the thickness. The forms of K for various load and crack configurations have been calculated and are available in various handbooks. Some of the more common configurations and the corresponding expressions for K are presented in Figure 7.13.

For samples of finite dimensions, the general practice is to consider the solution for an infinite plate and modify it by an algebraic or trigonometric function that would make the surface tractions vanish. Thus, for a central through-the-thickness crack of length $2a$, in a plate of width W, we have

$$K = \sigma \left(W \tan \frac{\pi a}{W} \right)^{1/2}. \tag{7.26}$$

For the same crack in an infinite plate, we have

$$K = \sigma \sqrt{\pi a}.$$

If we expand $\tan \pi a/W$ in a series (Equation 7.26), we get

$$\begin{aligned} K &= \sigma W^{1/2} \left(\frac{\pi a}{W} + \frac{\pi^3 a^3}{3W^3} + \cdots \right)^{1/2} \\ &= \sigma \sqrt{\pi a} \left(1 + \frac{\pi^3 a^3}{3W^3} + \cdots \right)^{1/2}. \end{aligned}$$

Thus, for an infinite solid, $a/W = 0$, and we have $K = \sigma \sqrt{\pi a}$, as expected. For an edge crack in a semi-infinite plate, we have $K = 1.12 \sigma \sqrt{\pi a}$. The factor 1.12 here takes care of the fact that stresses normal to the free surface must be zero.

At this point, it is appropriate to make some comments on the limitations of LEFM. It was pointed out earlier that the expressions for stress components (Equations 7.21–7.23) are valid only in the neighborhood of the crack tip. The reader will have noticed that these stress components tend to infinity as we approach the tip (i.e., as r goes to zero). Now, there does not exist a material in real life that can resist an infinite stress. The material in the neighborhood of the crack tip, in fact, would inevitably deform plastically. Thus, these expressions for stress components based on linear elasticity theory are not valid in the plastic zone at the crack tip. The deformation process in a plastic zone, as is well known, will be a sensitive function of the microstructure, among other things. However, in spite of ignorance of the exact nature of the plastic zone, the LEFM treatment is valid for low-enough stresses such that the size of the plastic zone at the crack tip is small with respect to the crack length and the dimensions of the sample. We shall see in the next section how to incorporate a correction term for the presence of a plastic zone at the crack tip.

7.6.6 Plastic-Zone Size Correction

Equations 7.21–7.23 show a $\sqrt{r}$ singularity; that is, σ_{11}, σ_{22}, and σ_{12} go to infinity when $\sqrt{r}$ goes to zero. For a great majority of materials, local yielding will occur at the crack tip, which would relax the peak stresses. As we shall see shortly, the utility of the elastic stress field equations is not affected by the presence of this plastic zone as long as the nominal stress in the material is below the general yielding stress of the material.

When yielding occurs at the crack tip, it becomes blunted; that is, the crack surfaces separate without any crack extension. (See

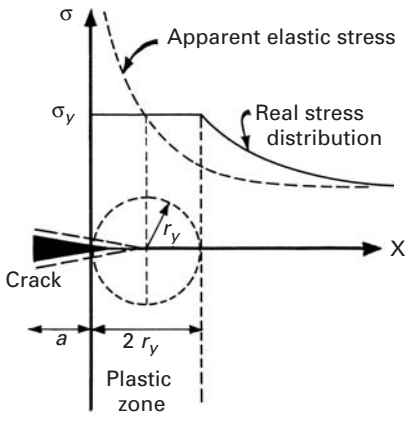

Fig. 7.14 Plastic-zone correction. The effective crack length is $(a + r_y)$.

Figure 7.14.) The plastic zone (radius r_y) will then be embedded in an elastic stress field. Outside and far away from the plastic zone, the elastic stress field "sees" the crack and the perturbation due to the plastic zone, as if there were present a crack in an elastic material with the leading edge of the crack situated inside the plastic zone. A crack of length $2(a + r_y)$ in an ideal elastic material produces stresses almost identical to elastic stresses in a locally yielded member outside the plastic zone. If the stress applied is too large, the plastic zone increases in size in relation to the crack length, and the elastic stress field equations lose precision. When the whole of the reduced section yields, the plastic zone spreads to the edges of the sample, and K does not have any validity as a parameter defining the stress field.

When the plastic zone is small in relation to the crack length, it can be visualized as a cylinder (Figure 7.14) of radius r_y at the crack tip. From Equation 7.24, for $\theta = 0$, $r = r_y$, and $\sigma_{22} = \sigma_y$, the yield stress, we can write

$$\sigma_y = \frac{K}{\sqrt{2\pi r_y}},$$

and, to a first approximation, the plastic-zone radius will be

$$r_y = \frac{1}{2\pi}\left(\frac{K}{\sigma_y}\right)^2. \tag{7.27}$$

In fact, the plastic-zone radius is a little bigger than $(1/2\pi)(K/\sigma_y)^2$, due to redistribution of load in the vicinity of the crack tip. Irwin,[7] taking into account the plastic constraint factor in the case of plane strain, gave the following expressions for the size of the plastic zone:

$$\boxed{r_y \approx \frac{1}{2\pi}\left(\frac{K}{\sigma_y}\right)^2} \quad \text{(plane stress)},$$

$$\boxed{r_y \approx \frac{1}{6\pi}\left(\frac{K}{\sigma_y}\right)^2} \quad \text{(plane strain)}.$$

[7] G. R. Irwin, in *Encyclopaedia of Physics*, Vol. VI (Heidelberg: Springer-Verlag, 1958); see also *J. Basic Eng., Trans. ASME*, 82 (1960) 417.

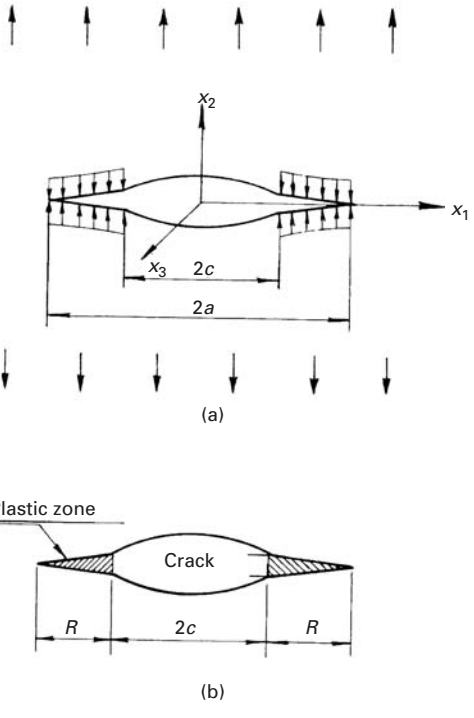

Fig. 7.15 Dugdale–Bilby–Cottrell–Swinden (BCS) model of a crack.

Thus, the center of perturbation, the apparent crack tip, is located a distance r_y from the real crack tip. The effective crack length is, then,

$$(2a)_{\text{eff}} = 2(a + r_y).$$

Substituting $(a + r_y)$ for a in the elastic stress field equations gives an adequate adjustment for the crack-tip plasticity under conditions of small-scale yielding. With this adjustment, the stress intensity factor K is useful for characterization of the fracture conditions.

There is another model for the plastic zone at the crack tip for the plane-stress case, called the Dugdale–BCS model.[8] In this model, the plasticity spreads out at the two ends of a crack in the form of narrow strips of length R (Figure 7.15). These narrow plastic strips in front of the actual crack tips are under the yield stress σ_y that tends to close the crack. Mathematically, the internal crack of length $2c$ is allowed to extend elastically a distance $2a$, and then internal stress is applied to reclose the crack in this region. Combining the internal stress field surrounding the plastic enclaves with the external stress field associated with the applied stress σ acting on the crack, Dugdale showed that

$$\frac{c}{a} = \cos\frac{\pi\sigma}{2\sigma_y}.$$

[8] B. A. Bilby, A. H. Cottrell, and K. H. Swinden, *Proc. Roy. Soc.*, A272 (1963) 304; D. S. Dugdale, *J. Mech. Phys. Solids*, 8 (1960) 100.

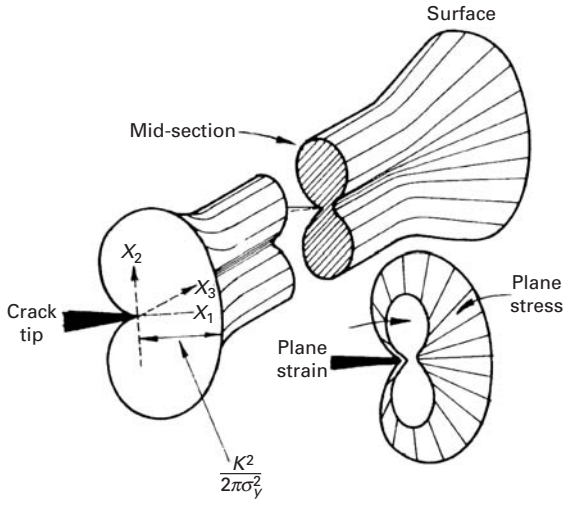

Fig. 7.16 Formal representation of the plastic zone at the crack tip for a through-the-thickness crack in a plate.

From this relation, one notes that as $\sigma \to \sigma_y$, $c/a \to 0$, $a \to \infty$ (i.e., general yielding occurs). On the other hand, as σ/σ_y decreases, we can write (using the series expansion for cosine),

$$\frac{c}{a} = 1 - \frac{\pi^2\sigma^2}{8\sigma_y^2} + \cdots.$$

Noting that $a = c + R$ and using the binomial expansion, we have

$$\frac{c}{a} = \frac{c}{c+R} = \left(1 + \frac{R}{c}\right)^{-1} = 1 - \frac{R}{c} + \cdots.$$

Thus, for $\sigma \ll \sigma_y$,

$$\frac{R}{c} \approx \frac{\pi^2}{8}\left(\frac{\sigma}{\sigma_y}\right)^2,$$

or

$$R \approx \frac{\pi}{8}\left(\frac{K}{\sigma_y}\right)^2. \tag{7.28}$$

Comparing Equation 7.28 with Equation 7.27, we see that there is good agreement between the two ($\pi/8 \approx 1/\pi$). In fact, the size of the plastic zone varies with θ also. A formal representation of the plastic zone at the crack front through the plate thickness is shown in Figure 7.16.

7.6.7 Variation in Fracture Toughness with Thickness

The elastic stress state is markedly influenced by the plate thickness, as indicated by Equation 7.24. The material in the plastic zone deforms in such a way that its volume is kept constant. Thus, the large deformations in the x_1 and x_2 directions tend to induce a contraction in the x_3 direction (parallel to the direction of the crack front or the plate thickness), which is resisted by the surrounding elastic material. We next perform a dimensional analysis. Since the elastic material

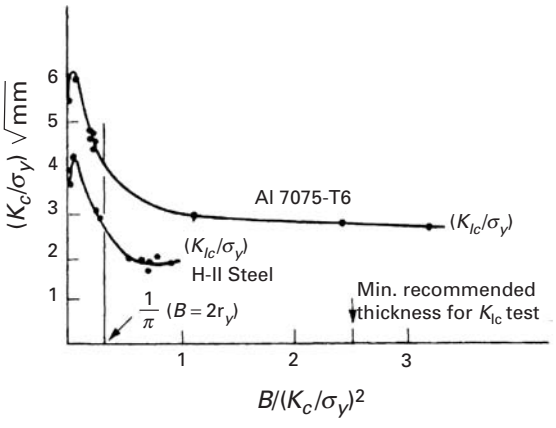

(a)

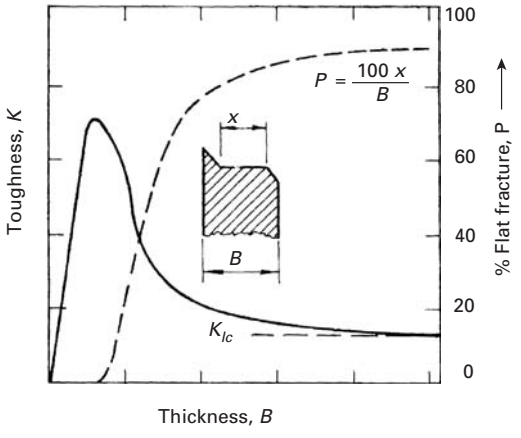

(b)

Fig. 7.17 (a) Variation in fracture toughness (K_c) with plate thickness (B) for Al 7075-T6 and H-11 Steel. (Reprinted with permission from J. E. Srawley and W. F. Brown, ASTM STP 381 (Philadelphia: ASTM, 1965), p 133, and G. R. Irwin, in *Encyclopaedia of Physics*, Vol. VI (Heidelberg: Springer Verlag, 1958); see also *J. Basic Eng., Trans. ASME*, 82 (1960) 417.) (b) Schematic variation of fracture toughness K_c and percentage of flat fracture P with the plate thickness B.

surrounding the plastic zone is the primary source of constraint, the size of the plastic zone, $2r_y$, should be compared with the plate thickness B. The ratio of the plate thickness B to the size of the plastic zone, $2r_y$, is given by

$$\frac{B}{2r_y} = \pi \frac{B}{(K_c/\sigma_y)^2},$$

and this would be a convenient parameter to characterize the variation of fracture toughness, K_c, with thickness. Data for Al 7075-T6 and H-11 steel are plotted in Figure 7.17(a) in the form[9] of K_c/σ_y versus $B/(K_c/\sigma_y)^2$. Observe that when $B/(K_c/\sigma_y)^2$ is greater than $1/\pi$ (i.e., $B \gg 2r_y$), the fracture toughness value K_c does not change with B. Apparently, beyond a thickness $B \gg 2r_y$, the constraint in the thickness direction (x_3) is completely effective, and additional plate thickness

[9] J. E. Srawley and W. F. Brown, American Society for Testing and Materials, Special Technical Publication (ASTM STP) 381 (Philadelphia: ASTM, 1965), p. 133; W. F. Brown and J. E. Srawley, ASTM STP 410 (Philadelphia: ASTM, 1966), p. 1.

does not change K_c. This particular value of K_c that is independent of the thickness of the specimen is labeled the fracture toughness of the material, and the symbol K_{Ic} is used to denote it.

On the other extreme, when the ratio $B/(K_c/\sigma_y)^2$ is much smaller than $1/\pi$ (i.e., $B \ll 2r_y$), we expect the fracture toughness to increase linearly with the plate thickness. In the region of $B/(K_c/\sigma_y)^2 = 1/\pi$ corresponding to $B = 2r_y$, the data for both materials show a rapid fall to a constant level of K_{Ic}. This decrease in the peak value of K_c (Figure 7.17(b)) to the K_{Ic} level represents a change in the fracture mode from a plane-stress type to a plane-strain condition. The fracture in a relatively thin plate (plane stress) usually consists of a certain fraction of slant fracture (high energy) and another fraction of flat fracture (low energy). In general, with increasing thickness of the specimen, the percentage of slant fracture decreases, and the energy necessary for crack propagation also decreases – hence the fall in the K_c value. At a certain critical thickness, the crack propagates under plane-strain conditions, and the stress intensity factor reaches the minimum value designated as K_{Ic}. Figure 7.17(b) shows schematically the variation of K_c and the percentage of flat fracture P with the plate thickness B. K_{Ic} is especially relevant in the evaluation of the material, as it is a constant that is essentially independent of the dimensions of the specimen.

Example 7.5

Establish the maximum load that the component shown in Figure E7.5, made of Ti-6Al–4V alloy, can withstand ($\sigma_y = 900$ MPa, $K_{Ic} = 100\ MPa\ \mathrm{m}^{1/2}$).

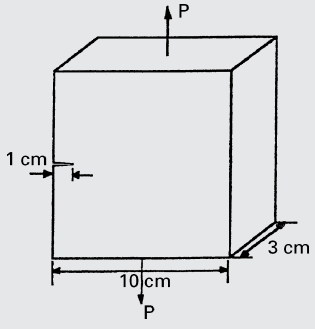

Fig. E7.5

Solution:

$$
\begin{aligned}
a &= 1\,\mathrm{cm},\\
W &= 1\,\mathrm{cm}.\\
K_{Ic} &= Y\sigma\sqrt{\pi a}, \qquad (1)\\
Y &= 1.12 - 0.231\left(\frac{a}{W}\right) + 10.55\left(\frac{a}{W}\right)^2\\
&= 1.12 - 0.231\left(\frac{1}{10}\right) + 10.55\left(\frac{1}{10}\right)^2\\
&= 1.20.
\end{aligned}
$$

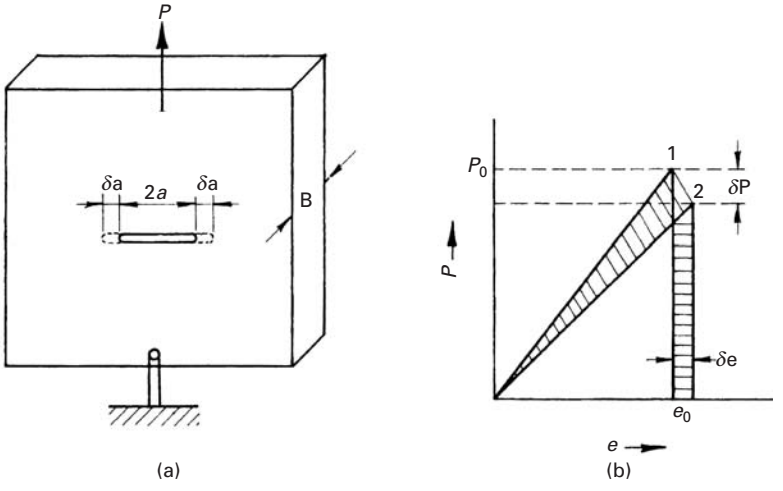

Fig. 7.18 (a) Elastic body containing a crack of length $2a$ under load P. (b) Diagram of load P versus displacement e.

We rewrite Equation 1 as

$$\sigma = \frac{K_{Ic}}{Y\sqrt{\pi a}}$$

to get

$$\sigma = \frac{100}{1.20\sqrt{\pi \times 10^{-2}}} = 470 \text{ MPa} < \sigma_y.$$

Therefore,

$$\frac{P}{A} = \sigma \quad \text{and} \quad P = \sigma A = (470 \times 10^6) \times (10 \times 10^{-2} \times 3 \times 10^{-2})$$
$$= 1{,}410 \text{ kN}.$$

Hence, the existing flaw, and not the yield stress, limits the maximum load.

7.7 Fracture Toughness Parameters

In this section, we describe the variety of fracture toughness parameters that have come into being.

7.7.1 Crack Extension Force *G*

The concept of the crack extension force G, attributed to Irwin, can be interpreted as a generalized force. One can say that fracture mechanics is the study of the response of a crack (measured in terms of its velocity) to the application of various magnitudes of the crack extension force. Let us consider an elastic body of uniform thickness B, containing a through-the-thickness crack of length $2a$. Let the body be loaded as shown in Figure 7.18(a). With increasing load P, the displacement e of the loading point increases. The load–displacement diagram is shown in Figure 7.18(b). At point 1, we have the load as P_0 and displacement as e_0. Now let us consider a "gedanken" experiment in which the crack extends by a small increment, δa. Due to this

small increment in crack extension, the loading point is displaced by δe, while the load falls by δP. Now, before the crack extension, the potential energy stored in body was

$$U_1 = \frac{1}{2} Pe,$$

represented by the area of the triangle through point 1 in the figure. After the crack extension, the potential energy stored in the body is

$$U_2 = \frac{1}{2}(P - \delta P)(e + \delta e),$$

represented by the area of the triangle passing through point 2 in the figure. In this process of crack extension, the change in potential energy, $U_2 - U_1$ is given by the difference in the areas of the two crosshatched regions in the figure. Considering the small increment δa in crack length, we can write an equation for G, the crack extension force per unit length, as

$$GB\ \delta a = U_2 - U_1 = \delta U.$$

The change in elastic strain energy with respect to the crack area, in the limit of the area going to zero, equals the crack extension force; that is,

$$G = \lim_{\delta A \to 0} \frac{\delta U}{\delta A},$$

where $\delta A = B\ \delta a$.

It is convenient to evaluate G in terms of the compliance c of the sample, defined as

$$e = cP. \tag{7.29}$$

Now,

$$\delta U = U_2 - U_1 = \frac{1}{2}(p - \delta P)(e + \delta e) - \frac{1}{2} Pe,$$

or

$$\delta U = \frac{1}{2} P\ \delta e - \frac{1}{2} e\ \delta P - \frac{1}{2} \delta P\ \delta e. \tag{7.30}$$

Differentiating Equation 7.29, we have

$$\delta e = c\ \delta P + P\ \delta c. \tag{7.31}$$

Substituting Equation 7.31 in Equation 7.30, we obtain

$$\delta U = \frac{1}{2} Pc\ \delta P + \frac{1}{2} P^2 \delta c - \frac{1}{2} e\ \delta P - \frac{1}{2} e(\delta P)^2 - \frac{1}{2} P\ \delta P\ \delta c. \tag{7.32}$$

Remembering that $e = cP$ and ignoring the higher order product terms, we can write

$$\delta U = \frac{1}{2} Pc\ \delta P + \frac{1}{2} P^2 \delta c - \frac{1}{2} Pc\ \delta P,$$

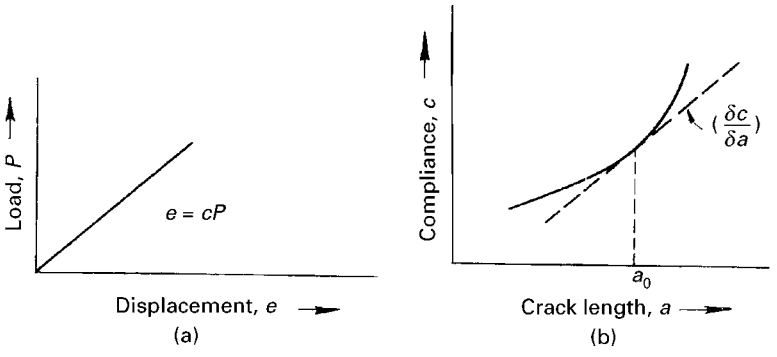

Fig. 7.19 (a) Load P versus displacement e. Compliance c is the inverse of the slope of this curve. (b) Compliance c versus crack length a. a_0 is the initial crack length.

or

$$\delta U = \frac{1}{2} P^2 \, \delta c. \tag{7.33}$$

Then

$$G = \lim_{\delta A \to 0} \frac{\delta U}{\delta A} = \lim_{\delta A \to 0} \frac{\frac{1}{2} P^2 \delta c}{\delta A},$$

or

$$\boxed{G = \frac{1}{2} \frac{P^2}{B} \frac{\delta c}{\delta a}.} \tag{7.34}$$

From Equation 7.34, we see that G is independent of the rigidity of the surrounding structure and the test machine. In fact, G depends only on the change in compliance of the cracked member due to crack extension. Thus, to obtain G for a specimen, all we need to do is to determine the compliance of the specimen as a function of crack length and measure the gradient of the resultant curve, $\delta c/\delta a$, at the appropriate initial crack length (Figure 7.19).

This method is more useful for relatively small test samples, on which exact measurements can be made in the laboratory. One of the important uses of Equation 7.34 is that it provides a value of G (or K) for complex structures that have not been (or cannot be) treated analytically. An experimental determination of G_c, the critical crack extension force, using this equation requires the value of fracture load (measured experimentally) and the value of $\delta c/\delta a$. The compliance can be measured by calibrating a series of samples with different crack lengths. We obtain a diagram of c versus a, and $\delta c/\delta a$ is evaluated as the slope at the appropriate initial crack length.

Example 7.6

A titanium alloy (Ti–6% Al–4% V) is used for aircraft applications. The NDE methods used cannot detect flaws whose size is smaller than 1 mm. You are asked, as the design engineer, to specify the maximum tensile stress that the part can bear in plane-stress and plane-strain

situations. The yield stress of the alloy is 1,450 MPa.

$$E = 115 \text{ GPa},$$
$$\nu = 0.312,$$
$$G_c = 23.6 \text{ kN/m}.$$

Solution: We have

$$2a = 1 \text{ mm},$$

so that

$$a = 0.5 \times 10^{-3} \text{ m}.$$

The critical stress in plane stress is

$$\sigma_c = \sqrt{\frac{E G_c}{\pi a}}$$
$$= \left(\frac{115 \times 10^9 \times 23.6 \times 10^3}{\pi \times 0.5 \times 10^{-3}} \right)^{1/2}$$
$$= 1.31 \times 10^9 \text{ Pa}.$$

The critical stress in plane strain is

$$\sigma_c = \sqrt{\frac{E G_c}{\pi a(1 - \nu^2)}}$$
$$= 1.385 \times 10^9 \text{ Pa}.$$

Thus, the maximum stresses are 1.31 GPa (plane stress) and 1.385 GPa (plane strain).

From consideration of fracture toughness, the maximum stress is lower than the yield stress; hence, the former is the limiting stress.

7.7.2 Crack Opening Displacement

The development of a plastic zone at the tip of the crack results in a displacement of the faces without crack extension. This relative displacement of opposite crack edges is called the crack opening displacement (COD) (Figure 7.20). Wells[10] suggested that when this displacement at the crack tip reaches a critical value δ_c, fracture would ensue.

LEFM is applicable only when the plastic zone is small in relation to the crack length (i.e., well below the yield stress and in plane strain). Consider a small crack in a brittle material. We have

$$\sigma_c = K_{Ic}(\sqrt{\pi a})^{-1}, \quad \text{as} \quad a \to 0, \quad \sigma_c \to \infty.$$

But this, as we very well know, does not occur. Instead, a plastic zone develops and may extend through the section such that

$$\sigma_{\text{net}} = \sigma \frac{W}{W - a} \geq \sigma_y,$$

[10] A. A. Wells, *Brit. Weld. J.*, 13 (1965) 2.

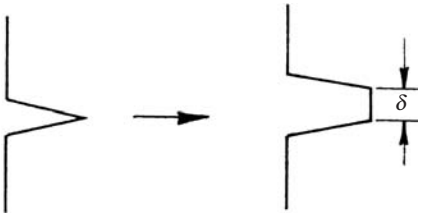

Fig. 7.20 Crack opening displacement.

where W is the width of sample and σ_y is the yield stress. In practice, $\sigma_c \leq 0.66\sigma_y$ for the K_{Ic} validity.

In more ductile materials, the critical stress predicted by LEFM will be higher than σ_y. One can use the concept of COD in such cases. In the elastic case (Figure 7.20),

$$COD = \Delta = \frac{4\sigma}{E}\sqrt{(a^2 - x^2)}. \tag{7.35}$$

At the center of the crack ($x = 0$), the maximum opening is

$$\Delta_{\max} = \frac{4\sigma a}{E}.$$

Applying the plastic zone correction, we have, from Equation 7.35,

$$\Delta = \frac{4\sigma}{E}\sqrt{(a + r_y)^2 - x^2},$$

where $(a + r_y)$ is the effective crack length.

The crack-tip opening displacement (CTOD), δ, is given for $x = a$ and $r_y \ll a$ as

$$\delta = \frac{4\sigma}{E}\sqrt{2ar_y}. \tag{7.36}$$

A displacement of the origin to the crack tip gives a general expression for the crack opening:

$$\Delta = \frac{4\sigma}{E}\sqrt{2a_{\text{eff}}r_y}.$$

Substituting $r_y = \sigma^2 a/2\sigma_y^2$ (see Equation 7.27) in Equation 7.36 gives

$$\delta = \frac{4}{\pi}\frac{K_I^2}{\mathrm{E}\sigma_y}. \tag{7.37}$$

Equation 7.37 is valid in the LEFM regime, and fracture occurs when $K_I = K_{Ic}$, which corresponds to $\delta = \delta_{Ic}$, a material constant.

The use of the COD criterion demands the measurement of δ_c. Direct measurement of δ_c is not easy. An indirect way is the following. We have

$$\begin{aligned}\Delta &= \frac{4\sigma}{E}\sqrt{(a + r_y)^2 - x^2} \\ &= \frac{4\sigma}{E}\sqrt{a + 2ar_y + r_y^2 - x^2}.\end{aligned}$$

Ignoring the r_y^2 term and using the relationship of Equation 7.36, we can write

$$\Delta = \frac{4\sigma}{E}\left(a^2 - x^2 + \frac{E^2}{16\sigma^2}\delta^2\right)^{1/2}. \tag{7.38}$$

According to this equation, δ can be measured indirectly from a COD measurement (e.g., at $x = 0$, at the center of the crack) without making any simplifications about the plastic-zone size correction. Δ can be measured by means of a clip gage.

Another way of obtaining δ is to use the equations of Dugdale–BCS model of the crack. (See Section 7.6.6.) According to Dugdale–BCS model (Bilby, Cotrell, Swinden, op. cit.; Dugdale, op. cit.)

$$\delta = \frac{8\sigma_y a}{\pi E}\log\sec\frac{\pi\sigma}{2\sigma_y}.$$

Expanding the log sec function in series, we get

$$\delta = \frac{8\sigma_y a}{\pi E}\left[\frac{1}{2}\left(\frac{\pi\sigma^2}{2\sigma_y}\right)^2 + \frac{1}{12}\left(\frac{\pi\sigma}{2\sigma_y}\right)^4 + \cdots\right].$$

For $\sigma \ll \sigma_y$, we can write (neglecting fourth- and higher-order terms)

$$\delta = \frac{\pi\sigma^2}{E\sigma_y} = \frac{G_I}{\sigma_y}. \tag{7.39}$$

Comparing Equation 7.39 with Equation 7.37, we note that the difference is in the factor $4/\pi$, which comes from the plastic-zone correction. In general,

$$\boxed{\delta = \frac{G_I}{\lambda\sigma_y} = \frac{K_I^2(1-\nu^2)}{E\lambda\sigma_y} \quad \text{(for plane strain).}} \tag{7.40}$$

The factor $(1 - \nu^2)$ should be ignored in the case of plane stress.

In the literature, we encounter various values of λ. These depend on the exact location where CTOD is determined (i.e., the exact location of the crack tip). Wells[11] suggested that, experimentally, $\lambda \approx 2.1$ for compatibility with LEFM (i.e., limited plasticity). For cases involving extensive plasticity, the engineering design application approach is to take $\lambda \approx 1$.

Thus, at unstable fracture, $G_{Ic} = \lambda\sigma_y\,\delta_c$. The important point about COD is that, theoretically, δ_c can be computed for both elastic and plastic materials, whereas G_{Ic} is restricted only to the elastic regimen. The COD thus allows one treat fracture under plastic conditions. A word of caution is in order, however. Figure 7.21 presents a comparison between COD and CTOD. We should realize that the strain fields and crack opening displacements associated with a crack tip will be different for different specimen configurations. Thus, we cannot define a single critical COD value for a given material in a manner

[11] A. A. Wells, *Eng. Fract. Mech.*, 1 (1970) 399.

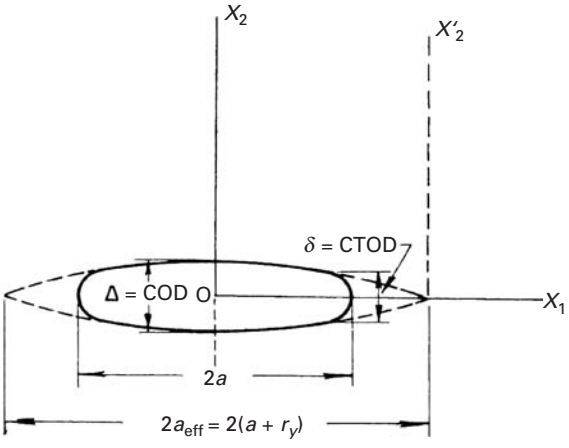

Fig. 7.21 Relationship between crack opening displacement (COD, Δ), crack-tip opening displacement (CTOD, δ), crack length ($2a$), and size of plastic zone (r_y).

equivalent to that of K_{Ic}, as the COD value will be affected by the geometry of the test specimen.

Example 7.7

If the toughness of a thermoplastic polymer $G_c = 103\ \text{J m}^{-2}$, what would be the critical crack length under an applied stress of 200 MPa? Take Young's modulus of the polymer to be 10 GPa.

Solution: We have

$$G_c = 10^3\ \text{J m}^{-2}, \quad E = 10\ \text{GPa}, \quad \sigma = 200\ \text{MPa}.$$

Thus, the critical crack length $a_c = EG_c/\pi\sigma^2 = 10 \times 10^9 \times 10^3/\pi\ (200 \times 10^6)^2 = 0.08$ mm.

7.7.3 *J* Integral

J integral is another variant for fracture toughness analysis. It provides a value of energy required to propagate a crack in an elastic–plastic material. The mathematical foundation for the *J* integral was laid by Eshelby,[12] who applied it to dislocations. Cherepanov[13] and Rice[14] applied it, independently, to cracks. Figure 7.22 shows a closed contour Γ in a two-dimensional body. When such a body is subjected to external forces, internal stresses arise in it. On the basis of the theory of conservation of energy, Eshelby showed that the integral *J* is equal to zero for a closed contour; that is,

$$J = \int_{\Gamma} \left(W dx_2 - T \frac{\partial u}{\partial x_1} ds \right) = 0, \tag{7.41}$$

[12] J. D. Eshelby, *Phil. Trans. Roy. Soc London*, A244 (1951) 87.
[13] G. P. Cherepanov, *Appl. Math. Mech.* (*Prinkl. Mat. Mekh.*), 31, no. 3 (1967) 503.
[14] J. R. Rice, *J. Appl. Mech.*, 35 (1968) 379.

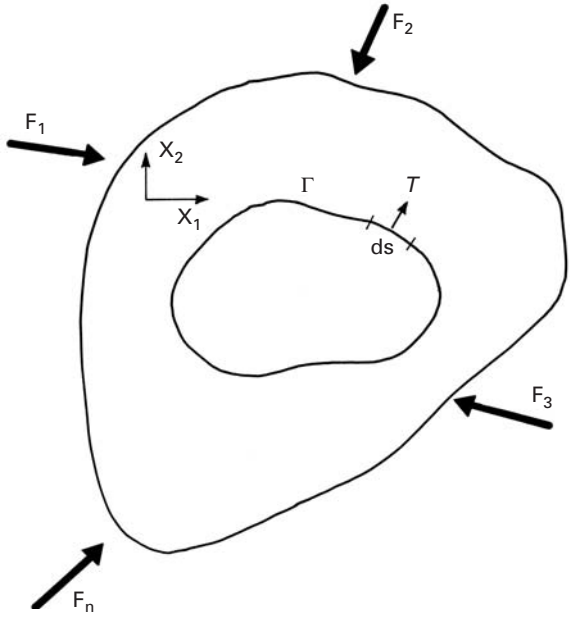

Fig. 7.22 A body subjected to external forces $F_1, F_2, \ldots, F_n$ and with a closed contour Γ.

where

$$W = \int_0^{\Sigma_{ij}} \sigma_{ij} d\varepsilon_{ij}$$

is the strain energy per unit volume (see Chapter 2), T is the tension vector (traction) perpendicular to Γ and pointing to the outside of the contour, ds is an element of length along the contour, and u is the displacement in the x_1 direction. The J integral is an energy related quantity; similar to the crack extension force G, J has the units of energy per unit area (J/m^2) or force per unit length (N/m).

Figure 7.23 shows a crack, around which a contour *ABCDEFA* is made. The total J must be zero, i.e.,

$$J = J_{\Gamma_1+\Gamma_2} = 0.$$

Along *AF* and *CD* (crack surfaces), the tractions T are equal to zero. The same is true for the normal and shear stresses. Thus, $J_{AF} = J_{CD} = 0$. It can therefore be concluded that

$$J_{\Gamma_1+\Gamma_2} = J_{\Gamma_1} + J_{\Gamma_2} + J_{AF} + J_{CD} = 0, \quad J_{\Gamma_1} = -J_{\Gamma_2}.$$

Hence, the J integral along two different paths around a crack has the same value. That is, in general, the J integral around a crack is path independent.

From a physical point of view, the J integral represents the difference in the potential energies of identical bodies containing cracks of length a and $a + da$; in other words, the J integral around a crack is equal to the change in potential energy for a crack extension da. For a body of thickness B, this can be written as

$$J = \frac{1}{B}\frac{\delta U}{\delta a}, \tag{7.42}$$

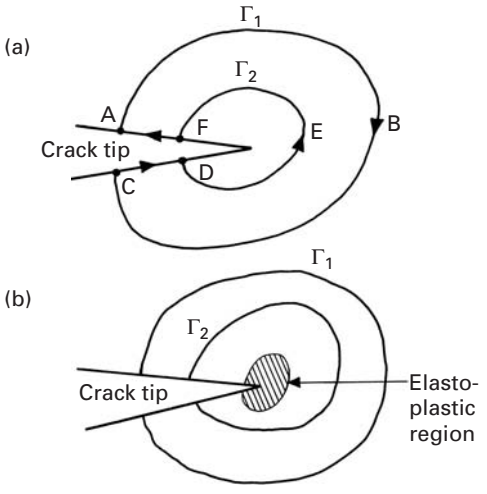

Fig. 7.23 Eshelby contours around cracks.

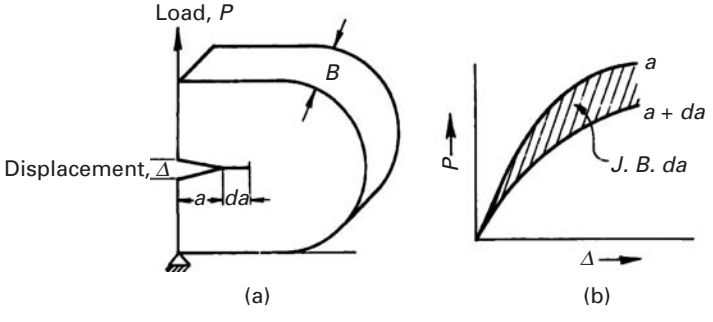

Fig. 7.24 Physical interpretation of the J integral. The J integral represents the difference in potential energy (shaded area) of identical bodies containing cracks of length a and $a + da$.

where U is the potential energy, a the crack length, and B the plate thickness. U is equal to the area under the curve of load versus displacement. Figure 7.24 shows this interpretation, where the shaded area is $\delta U = JB\ \delta a$. Like G_{Ic}, J_{Ic} measures the critical energy associated with the initiation of crack growth, but in this case accompanied by substantial plastic deformation. In fact, Begley and Landes[15] showed the formal equivalence of J_{Ic} and G_{Ic} by measuring the J_{Ic} from small fully plastic specimens and the G_{Ic} from large elastic specimens satisfying the plane-strain conditions for the LEFM test.

The path independence of the J integral, together with this interpretation in terms of energy, makes it a powerful analytical tool. The J integral is path independent in the case of either linear or nonlinear materials behaving elastically. When extensive plastic deformation occurs, the practice is to assume that the plastic yielding can be described by the deformation theory of plasticity. According to this theory, stresses and strains are functions only of the point of measurement and not of the path taken to get to that point. As in the case of slow, stable crack growth, there will be a relaxation of stresses at the crack tip, so there will be a violation of this postulate.

[15] J. A. Begley and J. D. Landes, ASTM STP 514, (Philadelphia: ASTM, 1972), p. 1.

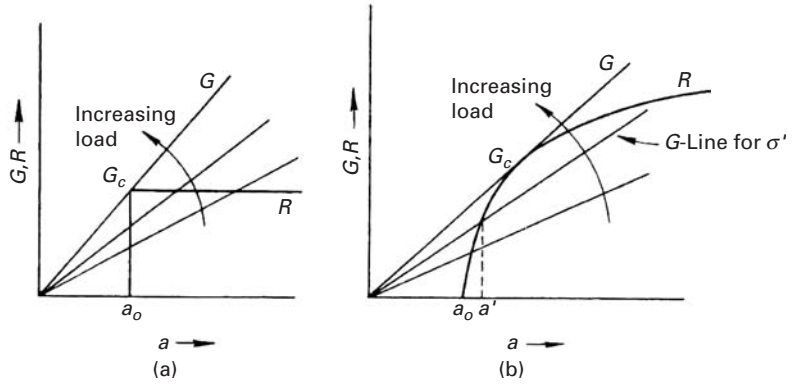

Fig. 7.25 *R* curves for (a) brittle material and (b) ductile material.

Thus, the use of the J integral should be limited to the initiation of crack propagation, by stable or unstable processes. Studies using incremental plasticity or flow theories with finite elements indicate the path independence of the J integral.

7.7.4 *R* Curve

The R curve characterizes the resistance of a material to fracture during slow and stable propagation of a crack. An R curve graphically represents this resistance to crack propagation of the material as a function of crack growth. With increasing load in a cracked structure, the crack extension force G at the crack tip also increases. (See Equation 7.34.) However, the material at the tip presents a resistance R (sometimes, the symbol K_R is used) to crack growth. According to Irwin, failure will occur when the rate of change of the crack extension force ($\partial G/\partial a$) equals the rate of change of this resistance to crack growth in the material ($\partial R/\partial a$). The resistance of the material to crack growth, R, increases with an increase in the size of the plastic zone. Since the plastic zone size increases nonlinearly with a, R will also be expected to increase nonlinearly with a. G increases linearly with a. Figure 7.25 shows the instability criterion: the point of tangency between the curves of G versus a and R versus a. Figure 7.25(a) shows the R curve for a brittle material, and Figure 7.25(b) shows the R curve for a ductile material. Crack extension occurs for $G > R$. Consider the G line for a stress σ', shown in Figure 7.25(b). At the stress σ', the crack in the material will grow only from a_0 to a', since $G > R$ for $a < a'$, $G < R$ for $a > a'$, and the crack does not extend beyond a'. As the load is increased, the position of the G line changes, as indicated in the figure. When G becomes tangent to R, unstable fracture ensues. The R curve for a brittle material (Figure 7.25(a)) is a "square" curve, and the crack does not extend at all until the contact is reached, at which point $G = G_c$ and the unstable fracture follows.

The R-curve method is another version of the Griffith energy balance. One can conveniently make this kind of analysis if an analytical expression for the R curve is available. Experimental determination of R curves, however, is complicated and time consuming.

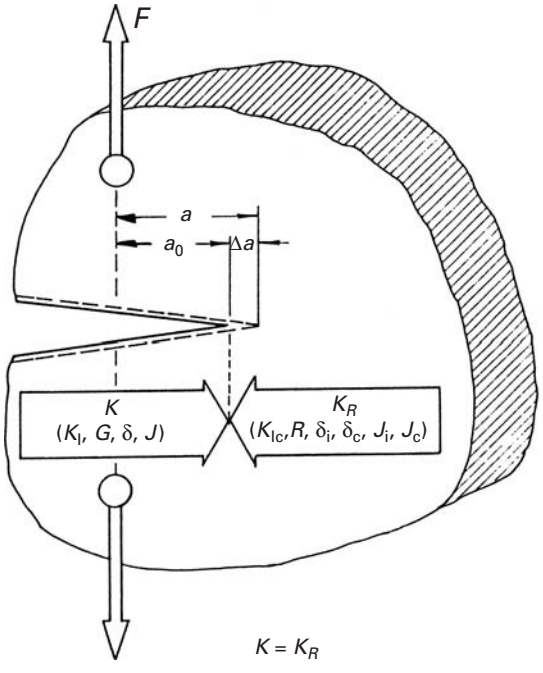

Fig. 7.26 Different parameters describing the growth of a crack.

7.7.5 Relationships among Different Fracture Toughness Parameters

So far, we have seen that, in our effort to develop a quantitative description of fracture toughness, various parameters, such as K, G, J, δ, R, etc., have been developed. Since all these parameters define the same physical quantity, it is not unexpected that they are interrelated. And we have mentioned in different sections the relationships among the parameters. Figure 7.26 summarizes these relationships. It would, however, be helpful to the reader to recapitulate these relationships, even at the risk of repeating. That is what we will do in this section.

If we take into account the stress distribution around the tip of a crack, we get the stress-intensity-factor (K) approach. The magnitude or the intensity of the local stresses is determined by K, because the form of the local crack-tip stress field is the same for all situations involving a remote stress σ. Thus, K, and not σ, is the local characterizing parameter. The fracture then occurs when the applied K attains the critical value K_c. In particular, when the specimen's dimensions satisfy the plane-strain condition, we call this value the plane-strain fracture toughness and denote it by K_{Ic}. The stress and the crack length corresponding to K_{Ic} are the fracture stress σ_c and the fracture crack length a_c. Note that the elastic constants of the material are not involved. The energy-release-rate approach gives us the crack extension force G, which is related to the parameters K by the equation

$$K^2 = E'G,$$

where $E' = E$, Young's modulus, in the case of plane stress and $E' = E/(1 - \nu^2)$ in the case of plane strain. Note that, in characterizing the fracture behavior in terms of G, we need to know the elastic constants of the material. Because in the case of polymers E is time dependent and very precise modulus data are not available, there is some advantage to using the K approach.

The critical crack opening displacement δ_c is another useful parameter. It is related to K by the equation

$$\delta_c = K_{Ic}^2/\lambda E\,\sigma_y,$$

where λ is a dimensionless constant that depends on the geometry of the specimen, its state of stress, and the work-hardening capacity of the material. λ has a value between 1 and 2. In particular, for the strip-yielding model of Dugdale–BCS, $\lambda = 1$.

The J integral provides yet another measure of fracture toughness. And, for small-scale yielding, we have

$$J = \lambda\delta\sigma_y.$$

In short, for small-scale yielding, we can sum up the relationships among the different fracture toughness parameters as

$$\boxed{J = G = K^2/E' = \lambda\sigma_y\delta,}$$

where the symbols have the usual meaning.

7.8 Importance of K_{Ic} in Practice

K_{Ic} is the critical stress intensity factor under conditions of plane strain ($\varepsilon_{33} = 0$), which is characterized by small-scale plasticity at the crack tip. The material is fully constrained in the direction of thickness. When determined under these rigorous conditions, K_{Ic} will be a material constant. Thus, when one needs to characterize materials by their toughness (in the same way that one characterizes materials by their ultimate tensile strength or tensile yield strength), only valid K_{Ic} data should be considered. This will be explained in Chapter 8.

K_c is the critical stress intensity factor under conditions of plane stress ($\sigma_{33} = 0$), which is characterized by large plasticity at the crack tip. In this case, the through-thickness constraint is negligible. K_c values can be up to two times greater than the K_{Ic} values of the same material. K_{Ic} depends on the temperature T, on the strain rate $\dot{\varepsilon}$, and on microstructural variables.

In general, K_c or K_{Ic} decreases as the (yield or ultimate) strength of a material increases. This inverse relationship between fracture toughness and strength is shown schematically in Figure 7.27. With concurrent improvement in the material's strength and toughness, this curve shifts in the direction of the arrow. The dependence of K_{Ic} on tensile strength and on sulfur level in a steel is shown in Figure 7.28. As expected, K_{Ic} decreases monotonically with increases in tensile

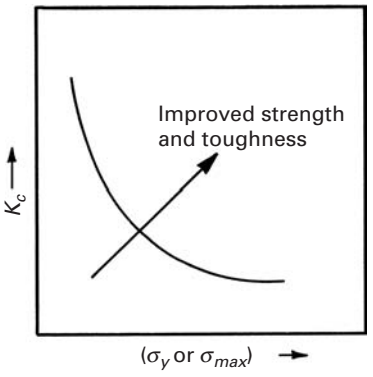

Fig. 7.27 Relationship between fracture toughness and yield stress.

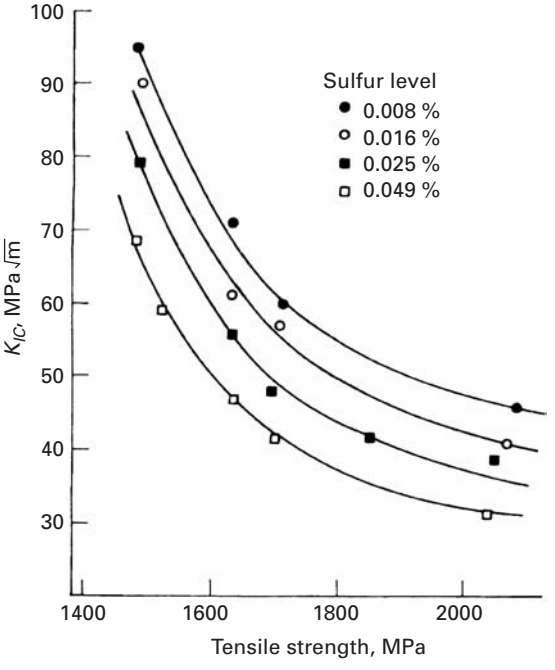

Fig. 7.28 Variation of fracture toughness K_{Ic} with tensile strength and sulfur content in a steel. (Adapted from A. J. Birkle, R. P. Wei, and G. E. Pellissier, *Trans. ASM*, 59 (1966) 981.)

strength or sulfur content. (Sulfur is well known to embrittle steels.) Figure 7.29 shows that the same holds for K_{Ic} as a function of the yield strength. K_c also depends on these variables.

Table 7.2 shows representative fracture toughnesses for selected materials. Metals have the highest toughness. For most ceramics, K_{Ic} does not exceed 5 MPa $\sqrt{\text{m}}$. The addition of partially stabilized zirconia to alumina increases K_{Ic} to 10 MPa $\sqrt{\text{m}}$ and even higher. The reason for this is a martensitic transformation that is described in greater detail in Chapter 11. Plastics have low K_{Ic}; however, we should remember that their density is only a small fraction of that of metals.

Table 7.2 Plane-Strain Fracture Toughnesses for Representative Materials

	Material	K_{Ic} (MPa $m^{1/2}$)
(a)	*Metals*	
	300M steel 300 °C temper	65
	300M steel 650 °C temper	152
	18-Ni maraging steel, vacuum melted	176
	18-Ni maraging steel, air melted	123
	AISI 4130 steel	110
	2024-T651 aluminum	24
	2024-T351 aluminum	34
	6061-T651 aluminum	34
	7075-T651 aluminum	29
	Ti-6Al-4V, mill annealed	106–123
	Ti-6Al-4V, recrystallized, annealed	77–116
(b)	*Ceramics*	
	Cement/concrete	0.2
	Soda–lime glass	0.7–0.9
	MgO	3
	Al_2O_3	3–5
	Al_2O_3 + 15% ZrO_2	10
	SiC	3–4
	Si_3N_4	4–5
(c)	*Polymers*	
	Epoxy	0.3–0.6
	Polyethylene, high-density	2
	Polyethylene, low-density	1
	Polypropylene	3
	ABS	3–4
	Polycarbonate	1–2.6
	PVC	2.4
	PVC (rubber modified)	3.4
	PMMA	1.8

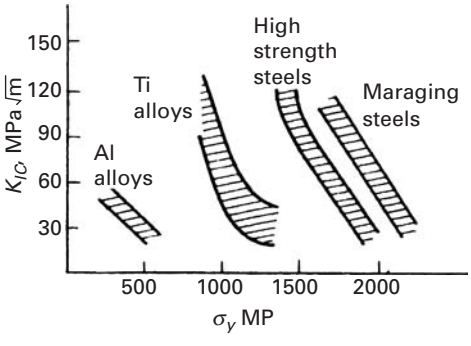

Fig. 7.29 Variation of fracture toughness K_{Ic} with yield strength σ_y for a series of alloys. (Adapted from D. Broek, *Elementary Engineering Fracture Mechanics*, 3rd ed. (Amsterdam: Martinus Nijhoff, 1978), p. 270.)

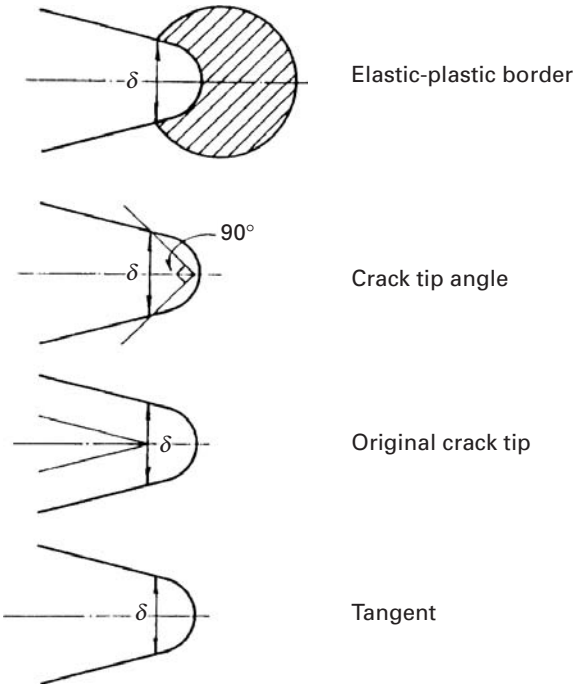

Fig. 7.30 Different measures of crack-tip opening displacement.

7.9 Post-Yield Fracture Mechanics

The concepts of crack opening displacement and the J integral are complementary. The crack tip opening displacement (CTOD), δ, is the parameter that controls crack extension. But the notion of CTOD is not problem free. For example, there exists a considerable amount of diversity in its very definition. Figure 7.30 shows some ways of measuring δ. The experimental determination of δ and the calculation of the relevant value for a cracked structure also involve uncertainties. We can split the CTOD value into an elastic and a plastic component, to wit:

$$\delta_t = \delta_{el} + \delta_{pl}.$$

The elastic portion is, of course, related to K or G, as indicated earlier. In particular, K_{Ic} and G_{Ic} correspond to δ_{Ic}, the CTOD value at the initiation of unstable fracture. The plastic portion is not strictly a material property, in as much as it depends on the specimen's dimensions, constraints, etc.

The J integral is, mathematically, a path-independent integral. From a practical engineering point of view, the J integral represents, similarly to G, a strain energy release rate and is related to the area under the curve load, P, and the *load line displacement*.

Just as we did for the concept of COD, we can write, for J,

$$J_{total} = J_{el} + J_{pl},$$

where J_{el} is the elastic portion, equal to K_I^2/E'. Here again, E' equals E for plane stress and $E/(1 - \nu^2)$ for plane strain. J_{pl} is a function of the geometry of the component and the crack load corresponding to extensive plastic deformation, and the material characteristics such as the yield strength, ultimate tensile strength, etc.

This division of the crack driving force into elastic and plastic parts is conceptually very convenient. Tests for the J integral, as well as for COD, are based on the fact that a ductile structure containing a crack is characterized by three successive stages:

1. Crack blunting and the initiation of propagation.
2. Slow and stable crack growth under increasing load.
3. Unstable crack growth, i.e., the instability.

A curve showing these stages is called a *resistance curve* (δ–R or J–R). It describes the material resistance as a function of stable crack growth a.

7.10 Statistical Analysis of Failure Strength

As we have repeatedly pointed out, materials in real life are never perfect. No matter how carefully processed a material is, it will always contain a distributions of flaws. The presence of flaws in ductile metals is not very serious, because these metals have the ability to deform plastically and thus attenuate, at least to some extent, the insidious effect of flaws on strength. The same cannot be said of brittle materials. Such preexisting flaws are responsible for the phenomenon of catastrophic fracture in these materials. In general, flaws vary in size, shape, and orientation; consequently, the strength of a material will vary from specimen to specimen. When we test a brittle material, one or several of the larger flaws propagate. In the case of a ductile material such as aluminum, most of the flaws get blunted because of plastic deformation, and only after considerable plastic deformation do microvoids form and coalesce, leading to an eventual fracture. (See Chapter 8.) If we were to test a large number of identical samples and plot the strength distribution of a brittle and a ductile solid, we would get the curves shown in Figure 7.31. The strength distribution curve for the ductile solid is very narrow and close to a Gaussian or normal distribution, while that for the brittle solid is very broad with a large tail on the high-strength side – that is, a non-Gaussian distribution. It turns out that the strength distribution of a brittle solid can be explained by a statistical distribution called the *Weibull distribution*, named after the Swedish engineer who first proposed it.[16] We next describe this distribution and its application to the analysis of the strength of brittle solids.

The basic assumption in Weibull distribution is that a body of material with volume V has a statistical distribution of noninteracting

[16] W. Weibull, *J. App. Mech.*, 18 (1951), 293.

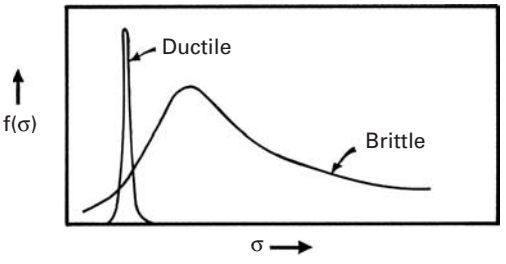

Fig. 7.31 Strength distribution of a brittle and a ductile solid.

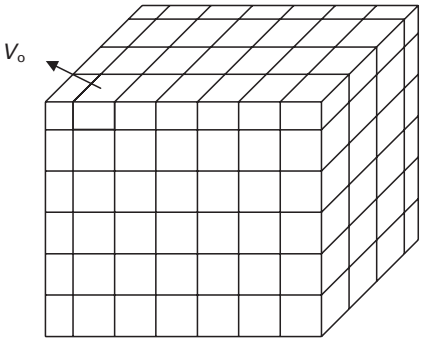

Fig. 7.32 Solid body with volume V composed of n cubes with volume V_0 each.

flaws. Thus, the body of volume V can be considered to be made up of n volume elements, each of unit volume V_0 and having the same flaw distribution. (See Figure 7.32.) Now, if we subject such a solid to an applied stress σ, the probability that the solid will survive can be written as

$$P(V) = P(V_0)P(V_0)\ldots\ldots P(V_0) = P(V_0)^n, \tag{7.43}$$

where V_0 is the volume of an element and n is the number of volume elements. Taking logarithms, we have

$$\ln P(V) = n \ln P(V_0),$$

or

$$P(V) = \exp[n \ln P(V_0)]. \tag{7.44}$$

Weibull defined a risk-of-rupture parameter

$$R = -[\ln P(V_0)], \tag{7.45}$$

or, alternatively,

$$P(V_0) = \exp(-R). \tag{7.46}$$

He then postulated that this parameter is given by

$$R = [(\sigma - \sigma_u)/\sigma_0]^m, \tag{7.47}$$

where σ is the applied stress and m, σ_0, and σ_u are material constants for a constant-flaw population, i.e., the flaw population does

Table 7.3 Typical Values of the Weibull Modulus m for Some Materials

Material	m
Traditional Ceramics: Brick, Pottery, Chalk	<3
Engineered Ceramics: SiC, Al_2O_3, Si_3N_4	5–10
Metals: Aluminum, Steel	90–100

not change from element to element. σ_u is the stress below which the probability of failure is zero. If we assume that any tensile stress will cause failure in a brittle solid, then we can take σ_u to be zero. For such a material, σ_0 is a characteristic strength – often taken to be approximately the mean strength – of the material, and m, called the *Weibull modulus*, is a measure of the variability of the strength of the material; the higher the value of m, the less is the material's variability in strength. m can have any value between 0 and ∞, i.e., $0 < m < \infty$. As $m \to 0$, $R \to 1$, and the material will fail at any stress. Also, when $m \to \infty$, the material will not fracture at any stress below σ_0. Table 7.3 gives some typical values of m for some materials.

From Equations (7.46) and (7.47), we can write, for the survival probability of a brittle material

$$P(V_0) = \exp\left[-\left(\frac{\sigma - \sigma_u}{\sigma_0}\right)^m\right]. \tag{7.48}$$

We can write the failure probability as

$$F(V_0) = 1 - P(V_0) = 1 - \exp\left[-\left(\frac{\sigma - \sigma_u}{\sigma_0}\right)^m\right]. \tag{7.49}$$

As explained in the preceding paragraph, we can take $\sigma_u = 0$ for a brittle material. This will make Equation 7.48 become

$$\boxed{P(V_0) = \exp\left[-\left(\frac{\sigma}{\sigma_0}\right)^m\right].} \tag{7.50}$$

Equation 7.50 says that when the applied stress $\sigma = 0$, the survival probability $P(V_0) = 1$, and all samples of the material tested survive. As the applied stress increases, more samples fail, and the survival probability decreases. Eventually, as $\sigma \to \infty$, $P(V_0) \to 0$; that is, all samples fail at very high stresses. We can arrive at a value of σ_0 by noting that, when $\sigma = \sigma_0$,

$$P(V_0) = \frac{1}{e} = 0.37.$$

Thus, σ_0 is the stress corresponding to a survival probability of 37%. Taking logarithms of Equation 7.50, we get

$$\ln\left[\frac{1}{P(V_0)}\right] = \left(\frac{\sigma}{\sigma_0}\right)^m. \tag{7.51}$$

Thus, a double-logarithmic plot of Equation 7.51 will give a straight line with slope m. This yields a convenient way of obtaining a Weibull analysis of the strength of a given material. If N samples are tested, we rank their strengths in ascending order and obtain the probability of survival for the ith strength value as

$$P_i(V_0) = (N + 1 - i)/(N + 1).$$

Note that there will be $N + 1$ strength intervals for N tests. Alternatively, we can use the failure probability:

$$F_i(V_0) = 1 - P_i(V_0) = i/(N + 1).$$

We can incorporate a volume dependence into Equation 7.50. Let V_0 be a reference volume of a material with a survival probability of $P(V_0)$, i.e., fraction of samples, each of volume V_0, that survive when loaded to a stress, σ. Now consider a volume V of this material such that $V = nV_0$. Then, from Equation 7.43, we can write

$$P(V) = P(V_0)^n = [P(V_0)]^{V/V_0}.$$

Taking logarithms, we get

$$\ln P(V) = \frac{V}{V_0} \ln P(V_0),$$

or

$$P(V) = \exp\left[\frac{V}{V_0} \ln P(V_0)\right]. \tag{7.52}$$

From Equations 7.50 and 7.52, we have

$$\boxed{P(V) = \exp\left[-\frac{V}{V_0}\left(\frac{\sigma}{\sigma_0}\right)^m\right],} \tag{7.53}$$

or

$$\ln P(V) = -\frac{V}{V_0}\left(\frac{\sigma}{\sigma_0}\right)^m. \tag{7.54}$$

We can convert Equation 7.54 to the following form by taking logarithms again.

$$\ln\ln\left[\frac{1}{P(V)}\right] = \ln\frac{V}{V_0} + m\ln\frac{\sigma}{\sigma_0}.$$

Equation 7.54 tells us that, for a given probability of survival and for two volumes V_1 and V_2 of a material,

$$\ln P(V) = -\frac{V_1}{V_0}\left[\frac{\sigma_1}{\sigma_0}\right]^m = -\frac{V_2}{V_0}\left[\frac{\sigma_2}{\sigma_0}\right]^m,$$

where σ_1 and σ_2 are the strengths of the material in volumes V_1 and V_2, respectively.

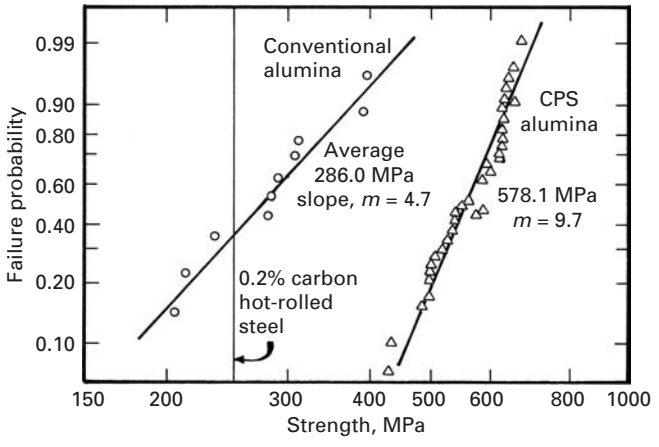

Fig. 7.33 A Weibull plot for a steel, a conventional alumina, and a controlled-particle-size (CPS) alumina. Note that the slope (Weibull modulus m) $\rightarrow \infty$ for steel. For CPS alumina, m is double that of conventional alumina. (After E. J. Kubel, *Adv. Mater. Proc.*, Aug (1988) 25.)

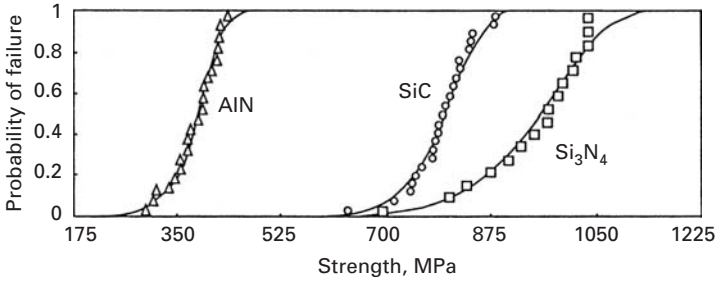

Fig. 7.34 Cummulative probability of flexural strengths (four-point bend test with inner and outer spans 20 and 40 mm, respectively, and cross section of 3 × 4 mm) for three ceramics. (Courtesy of C. J. Shih.)

Hence,

$$V_1\sigma_1^m = V_2\sigma_2^m,$$

or

$$\boxed{\frac{\sigma_1}{\sigma_2} = \left(\frac{V_2}{V_1}\right)^{1/m}}. \tag{7.55}$$

Thus we see that, for an equal probability of survival, the larger the volume ($V_2 > V_1$), the smaller must be the fracture strength ($\sigma_1 < \sigma_2$).

An interesting application of the Weibull distribution is illustrated in Figure 7.33, which shows a double-logarithmic plot as per Equation 7.51. Note that the failure probability $F(V) = 1 - P(V)$, rather than the survival probability $P(V)$ is plotted. The figure shows the following items:

1. The Weibull modulus m of steel $\rightarrow \infty$. (Note the vertical line.)
2. The Weibull modulus m of conventionally processed alumina is 4.7.
3. If we process alumina carefully – say, by using a controlled particle size (CPS in Figure 7.33) – the value of m is doubled, to 9.7. By a controlled particle size, we mean a monosize powder that enhances packing, less use of a binder material (which produces flaws after sintering), more uniform shrinkage, etc.

Figure 7.34 shows the cummulative probability of failure as a function of stress for three important engineering ceramics: AlN, SiC, and

Si_3N_4. As the Weibull modulus increases, the slope of the curve becomes steeper. When we plot the curves on logarithmic abscissa and ordinate axes, a straight line is obtained that can be used to obtain m as shown in Figure 7.33.

Some words of caution regarding the use of Weibull probability plots are in order. The tail of the distribution (see Figure 7.31) must be included in the analysis. In practical terms, this means that the statistical sample size should be sufficiently large. Typically, for an allowable failure rate $P = 0.01$, the sample size would be greater than 100. Also, the preceding analysis assumes a "well-behaved flaw population." Bimodal flaw populations can result in two linear parts on the Weibull plot, indicating two values of the Weibull modulus.

Example 7.8

The data obtained in four-point bend (or flexure) tests on SiC specimens processed in three different ways are reported in Table E7.8.1. Calculate the Weibull modulus m and the characteristic strength σ_0, and make the Weibull plot, for each specimen. Each specimen had outer and inner spans of 40 and 20 mm, respectively. The height and width of the specimens are 3 mm and 4 mm, respectively.

Table E7.8.1 Fracture Load (N) of Three Hot-Pressed SiC Specimens

Test No.	SiC-A	SiC-B	SiC-N
1	497	421	466
2	291	690	618
3	493	556	529
4	605	573	627
5	511	618	564
6	524	609	564
7	327	690	573
8	484	654	394
9	394	618	618
10	448	645	493
11	511	591	511
12	497	739	475
13	426	739	618
14	345	703	493
15	358	569	591
16	287	685	627
17	412	708	618
18	466	573	600
19	493	717	645
20	591	676	614

Solution: We first obtain the stresses from the loads in Table E7.8.1. The moment is

$$M = \frac{P}{2} \times \frac{L}{4}.$$

(See Figure E7.8.1.) The maximum tensile stress is

$$\sigma = \frac{Mc}{I},$$

where h is the height, b is the breadth, I is the moment of inertia of the beam, and

$$c = \frac{h}{2},$$
$$I = \frac{bh^3}{12}.$$

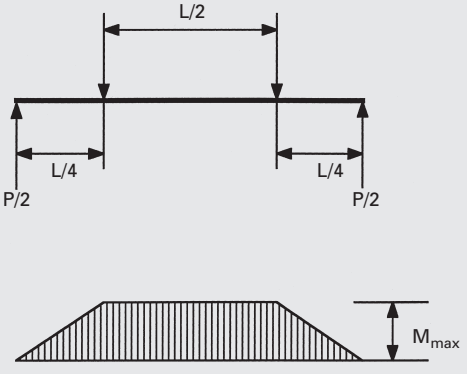

Fig. E7.8.1

The calculated stresses are shown in Figure E7.8.2. Hence,

$$\sigma = \frac{pL\,h \times 12}{8 \times bh^3} = \frac{3}{4}\frac{PL}{bh^2}.$$

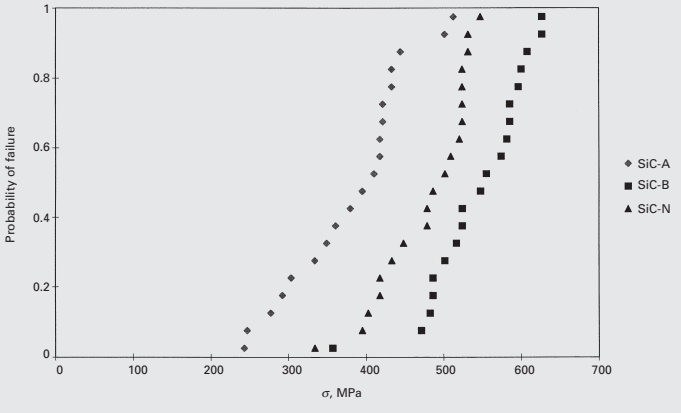

Fig. E7.8.2

To obtain the Weibull parameters, we use Equation 7.50:

$$P(V) = \exp\left[-\left(\frac{\sigma}{\sigma_0}\right)^m\right],$$

or

$$1 - F(V) = \exp\left[-\left(\frac{\sigma}{\sigma_0}\right)^m\right].$$

Taking logarithms yields

$$\ln[1 - F(V)] = -\left(\frac{\sigma}{\sigma_0}\right)^m.$$

Taking logarithms again results in

$$\ln\ln[1 - F(V)] = -m(\ln\sigma - \ln\sigma_0),$$

or

$$\ln\ln\left[\frac{1}{1 - F(V)}\right] = m(\ln\sigma - \ln\sigma_0).$$

To obtain $F(V)$ for each point, we use the following equation:

$$1 - P_i(V) = F_i(V) = \frac{i}{N+1},$$

where N is the total number of specimens tested.

In the present case, $N = 20$. Hence, $F_1(V) = 1/21$, $F_2(V) = 2/21$, $F_3(V) = 3/21$. . . . These results are plotted in Figure E7.8.3. We use a double logarithm for $1/[1– F(V)]$ and the logarithm for σ. The slope of this plot provides m. The horizontal line passing through zero gives the values of the characteristic strengths. We summarize our results in Table E7.8.2. Figure E7.8.4 shows the Weibull curves with the preceding parameters superimposed on the data points of Figure E7.8.3.

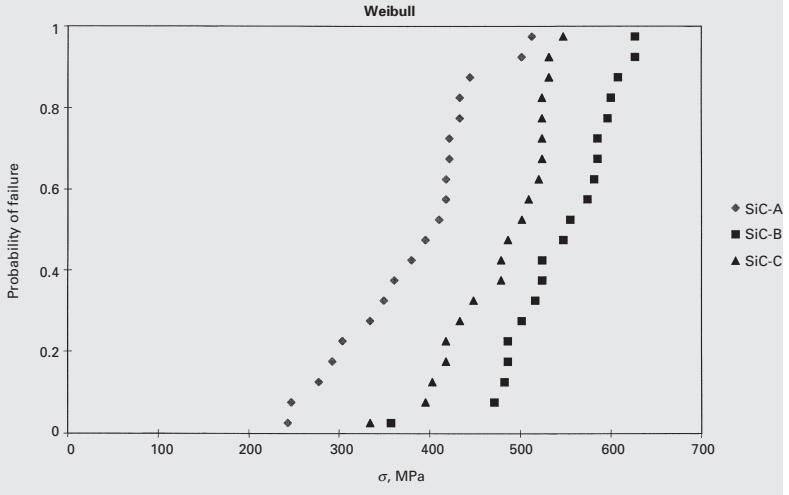

Fig. E7.8.3

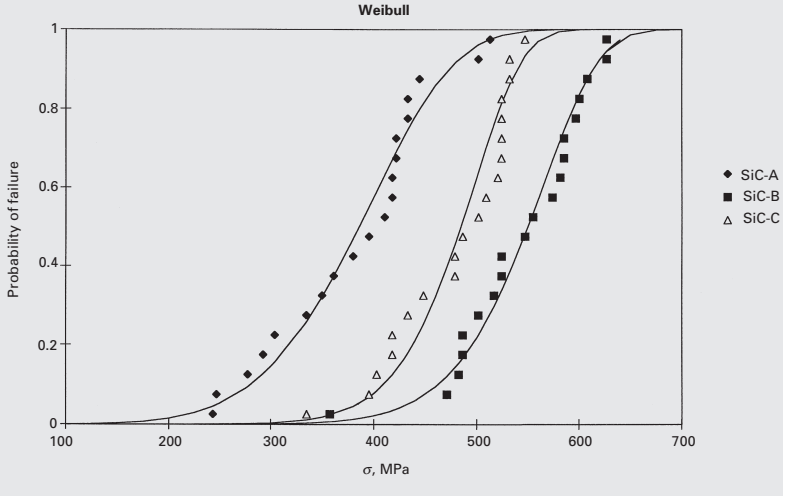

Fig. E7.8.4

Table E7.8.2

Specimen	m	σ_0 (MPa)	Average Stress ± S.D. (MPa)
SiC-A	5.61	411.3	380.7 ± 63.1
SiC-B	9.10	572.1	542.0 ± 52.6
SiC-N	9.22	502.9	476.8 ± 48.7

S.D. = Standard deviation.

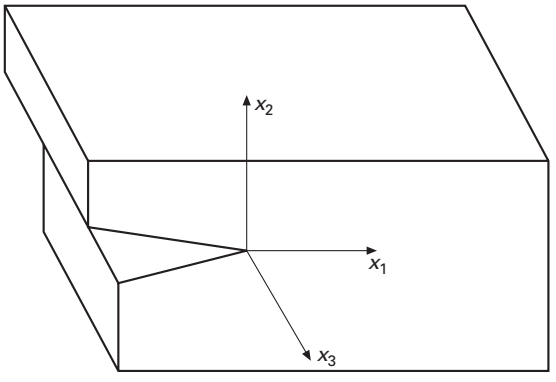

Fig. A1

Appendix: Stress Singularity at Crack Tip

It is relatively simple to obtain the stress singularity close to a crack in Mode III. (See Figure A1.) For Modes I and II, other more complex solutions exist.

The displacements are, for the three directions (X_1, X_2, and X_3):

$$u = 0,$$
$$v = 0,$$
$$w = 0.$$

The strains are:

$$\gamma_{31} = \gamma_{13} = \frac{\partial w}{\partial x_1},$$
$$\gamma_{32} = \gamma_{23} = \frac{\partial w}{\partial x_2}.$$

All the other components are zero.

The stresses are given by

$$\sigma_{13} = G\,\gamma_{13},$$
$$\sigma_{23} = G\,\gamma_{23}.$$

The equilibrium equation is

$$\frac{\partial \sigma_{ij}}{\partial x_j} = \rho \ddot{u}_i.$$

In our case, since the acceleration is zero

$$\frac{\partial \sigma_{ij}}{\partial x_j} = 0.$$

In the extended notation we can write:

$$\frac{\partial \sigma_{13}}{\partial x_1} + \frac{\partial \sigma_{23}}{\partial x_2} = 0,$$
$$G\,\frac{\partial^2 w}{\partial x_1^2} + G\,\frac{\partial^2 w}{\partial x_2^2} = 0,$$
$$\nabla^2 w = 0.$$

We now change to radial coordinates. (See Figure A2.)

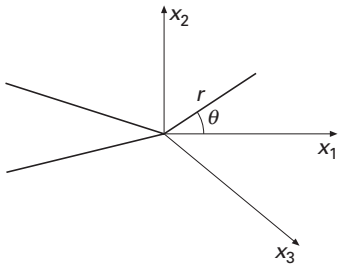

Fig. A2

The form of Laplacian operator in radial coordinates is:

$$\nabla^2 = \frac{\partial^2}{\partial x_1^2} + \frac{\partial^2}{\partial x_2^2} = \frac{\partial^2}{\partial r^2} + \frac{1}{r}\frac{\partial}{\partial r} + \frac{1}{r}\frac{\partial^2}{\partial \theta^2}.$$

The solution to this equation is given in differential equation books.[17]

$$w = r^{\lambda} f(\theta),$$

$$\nabla^2 w = \lambda(\lambda - 1) r^{\lambda-2} f(\theta) + \frac{1}{r}\lambda r^{\lambda-1} f(\theta) + \frac{1}{r^2} r^{\lambda} f''(\theta),$$

$$r^{\lambda-2}\left(\lambda(\lambda - 1) f(\theta) + \lambda f(\theta) + f''(\theta)\right) = 0.$$

Apply for all r,

$$\lambda^2 f(\theta) + f''(\theta) = 0,$$

$$f(\theta) = A \sin\lambda\theta + B \cos\lambda\theta,$$

$$w = r^{\lambda}(A \sin\lambda\theta + B \cos\lambda\theta).$$

The boundary conditions are:

$$w(r, \theta) = -w(r, -\theta),$$

$$w(r, \theta) = r^{\lambda}(A \sin\lambda\theta + B \cos\lambda\theta),$$

$$w(r, -\theta) = r^{\lambda}(-A \sin\lambda\theta + B \cos\lambda\theta),$$

$$B = 0,$$

$$w(r, \theta) = r^{\lambda} A \sin\lambda\theta.$$

For $\theta = \pm\pi$, $\quad \sigma_{r\theta} = 0$.

$$\sigma_{z\theta} = G\frac{1}{r}\frac{\partial w}{\partial \theta} = 0,$$

$$\frac{\partial w}{\partial \theta} = r^{\lambda} A\lambda \cos\lambda\theta \quad \text{at} \quad \theta = \pi,$$

$$\lambda = \pm\frac{1}{2}, \ \pm\frac{3}{2}, \ \pm\frac{5}{2}, \quad \lambda = \frac{2n-1}{2}.$$

In a general way, one can write:

$$w(r, \theta) = \sum_{n=1}^{N}\left(r^{\frac{2n-1}{2}} A \sin\frac{2n-1}{2}\theta\right).$$

We will only use $A > 0$, then the first terms becomes:

$$w(r, \theta) = A_1 r^{\frac{1}{2}} \sin\frac{1}{2}\theta,$$

$$\sigma_{z\theta} = G\frac{1}{r}\frac{\partial w}{\partial \theta} = \frac{A_1}{r} G r^{\frac{1}{2}}\frac{1}{2}\cos\frac{\theta}{2},$$

$$\sigma_{z\theta} = \frac{A_1 G}{2r^{\frac{1}{2}}}\cos\frac{\theta}{2}.$$

where G is the shear modulus.

[17] See, for example, R. Haberman, *Elementary Applied Partial Differential Equations* (Upper Saddle River, NJ: Prentice Hall, 1998).

We use the term K_{III} to group the constants:

$$\sigma_{z\theta} = \frac{K_{III}}{\sqrt{2\pi r}} \cos\frac{\theta}{2},$$

$$\sigma_{r\theta} = G\frac{\partial w}{\partial r} = \frac{A_1 G}{2r^{\frac{1}{2}}} \sin\frac{\theta}{2},$$

or,

$$\sigma_{r\theta} = \frac{K_{III}}{\sqrt{2\pi r}} \sin\frac{\theta}{2}.$$

These expressions are equivalent to Equation 7.23 and demonstrate the square root singularity of the stresses at the tip of the crack.

Suggested Reading

T. L. Anderson. *Fracture Mechanics*, 2nd ed. Boca Raton, FL: CRC Press, 1995.

J. M. Barsom and S. T. Roffe. *Fracture and Fatigue Control in Structures*, 2nd ed. Englewood Cliffs, NJ: Prentice Hall, 1987.

D. Broek. *Elementary Engineering Fracture Mechanics*, 3rd ed. The Hague: Sijthoff and Noordhoff, 1978.

H. L. Ewalds and R. J. H. Wanhill. *Fracture Mechanics*. London: Arnold, 1984.

M. F. Kanninen and C. H. Popelar. *Advanced Fracture Mechanics*. New York, NY: Oxford University Press, 1985.

J. F. Knott. *Fundamentals of Fracture Mechanics*, 3rd ed. London: Butterworths, 1993.

R. J. Sanford, *Principles of Fracture Mechanics*. Upper Saddle River, NJ: Prentice Hall, 2003.

H. Tada, P. C. Paris, and G. R. Irwin, *The Stress Analysis of Cracks Handbook*, 3rd ed., New York, NY: ASME, 2000.

Exercises

7.1 In a polyvinyl chloride (PVC) plate, there is an elliptical, through-the-thickness cavity. The dimensions of the cavity are:

major axis = 1 mm,
minor axis = 0.1 mm.

Compute the stress concentration factor K_t at the extremities of the cavity.

7.2 Calculate the maximum tensile stress at the surfaces of a circular hole (in the case of a thin sheet) and of a spherical hole (in the case of a thick specimen) subjected to a tensile stress of 200 MPa. The material is Al_2O_3 with $\nu = 0.2$.

7.3 Calculate the maximum tensile stress if the applied stress is compressive for a circular hole for which $\sigma_c = 200$ MPa and $\nu = 0.2$.

7.4 The strength of alumina is approximately $E/15$, where E is the Young's modulus of alumina, equal to 380 GPa. Use the Griffith equation in the plane-strain form to estimate the critical size of defect corresponding to fracture of alumina.

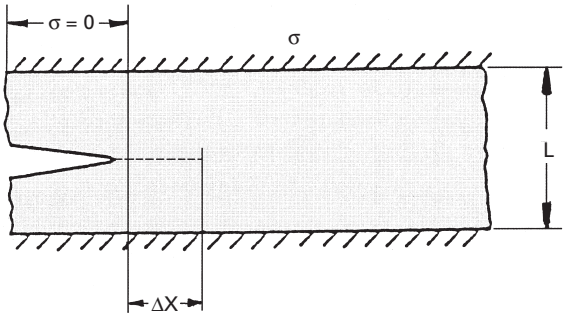

Fig. Ex7.7

7.5 Compute the ratio of stress required to propagate a crack in a brittle material under plane-stress and plane-strain conditions. Take Poisson's ratio ν of the material to be 0.3.

7.6 An Al_2O_3 specimen is being pulled in tension. The specimen contains flaws having a size of 100 μm. If the surface energy of Al_2O_3 is 0.8 J/m^2, what is the fracture stress? Use Griffith's criterion. $E = 380$ GPa.

7.7 A thin plate is rigidly fixed at its edges (see Figure Ex7.7). The plate has a height L and thickness t (normal to the plane of the figure). A crack moves from left to right through the plate. Every time the crack moves a distance Δx, two things happen:

1. Two new surfaces (with specific surface energy) are created.
2. The stress falls to zero behind the advancing crack front in a certain volume of the material.

Obtain an expression for the critical stress necessary for crack propagation in this case. Explain the physical significance of this expression. Assume the stress, σ, ahead of the crack is uniform.

7.8 A central through-the-thickness crack, 50 mm long, propagates in a thermoset polymer in an unstable manner at an applied stress of 5 MPa. Find K_c.

7.9 Machining of SiC produced surface flaws of a semielliptical geometry. The flaws that were generated have dimensions $a = 1$ mm, width $w = 100$ mm, and $c = 5$ mm, and the thickness of the specimen is $B = 20$ mm. Calculate the maximum stress that the specimen can withstand in tension. $K_{Ic} = 4$ MPa m$^{1/2}$.

7.10 (a) An AISI 4340 steel plate has a width W of 30 cm and has a central crack $2a$ of 3 mm. The plate is under a uniform stress σ. This steel has a K_{Ic} value of 50 MPa m$^{1/2}$. Find the maximum stress for this crack length. (b) If the operating stress is 1,500 MPa, compute the maximum crack size that the steel may have without failure.

7.11 A microalloyed steel, quenched and tempered at 250 °C, has a yield strength (σ_y) of 1,750 MPa and a plane-strain fracture toughness K_{Ic} of 43.50 MPa m$^{1/2}$. What is the largest disk-type inclusion, oriented most unfavorably, that can be tolerated in this steel at an applied stress of $0.5\sigma_y$?

7.12 A 25-mm^2 bar of cast iron contains a crack 5 mm long and normal to one face. What is the load required to break this bar if it is subjected to three-point bending with the crack toward the tensile side and the supports 250 mm apart?

7.13 Consider a maraging steel plate of thickness (B) 3 mm. Two specimens of width (W) equal to 50 mm and 5 mm were taken out of this plate. What is the largest through-the-thickness crack that can be tolerated in the two cases at an applied stress of $\sigma = 0.6\sigma_y$, where σ_y (yield stress) = 2.5 GPa? The plane-strain fracture toughness K_{Ic} of the steel is 70 MPa m$^{1/2}$. What are the critical dimensions in the case of a single-edge notch specimen?

7.14 An infinitely large plate containing a central crack of length $2a = 50/\pi$ mm is subjected to a nominal stress of 300 MPa. The material yields at 500 MPa. Compute:

(a) The stress intensity factor at the crack tip.
(b) The size of the plastic zone at the crack tip.

Comment on the validity of Irwin's correction for the size of the plastic zone in this case.

7.15 A steel plate containing a through-the-thickness central crack of length 15 mm is subjected to a stress of 350 MPa normal to the crack plane. The yield stress of the steel is 1,500 MPa. Compute the size of the plastic zone and the effective stress intensity factor.

7.16 The size of the plastic zone at the crack tip in the general plane-stress case is given by

$$r_y = \frac{K_I^2}{2\pi\sigma_y^2}\cos^2\frac{\theta}{2}\left(4 - 3\cos^2\frac{\theta}{2}\right).$$

(a) Determine the radius of the plastic zone in the direction of the crack.
(b) Determine the angle θ at which the plastic zone is the largest.

7.17 For the plane-strain case, the expression for the size of the plastic zone is

$$r_y = \frac{K_I^2}{2\pi\sigma_y^2}\cos^2\frac{\theta}{2}\left\{4[1 - \nu(1 - \nu)] - 3\cos^2\frac{\theta}{2}\right\}.$$

(a) Show that this expression reduces to the one for plane stress.
(b) Make plots of the size of the plastic zone as a function of θ for $\nu = 0$, $\nu = \frac{1}{3}$, and $\nu = \frac{1}{2}$. Comment on the size and form of the zone in the three cases.

7.18 A sheet of polystyrene has a thin central crack with $2a = 50$ mm. The crack propagates catastrophically at an applied stress of 10 MPa. The Young's modulus polystyrene is 3.8 GPa, and the Poisson's ratio is 0.4. Find G_{Ic}.

7.19 Compute the approximate size of the plastic zone, r_v, for an alloy that has a Young's modulus $E = 70$ GPa, yield strength $\sigma_v = 500$ MPa, and toughness $G_c = 20$ kJ/m^2.

7.20 300-M steel, commonly used for airplane landing gears, has a G_c value of 10 kN/m. A nondestructive examination technique capable of detecting cracks that are 1 mm long is available. Compute the stress level that the landing gear can support without failure.

7.21 A thermoplastic material has a yield stress of 75 MPa and a G_{Ic} value of 300 J/m^2. What would be the corresponding critical crack opening displacement? Take $\lambda = 1$. Also, compute J_{Ic}.

7.22 A pipe line with overall diameter of 1 m and 25-mm thickness is constructed from a microalloyed steel ($K_{Ic} = 60$ MPa m$^{1/2}$; $\sigma_y = 600$ MPa). Calculate the maximum pressure for which the leak-before-break criterion will be obeyed. The leak-before-break criterion states that a through-the-thickness crack ($a = t$) will not propagate catastrophically.

7.23 Al_2O_3 has a fracture toughness of approximately 3 MPa m$^{1/2}$. Suppose you carried out a characterization of the surface of the specimen and detected surface flaws with a radius $a = 50$ μm. Estimate the tensile and compressive strengths of this specimen; show by sketches, how flaws will be activated in compression and tension.

7.24 Using the Weibull equation, establish the tensile strength, with a 50% survival probability, of specimens with a length of 60 mm and a diameter of 5 mm. Uniaxial tensile tests carried out on specimens with a length of 20 mm and the same diameter yielded the following results in MPa (10 tests were carried out): 321, 389, 411, 423, 438, 454, 475, 489, 497, 501.

7.25 An engineering ceramic has a flexure strength that obeys Weibull statistics with $m = 10$. If the flexure strength is equal to 200 MPa at 50% survival probability, what is the flexure strength level at which the survival probability is 90%?

7.26 What would be the flexure strength, at 90% survival probability, if the ceramic in the preceding problem is subjected to a hot isostatic processing (HIP) treatment that greatly reduces the population of flaws and increases m to 60. Assume that the flexure strength at 50% survival probability is unchanged.

7.27 Ten rectangular bars of Al_2O_3 (10 mm wide and 5 mm in height) were tested in three-point bending, the span being 50 mm. The failure loads were 1,040, 1,092, 1,120, 1,210, 1,320, 1,381, 1,410, 1,470, 1,490, and 1,540 N. Determine the characteristic flexure strength and Weibull's modulus for the specimens. (See Section 9.6.1 for the flexure formula.)

7.28 Verify the values of m in Figure 7.34, and obtain the characteristic strengths σ_0 for the three materials. If the fracture toughness of SiC, Si_3N_4, and AlN are equal to 5.2, 5.7, and 2.4 MNm$^{3/2}$, respectively, what are the largest flaws that can be tolerated in these specimens?

7.29 Aluminum has a surface energy of 0.5 Jm^{-2} and a Young's modulus of 70 GPa. Compute the stress at the crack tip for two different crack lengths: 1 mm and 1 cm.

7.30 Determine the stress required for crack propagation under plane strain for a crack of length equal to 2 mm in aluminum. Take the surface energy equal to 0.048 J/m^2, Poisson's ratio to 0.345, and the modulus of $E = 70.3$ GPa.

7.31 Calculate the maximum load that a 2024-T851 aluminum alloy (10 cm × 2 cm) with a central through-the-thickness crack (length 0.1 mm) can withstand without yielding. Given: $\sigma_y = 500$ MPa and $K_{Ic} = 30$ MPa m$^{1/2}$.

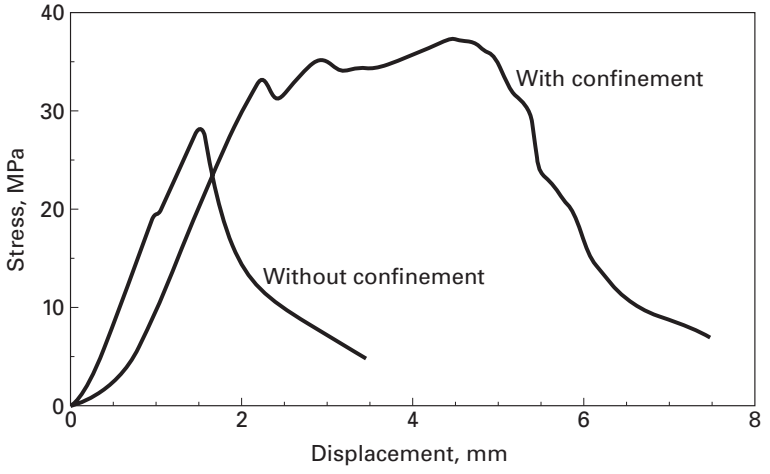

Fig. Ex7.34

7.32 An infinitely large sheet is subjected to a far-field stress of 300 MPa. The material has a yield strength of 600 MPa, and there is a central crack $7/\pi$ cm long.

(a) Calculate the stress intensity factor at the tip of the crack.
(b) Estimate the size of the plastic zone size at the tip of the crack.

7.33 What is the maximum allowable crack size for a material that has $K_{Ic} = 55$ MPa $m^{1/2}$ and $\sigma_y = 1{,}380$ MPa? Assume a plane-strain condition and a central crack.

7.34 Two specimens of concrete were tested in compression. One was wrapped with a very strong composite tape. They exhibited substantial differences in strength, shown in Figure Ex7.34. Explain, in terms of microstructural behavior, the reason for the difference in response. Use sketches.

7.35 An Al_2O_3 specimen is being pulled in tension. The specimen contains flaws having a size of 100 μm.

(a) If the surface energy of Al_2O_3 is 0.8 J/m^2, what is the fracture stress? Use the Griffith criterion. $E = 380$ GPa.
(b) Using your vast fracture mechanics knowledge and advanced equations, estimate the fracture stress if the fracture toughness is 4 MPa $m^{1/2}$. Assume two positions for flaw: in the center of an infinite body and at the edge.

7.36 A structural steel component has a surface crack of 2 mm. This steel has a fracture toughness of 75 MPa $m^{1/2}$. By how much can this crack grow before catastrophic failure?

7.37 A titanium alloy (Ti-6Al-4V) has a yield strength of 1280 MPa and a fracture toughness of 77 MPa $m^{1/2}$. If we apply a stress of $0.3\sigma_y$, what will be the size of the surface crack that will lead to catastrophic failure?

7.38 An AISI steel plate has a crack with the size of 2 mm in the center. If the plate is under a uniform stress, and the width of the plate is 24 cm:

(a) Find the maximum value of the stress if $K_{Ic} = 45$ MPa $m^{1/2}$.
(b) Find the maximum crack size that the plate can have, if it has to operate at a stress of 1,250 MPa.

7.39 In an Al alloy 7178-T651 (thick plate), find the critical crack length if it is under a stress of 500 MPa. Given: $K_{Ic} = 28$ MPa $m^{1/2}$.

7.40 What is the largest flaw size of a ceramic material that can support a strength of 280 MPa and $K_{Ic} = 2.2$ MPa $m^{1/2}$, assuming $Y = 1$?

7.41 Determine the tensile strength of an alumina specimen having a grain size of 1 μm, if the tensile strength of the same material with a grain size of 50 μm is 1 GPa. Assume that the flaw size is equal to one half the grain size.

7.42 A brittle material (Sialon) is used as a support plate. Sialon has a fracture toughness of 9 MPa $m^{1/2}$. The plate has to withstand a tensile load of 200kN. We have three non-destructive inspection techniques at our disposal: X-ray radiography (can detect flaws greater than 0.5 mm); gamma-ray radiography (flaws greater than 0.20 mm) and ultrasonic inspection (flaws greater than 0.125 mm). Calculate the cross-sectional area of the plate for the different NDE testing methods.

7.43
(a) An AISI steel plate has width $W = 30$ cm and a central crack with size of 3 mm. The plate is under a uniform stress. Find the maximum value of the stress is $K_{Ic} = 50$ MPa $m^{1/2}$.
(b) If the part has to operate at a stress of 1,500 MPa, compute the maximum crack size that the plate can have.

7.44 A polymer contains internal flaws (penny shaped) with a diameter of 2 mm and fails, in tension, at an applied stress of 30 MPa. What is the fracture toughness of this polymer?

7.45 Rank the estimated strength of three ceramic parts, made of Al_2O_3, with three different volumes: $V = 10$ cm^3; $V = 100$ cm^3; $V = 1$ m^3.

7.46 Establish the maximum tensile load that a block with a cross-section of 10×10 cm can take, if its fracture toughness is equal to 90 MPa $m^{1/2}$ and its yield stress is 1,000 MPa. This part contains an embedded crack with a radius of 10 mm.

7.47 Engineers are designing a ceramic component for a jet engine. The ceramic has a fracture toughness of 8 MPa $m^{1/2}$. The ceramic is subjected to a maximum tensile stress of 500 MPa. Calculate the maximum size of surface flaws that the part can have.

7.48 A cylindrical pressure vessel (length of 10 m; diameter of 1 m) is made from a high strength steel with $K_{Ic} = 100$ MPA $m^{1/2}$ and a yield strength of 1,600 MPa. The thickness of the vessel is 25 mm. NDE has revealed a longitudinal crack penetrating 7 mm into the cylinder wall.

(a) What maximum pressure can the cylinder be loaded to?
(b) What is the percentage reduction in maximum pressure due to the presence of flaw?

Chapter 8

Fracture: Microscopic Aspects

8.1 Introduction

In Chapter 7, we described the macroscopic aspects of the fracture behavior of materials. As with other characteristics, the microstructure of a material has a great influence on its fracture behavior. In what follows, we present a brief description of the microstructural aspects of crack nucleation and propagation, as well as the effect of the environment on the fracture behavior of different materials. Figure 8.1 shows, schematically, some important fracture modes in a variety of materials. These different modes will be analyzed in some detail in this chapter. Metals fail by two broad classes of mechanisms: *ductile and brittle* failure.

Ductile failure occurs by (a) the nucleation, growth, and coalescence of voids, (b) continuous reduction in the metal's cross-sectional area until it is equal to zero, or (c) shearing along a plane of maximum shear. Ductile failure by void nucleation and growth usually starts at second-phase particles. If these particles are spread throughout the interiors of the grains, the fracture will be transgranular (or transcrystalline). If these voids are located preferentially at grain boundaries, fracture will occur in an intergranular (or intercrystalline) mode. The appearance of a ductile fracture, at high magnification (500× or higher) is of a surface with indentations, as if marked by an ice-cream scooper. This surface morphology is appropriately called *dimpled*. Rupture by total necking is very rare, because most metals contain second-phase particles that act as initiation sites for voids. However, high-purity metals, such as copper, nickel, gold, and other very ductile materials, fail with very high reductions in their areas.

Brittle fracture is characterized by the propagation of one or more cracks through the structure. While totally elastic fracture describes the behavior of most ceramics fairly well, metals and some polymers undergo irreversible deformation at the tip of the crack, which affects its propagation. Figure 8.1 shows the variety of morphologies and processes occurring during fracturing of materials. For metals and ceramics, two modes of crack propagation: transgranular

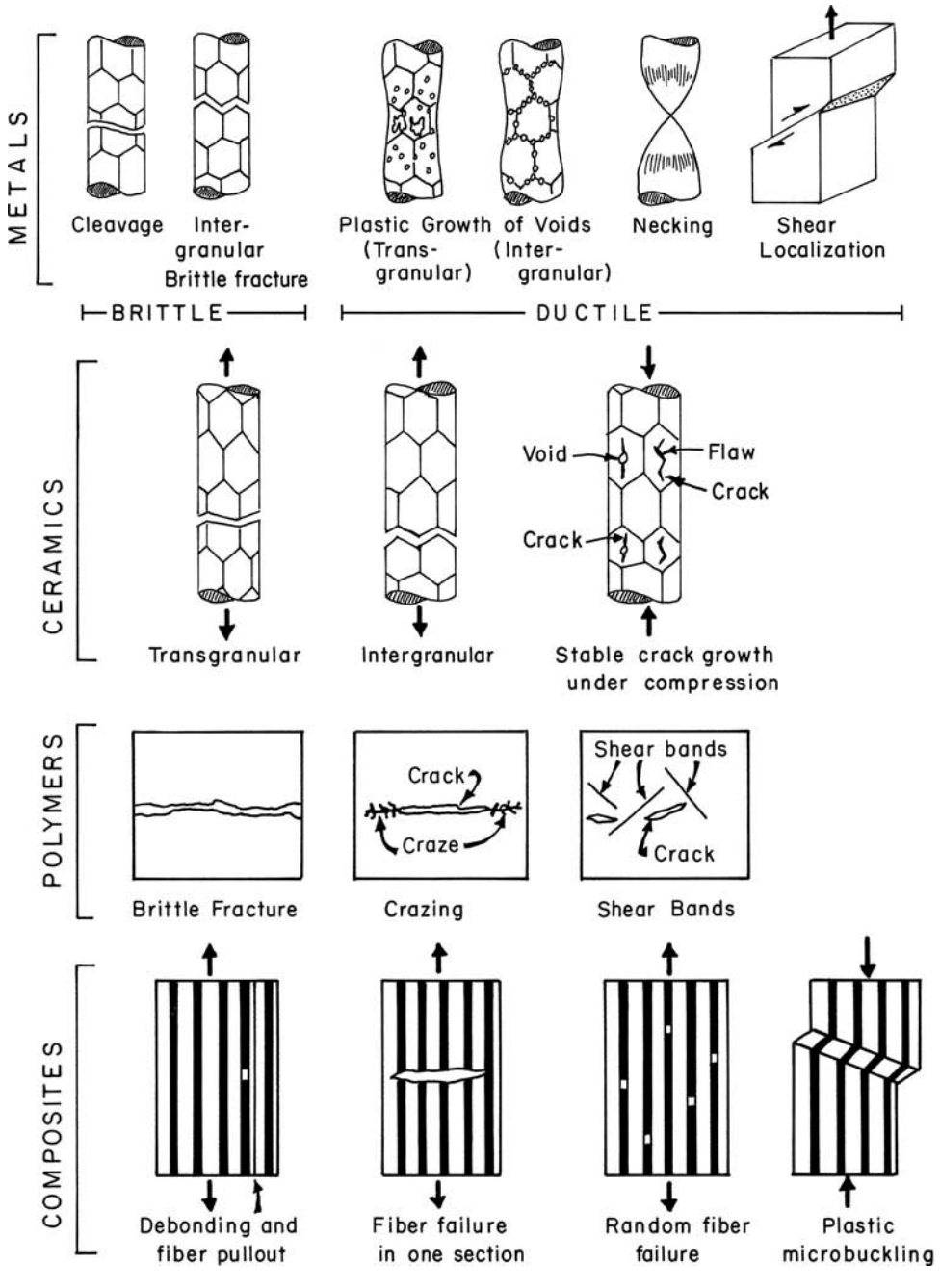

Fig. 8.1 Schematic classification of fracture morphologies and processes. (After M. F. Ashby.)

fracture (or cleavage) and intergranular fracture are observed. For energy-related reasons, a crack will tend to take the path of least resistance. If this path lies along the grain boundaries, the fracture will be intergranular.

Often, a crack also tends to run along specific crystallographic planes, as is the case for brittle fracture in steel. Upon observation at high magnification, transgranular brittle fracture is characterized by

clear, smooth facets that have the size of the grains. In steel, brittle fracture has the typical shiny appearance, while ductile fracture has a dull, grayish aspect. In addition to brittle fracture, polymers undergo a mode of fracture involving *crazing*, in which the polymer chains ahead of a crack align themselves along the tensile axis, so that the stress concentration is released.

Another mode of deformation that is a precursor to fracture is the phenomenon of *shear banding* in a polymer. If one stretches the polymer material, one observes the formation of a band of material with a much higher flow stress than exists in the unstretched state. Shear banding (or localization) is also prevalent in metals.

Composites – especially fibrous ones – can exhibit a range of failure modes that is dependent on the components of the material (matrix and reinforcement) and on bonding. If the bond strength is higher than the strength of the matrix and reinforcement, the fracture will propagate through the latter (Figure 8.1). If the bonding is weak, one has debonding and fiber pullout. In compression, composites can fail by a kinking mechanism, also shown in the figure; the fibers break, and the entire structure rotates along a band, resulting in a shortening of the composite. This mechanism is known as *plastic microbuckling*.

8.2 Fracture in Metals

Metals are characterized by a highly mobile dislocation density, and they generally show a ductile fracture. In this section, we discuss the various aspects of void and crack nucleation and propagation in metals.

8.2.1 Crack Nucleation

Nucleation of a crack in a perfect crystal essentially involves the rupture of interatomic bonds. The stress necessary to do this is the theoretical cohesive stress, which was dealt with in Chapter 7, starting from an expression for interatomic forces. From this expression, we see that ordinary materials break at much lower stresses than do perfect crystals – on the order of $E/10^4$, where E is Young's modulus of the material. The explanation of this behavior lies in the existence of surface and internal defects that act as preexisting cracks and in the plastic deformation that precedes fracture. When both plastic deformation and fracture are eliminated – for example, in "whiskers" – stresses on the order of the theoretical cohesive stresses are obtained.

Crack nucleation mechanisms vary according to the type of material: brittle, semibrittle, or ductile. The brittleness of a material has to do with the behavior of dislocations in the region of crack nucleation. In highly brittle materials the dislocations are practically immobile, in semibrittle materials dislocations are mobile, but

Table 8.1 Materials of Various Degrees of Brittleness[a]

Type	Principal Factors	Materials
Brittle	Bond rupture	Structures of type diamond, ZnS, silicates, alumina, mica, boron, carbides, and nitrides
Semibrittle	Bond rupture, dislocation mobility	Structures of type NaCl, ionic crystals, hexagonal close-packed metals, majority of body-centered cubic metals, glassy polymers
Ductile	Dislocation mobility	Face-centered cubic metals, some body-centered cubic metals, semicrystalline polymers

[a] Adapted with permission from B. R. Lawn and T. R. Wilshaw, *Fracture of Brittle Solids* (Cambridge, U.K.: Cambridge University Press, 1975), p. 17).

only on a restricted number of slip planes, and in ductile materials there are no restrictions on the movement of dislocations other than those inherent in the crystalline structure of the material. Table 8.1 presents various materials classified according to this criterion regarding the mobility of dislocations.

The exposed surface of a brittle material can suffer damage by mechanical contact with even microscopic dust particles. If a glass fiber without surface treatment were rolled over a tabletop, it would be seriously damaged mechanically.

Any heterogeneity in a material that produces a stress concentration can nucleate cracks. For example, steps, striations, depressions, holes, and so on act as stress raisers on apparently perfect surfaces. In the interior of the material, there can exist voids, air bubbles, second-phase particles, etc. Crack nucleation will occur at the weakest of these defects, where the conditions would be most favorable. We generally assume that the sizes as well as the locations of defects are distributed in the material according to some function of standard distribution whose parameters are adjusted to conform to experimental data. In this assumption, there is no explicit consideration of the nature or origin of the defects.

In semibrittle materials, there is a tendency for slip initially, followed by fracture on well-defined crystallographic planes. That is, there exists a certain inflexibility in the deformation process, and the material, not being able to accommodate localized plastic strains, initiates a crack to relax stresses.

Various models are based on the idea of crack nucleation at an obstruction site. For example, the intersection of a slip band with a grain boundary, another slip band, and so on, would be an obstruction site.

8.2.2 Ductile Fracture

In ductile materials, the role of plastic deformation is very important. The important feature is the flexibility of slip. Dislocations can move

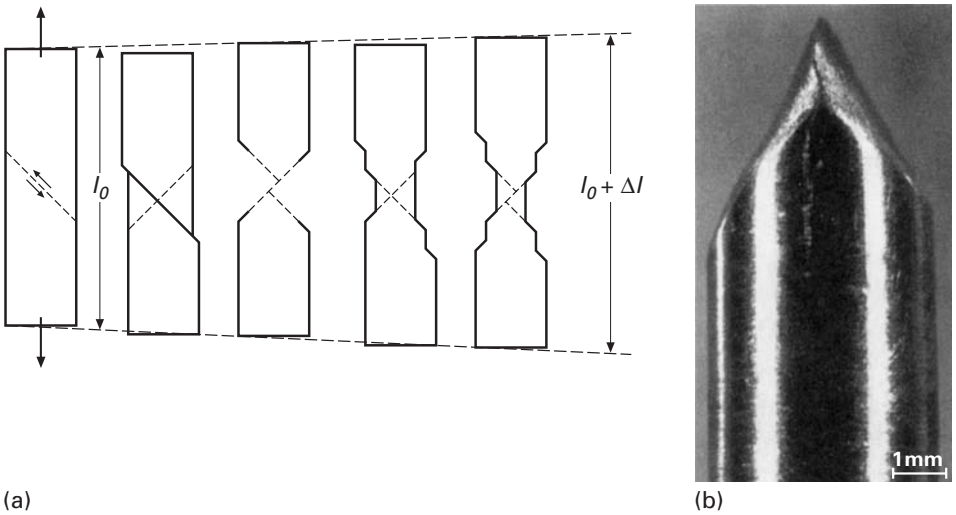

(a) (b)

Fig. 8.2 (a) Failure by shear (glide) in a pure metal. (Reprinted with permission from D. Broek, *Elementary Engineering Fracture Mechanics*, 3rd ed. (The Hague, Netherlands: Martinus Nijhoff, 1982), p. 33.) (b) A point fracture in a soft single-crystal sample of copper. (Courtesy of J. D. Embury.)

on a large number of slip systems and even cross from one plane to another (in cross-slip). Consider the deformation of a single crystal of copper, a ductile metal, under uniaxial tension. The single crystal undergoes slip throughout its section. There is no nucleation of cracks, and the crystal deforms plastically until the start of plastic instability, called necking. From this point onward, the deformation is concentrated in the region of plastic instability until the crystal separates along a line or a point. (See Figure 8.2(a).) In the case of a cylindrical sample, a soft single crystal of a metal such as copper will reduce to a point fracture. Figure 8.2(b) shows an example of such a fracture in a single crystal of copper. However, if, in a ductile material, there are microstructural elements such as particles of a second phase, internal interfaces, and so on, then microcavities may be nucleated in regions of high stress concentration in a manner similar to that of semibrittle materials, except that, due to the ductile material's large plasticity, cracks generally do not propagate from these cavities. The regions between the cavities, though, behave as small test samples that elongate and break by plastic instability, as described for the single crystal.

In crystalline solids, cracks can be nucleated by the grouping of dislocations piled up against a barrier. Such cracks are called *Zener–Stroh* cracks.[1] High stresses at the head of a pileup are relaxed by crack nucleation, as shown in Figure 8.3, but this would occur only in the case where there is no relaxation of stresses by the movement of dislocations on the other side of the barrier. Depending on the

[1] C. Zener, *The Fracturing of Metals* (Metals Park, OH: ASM, 1948).

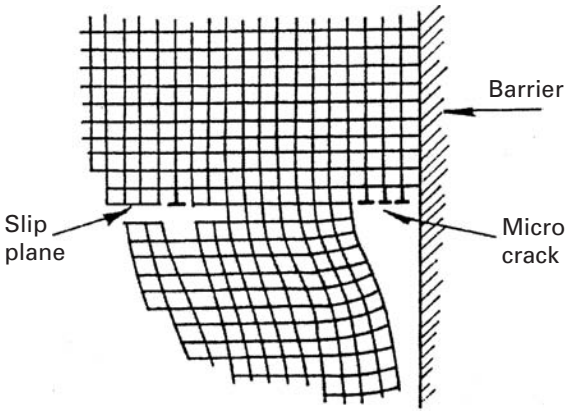

Fig. 8.3 Grouping of dislocations piled up at a barrier and leading to the formation of a microcrack (Zener–Stroh crack).

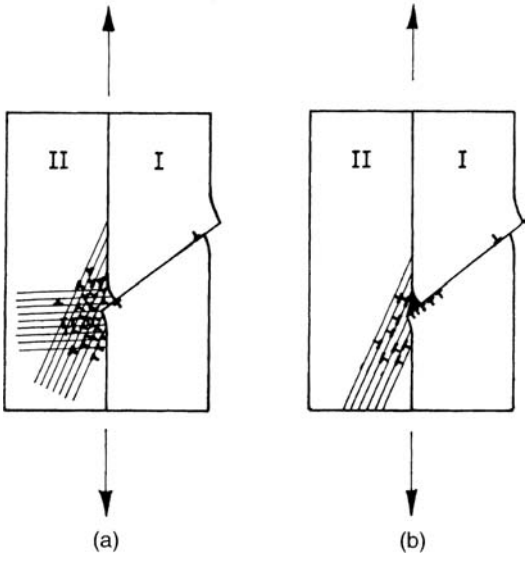

Fig. 8.4 Bicrystal with a slip band in grain I. (a) The stress concentration at the boundary of the barrier due to slip band is fully relaxed by multiple slip. (b) The stress concentration is only partially relaxed, resulting in a crack at the boundary.

slip geometry in the two parts and the kinetics of the motion and multiplication of dislocations, such a combination of events could occur. (See Table 8.1.) Figure 8.4(a) shows a bicrystal that has a slip band in grain I. The stress concentration at the barrier due to the slip band is completely relaxed by slip on two systems in grain II. Figure 8.4(b) shows the case of only a partial relaxation and the resulting appearance of a crack at the barrier. Lattice rotation associated with the bend planes and deformation twins can also nucleate cracks. Figure 8.5 shows crack nucleation in zinc as per the model shown in Figure 8.5(a). Cracks can also begin at the intersections of various boundaries in a metal, which represent sites at which there is a concentration of stress. Figure 8.6 presents examples of crack nucleation at the intersection of twin boundaries and at the intersection of twin steps and boundaries.

Fracture at high temperature can occur by a variety of other modes as well. For example, grain-boundary sliding occurs rather easily at high temperatures. Grain-boundary sliding can lead to the

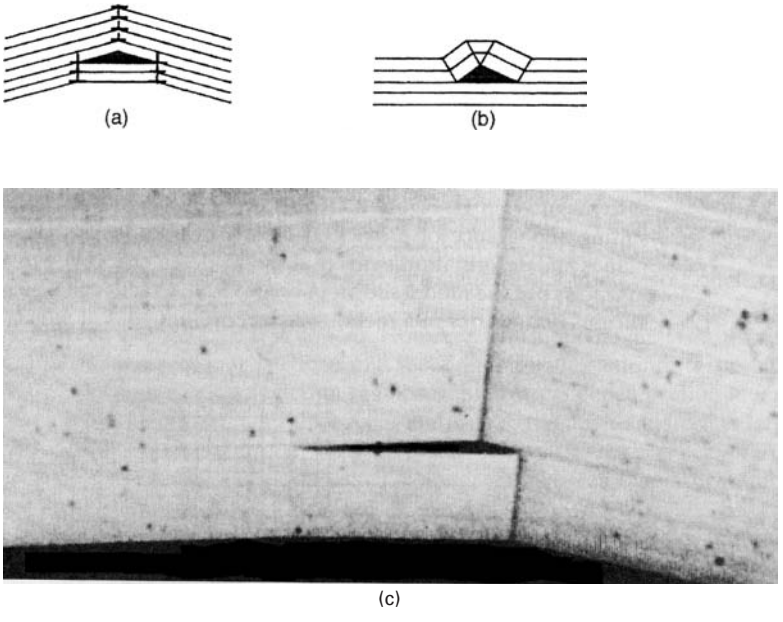

Fig. 8.5 Crack nucleation by (a) lattice rotation due to bend planes and (b) deformation twins. (c) Crack nucleation in zinc due to lattice rotation associated with bend planes. (Reprinted with permission from J. J. Gilman, *Physical Nature of Plastic Flow and Fracture*, General Electric Report No. 60-RL-2410M, April, 1960, p. 83.)

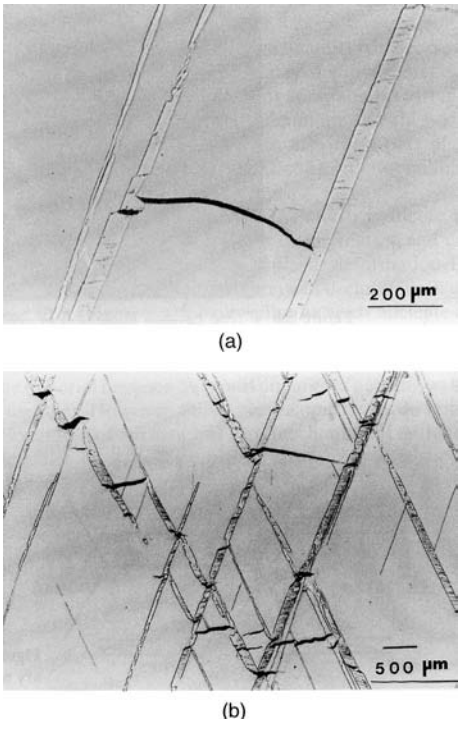

Fig. 8.6 Initiation of failure by microcrack formation in tungsten deformed at approximately 10^4 s^{-1} at room temperature. (a) Twin steps. (b) Twin steps and twin–twin intersection. (From T. Dümmer, J. C. LaSalvia, M. A. Meyers, and G. Ravichandran, *Acta Mater.*, 46 (1998) 959.)

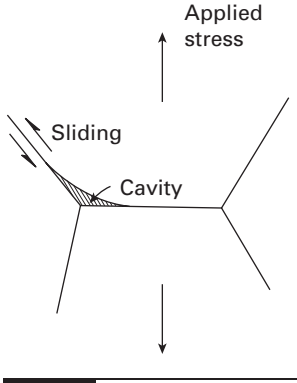

Fig. 8.7 *w*-type cavitation at a grain-boundary triple point.

development of stress concentrations at grain-boundary triple points (where three grain boundaries meet). Cracks nucleate at such triple points as shown schematically in Figure 8.7. Figure 8.8 shows a micrograph of copper in which such a crack nucleation has occurred. This type of crack is called *w-type cavitation* or *w-type cracking*. Yet

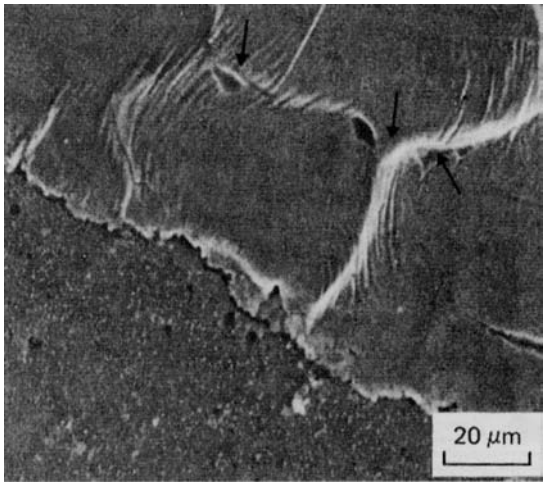

Fig. 8.8 *w*-type cavities nucleated at grain boundaries in copper; SEM.

another type of cracking occurs, characteristically, under conditions of low stresses and high temperature. Small cavities form at grain boundaries that are predominantly at approximately 90° to the stress axis, as shown in Figure 8.9. This is called *r-type cavitation* or *r-type cracking*. Figure 8.10 shows such intergranular voids in copper.

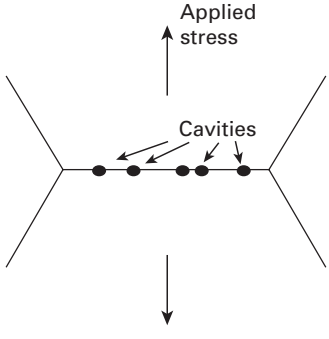

Fig. 8.9 *r*-type cavitation at a grain boundary normal to the stress axis.

The most familiar example of ductile fracture is that in uniaxial tension, giving the classic "cup and cone" fracture. When the maximum load is reached, the plastic deformation in a cylindrical tensile test piece becomes macroscopically heterogeneous and is concentrated in a small region. This phenomenon is called necking (see Section 3.2). The final fracture occurs in this necked region and has the characteristic appearance of a conical region on the periphery resulting from shear and a central flat region resulting from the voids created there. In extremely pure metal single crystals (e.g., those free of inclusions, etc.), plastic deformation continues until the sample section is reduced to a point, a geometric consequence of slip, as shown in Figure 8.2.

In practice, materials generally contain a large quantity of dispersed phases. These can be very small particles (1 to 20 nm) such as carbides of alloy elements, particles of intermediate size (50 to 500 nm) such as alloy element compounds (carbides, nitrides,

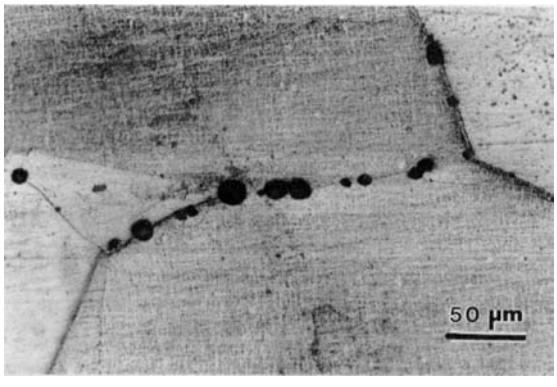

Fig. 8.10 *r*-type cavities nucleated at grain boundaries in copper, seen through an optical microscope.

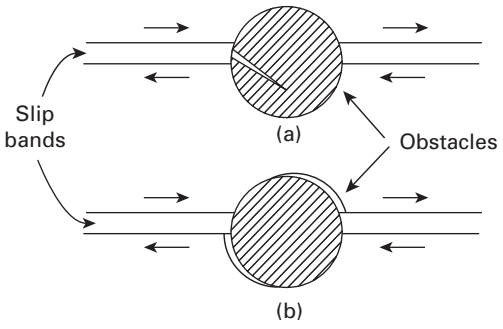

Fig. 8.11 Nucleation of a cavity at a second-phase particle in a ductile material. (Adapted with permission from B. R. Lawn and T. R. Wilshaw, *Fracture of Brittle Solids* (Cambridge: Cambridge University Press, 1975), p. 40.)

carbonitrides) in steels, or dispersions such as Al_2O_3 in aluminum and ThO_2 in nickel. Precipitate particles obtained by appropriate heat treatment also form part of this class (e.g., an Al–Cu–Mg system), as do inclusions of large size (on the order of millimeters) – for example, oxides and sulfides.

If the second-phase particles are brittle and the matrix is ductile, the former will not be able to accommodate the large plastic strains of the matrix, and consequently, these brittle particles will break in the very beginning of plastic deformation. In case the particle/matrix interface is very weak, interfacial separation will occur. In both cases, microcavities are nucleated at these sites (Figure 8.11). Generally, the voids nucleate after a few percent of plastic deformation, while the final separation may occur around 25%. The microcavities grow with slip, and the material between the cavities can be visualized as a small tensile test piece. The material between the voids undergoes necking on a microscopic scale, and the voids join together. However, these microscopic necks do not contribute significantly to the total elongation of the material. This mechanism of initiation, growth, and coalescence of microcavities gives the fracture surface a characteristic appearance. When viewed in the scanning electron microscope, such a fracture appears to consist of small dimples, which represent the microcavities after coalescence. In many of these dimples, one can see the inclusions that were responsible for the void nucleation. (See Figure 8.12.) At times, due to unequal triaxial stresses, these voids are elongated in one or the other direction. We describe the process of fracture by void nucleation, growth, and coalescence in some detail because of its great importance in metals.

Fracture by Void Nucleation, Growth, and Coalescence

Figure 8.13 shows the classic cup-and-cone fracture observed in many tensile specimens with a cylindrical cross section. The configuration is typical of ductile fracture, and upon observation at a higher magnification (1,000× or higher, best done in a scanning electron microscope), one sees the typical "dimple" features. The dimples are equiaxal in the central portion of the fracture and tend to be inclined in the sidewalls of the "cup." The top two pictures show scanning electron micrographs of these two areas. In the central region fracture is